ARCHIVES OF ACOUSTICS
11, 2, 119-136 (1986)

ACOUSTIC ASPECTS OF A RADIAL DIFFUSER

J. DE KRASINSKI, W. WAWSZCZAK, S. SUN

Department of Mechanical Engineering, University of Calgary
(Calgary, Alberta Canada TZN1N4)

The flow in a supersonic radial-diffuser is investigated experimentally and the results of the experiments are discussed in the light of existing theories From such an analysis it is concluded that a better understanding of this particular diffuser, which can be used as a sound attenuator, may lead to other applications in the field of propulsive units and jet flows*.

1. Introduction

The advent of high power propulsive units in aeronautics has brought an unwelcome by-product: the noise. It was first experienced in a drastic manner at the propeller tips when these surpassed the velocity of sound, later in turbo-jet units or rocket propulsive engines. Also industrial jets operating with compressed air are powerful noise generators with all the associated side effects.

Sound generated aerodynamically has focussed attention of prominent scientists since the early 1950' s. On the theoretical side the first break-through in the understanding of the mechanism of aerodynamically generated noise was done by H. J. LIGHTHILL [1], [2] and G. M. LILLEY [3] in Great Britain followed later by A. POWELL [4] in the U.S.A. and H. RIBNER [5], [6] in Canada, just to mention a few. It was followed with greater or smaller success by considerable experimental research on both of the Atlantic like E. MOLLO CHRISTENSEN [7], A. MICHALKE [8], [9], I. JONES [10], H. RIBNER [11], W. FFOWCS [12], M. HOLLINGWORTH [13], just to quote a few earlier studies.

In spite of the progress in the understanding of the nature of aerodynamic noise when it comes to the prediction of its intensity for a particular case and to the reduction of noise by applying the existing theories it appears that they fall short of expections. They have not yet reached sufficient refinement to be

---

* The Abstract was prepared by the Editorial Board.

of great use to the applied scientist, and engineer. Thus for example a multitube suppressor nozzle developed by the *Boeing Company* [14] is known to suppress the noise, yet the calculated value of the total acoustic power using LIGHTHILL'S power law is equal to that of a single jet. In defence of the existing theories one should say that they point out the nature of noise generation, can help to interpret results of measurements and indicate interesting possibilities in new design.

The concept of a radial diffuser in subsonic and supersonic flows is not very well known and its application as a noise suppressor of supersonic jets new to the knowledge of the authors of this paper. Supersonic diffusers tend to diminish the noise due to the reduction of the kinetic energy of the flow. Because a normal shock has to be situated downstream of the second throat, which is open to the atmosphere the noise attenuation is not substantial.

The use of a radial diffuser would not be applicable to the turbo-jet engines during flight operation because of the reduction of the momentum flux at the exit, yet the present study indicates that the main cause of the noise reduction may not be necessarily the process of recompression. There are several other factors all working in parallel to reduce the noise in the case of such a diffuser.

This paper deals in the first instance with the experimental results of sound attenuation and the necessary details related to a supersonic radial-diffuser-silencer. In the second part the results are discussed in the light of the existing theories. It is hoped that a better understanding of this particular sound attenuator may lead to other applications in the field of propulsive units and jet flows.

2. Details of the experiment

2.1 The radial diffuser-silencer and its installation

Fig. 1 shows a cross section of the radial diffuser. One observes in it: i) the supersonic nozzle, ii) the front plate forming the diffuser bell, iii) the adjustable back plate separated from the bell by a gap h, iv) a conical spike. If the diameter of the back-plate at the exit is D and the diameter of the nozzle is d then the area ratio of this diffuser is $4Dh/d^2$. By adjusting the back plate with the regulating screws one varies the gap h and also the area ratio and the area of the second throat situated in the region of the base of the conical spike. Three typical conical spikes are also shown, as well as a rounded dome-shaped piece used originally for subsonic tests.

Fig. 2 gives a typical distribution of the internal cross-section of this diffuser along the axis for various gaps h. The areas A^* and A^{**} as function of Mach number are also drawn for all the supersonic nozzles which have a constant diameter $d = 0.8$ inch.

For a typical gap $h = 0.118$ inch and back plate diameter $D = 7.0$ inch the area ratio of this diffuser is about 5.2. The smallest recorded gap which the diffuser was operating efficiently was $h = 0.06''$ reducting the area ratio quoted above by half.

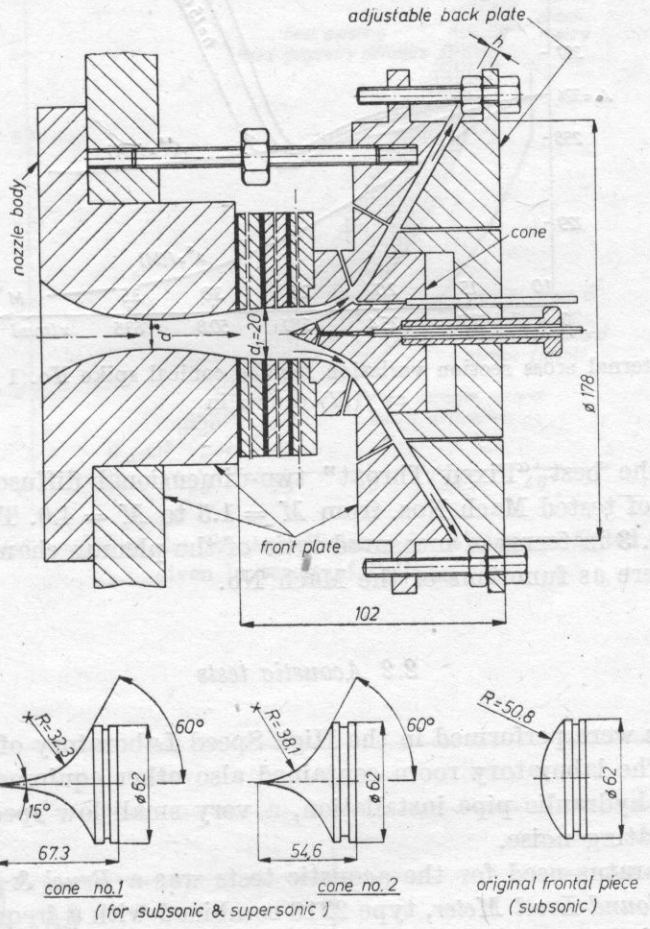

Fig. 1. A cross section of the radial diffuser with typical conical spikes and low speed rounded head

The diffuser was connected through a nozzle to a plenum chamber fed from a compressed air storage system having T_0 approximately at room temperature. Filling of the plenum chamber during the blow down operation through reduction valves was accompanied by a hissing noise similar to that of a pressurized water installation. No separate analysis of this noise has been done yet, although the background noise of the laboratory was recorded (sec below).

The aerodynamic characteristics of this diffuser are described separately [15]. It may be noted however that the efficiency of some configurations com-

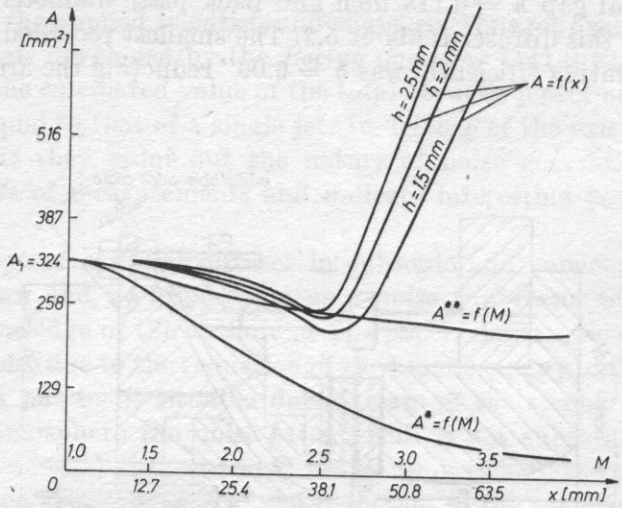

Fig. 2. The internal cross section variation for the conical spike No. 1 with A^* and A^{**} as $f(M)$ drawn in

pares with the best "Fixed Throat" two-dimensional diffusers through the whole range of tested Mach Nos. from $M = 1.5$ to $M = 4.0$. These results are shown in Fig. 3 in terms of measured ratio of the plenum chamber pressure to the atmosphere as functions of the Mach No.

2.2 Acoustic tests

The tests were performed in the High Speed Laboratory of the University of Calgary. The laboratory room contained also other equipment like a small water flume, hydraulic pipe installation, a very small low speed wind tunnel etc. all generating noise.

The apparatus used for the acoustic tests was a *Bruel & Kjaer Precision Intergrating Sound Level Meter*, type 2218 combined with a frequency analyzer. Also a *Bruel & Kjaer High Resolution Signal Analyzer* type 2033 with a plotter was used to obtain noise spectra. The frequency range was for most of the tests up to 20 kHz, but in some cases a microphone was used, sensitive to very high frequencies up to 50 kHz. The laboratory walls were made of cement. A typical background noise of the laboratory was recorded and is shown in Fig. 4. It does include the noise of the high pressure system required to run the nozzle.

Fig. 5 shows the results of directional tests at $M = 4.0$. The microphone was located at the level of the nozzle axis at a distance of 4.9′ from the nozzle exit and rotated through 90°. Without diffuser the highest noise level was 125 dB when on the nozzle axis. A typical "valley" of noise intersity was not recorded in the front of the nozzle which may be partly due to the bell of the diffuser

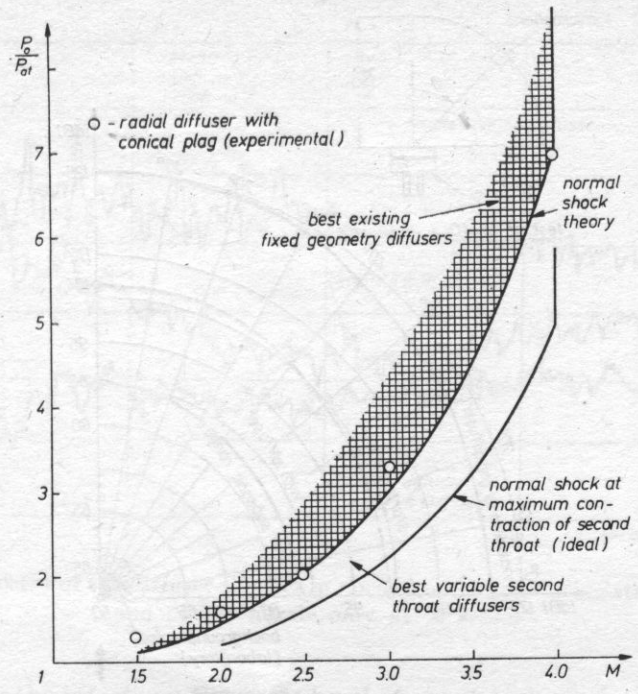

Fig. 3. Experimental results of the diffuser efficiency for a range of tested Mach Numbers given in terms of P_0/P_{atm}

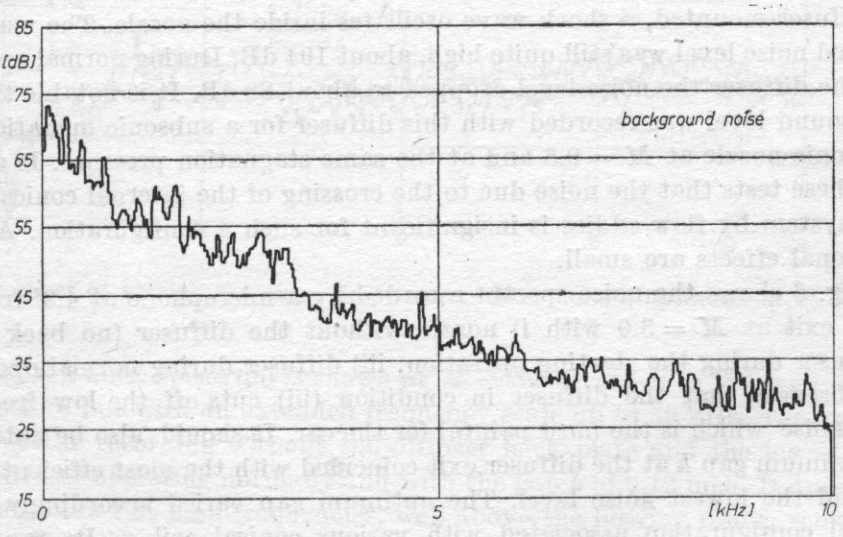

Fig. 4. Measured spectrum of the typical laboratory background noise

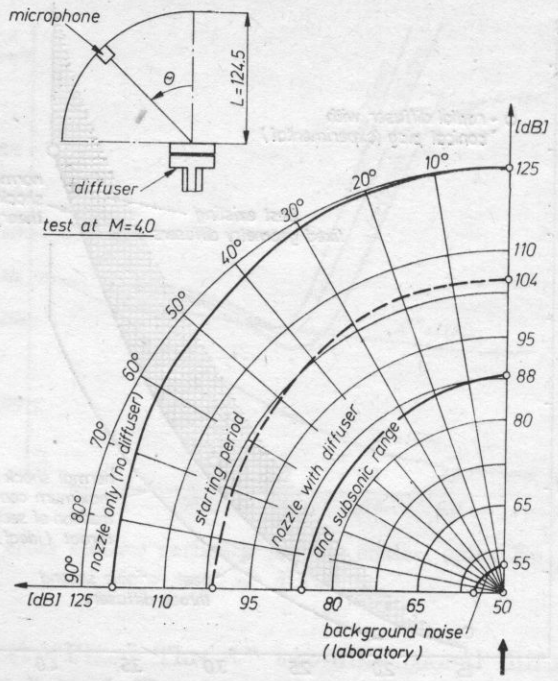

Fig. 5. Directional effects of measured noise measured noise intensity. Nozzle with diffuser (normal operation), starting period and nozzle only. $M = 4.0$ and approximately $M = 0.8$

which was not dismounted for those tests, and partly due to the reflections from the cement floor and walls of the laboratory. During the starting period with the diffuser mounted, a shock wave oscillates inside the nozzle. The maximum recorded noise level was still quite high, about 104 dB. During normal operation with the diffuser the noise level dropped to about 88 dB. It is notable that the same sound level was recorded with this diffuser for a subsonic operation with a subsonic nozzle at $M = 0.8$ and at the same stagnation pressure. It appears from these tests that the noise due to the crossing of the internal conical shock wave system by flow eddies is insignificant for such a configuration. Also the directional effects are small.

Fig. 6 shows the noise spectra recorded by a microphone at 4.9′ from the nozzle exit at $M = 3.0$ with i) nozzle without the diffuser (no back plate), ii) diffuser during the starting operation, iii) diffuser during normal operation. One observes that the diffuser in condition (iii) cuts off the low frequency range noise which is the most painful for the ear. It should also be noted that the minimum gap h at the diffuser exit coincided with the most efficient operation and the lowest noise level. The optimum gap varied accordingly to the internal configuration associated with various conical spikes. Its range was between 0.06 inch (1.5 mm) and 0.12 inch (3.0 mm).

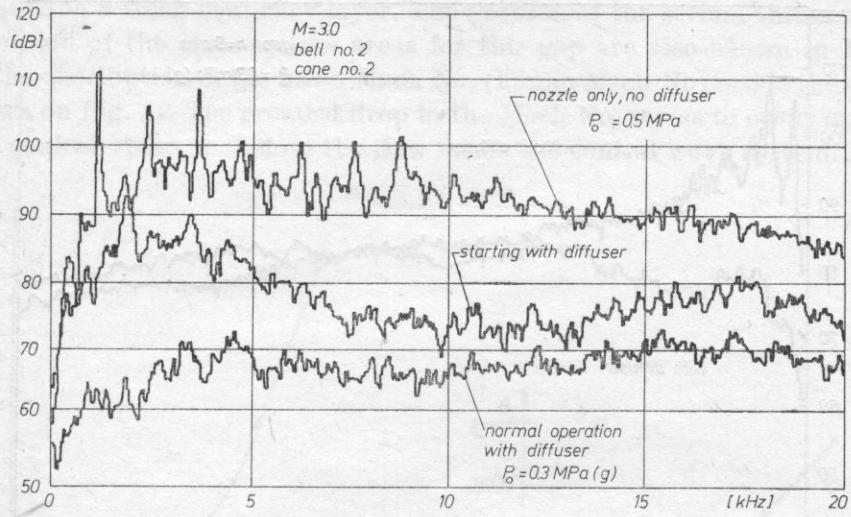

Fig. 6. Acoustic spectra of the diffuser-silencer in normal operation during starting procedure and of the nozzle only at $M = 3.0$

Fig. 7 shows the effects on the noise level of varying the stagnation pressure at $M = 3.0$ from about 44 psig (0.3 mPag) to 73 psig (0.5 mPag). One observes that this effect is small, and is about 17.0 dB/mPa.

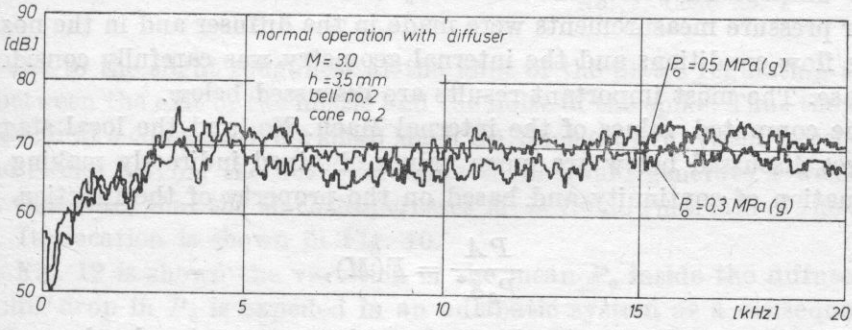

Fig. 7. The effect of varying the reservoir pressure during normal operation at $M = 3.0$

On Fig. 8 a noise spectrum is shown at $M = 3.0$ recorded in the same condition as before but with an extended frequency scale up to 50 kHz. The upper curve shows the recording without the diffuser back plate and the lower one with the diffuser operating normally and with the gap h of 0.12 inch. It appears that the noise level at high frequencies, well above the hearing range, remains approximately the same. The difference of an order of magnitude is recorded however at lower frequencies within the hearing range.

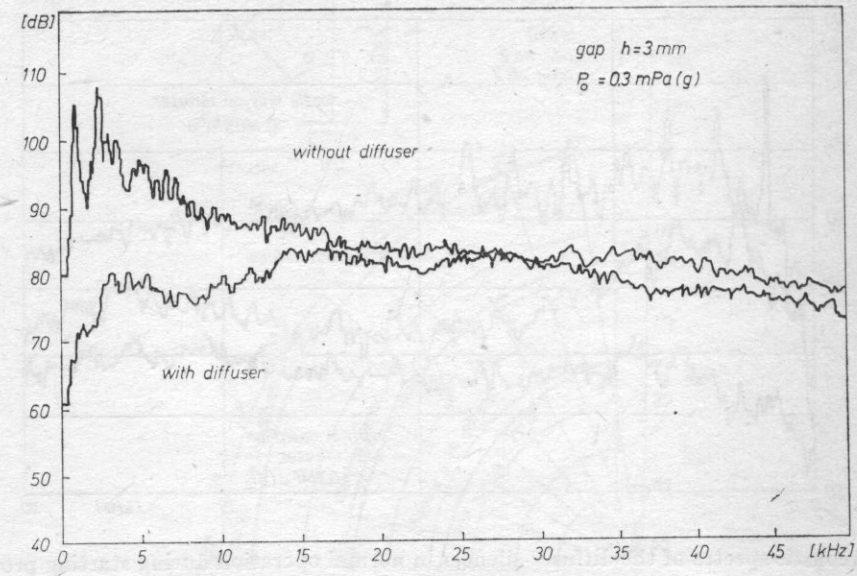

Fig. 8. Aerodynamic noise spectra at $M = 3.0$ with and without the diffuser for an extended range of frequencies up to 50 kHz

3. An analysis of the internal flow conditions

To understand better the unusually effective sound attenuation of this diffuser pressure measurements were made in the diffuser and in the nozzle for various flow conditions and the internal geometry was carefully considered in each case. The most important results are discussed below.

The computed values of the internal Mach. No. and the local stagnation pressures discussed below are mean values obtained indirectly making use of the equation of continuity and based on the property of the function

$$\frac{PA}{P_0 A^*} = F(M),$$

where P = local static pressure, P_0 = reservoir pressure, A = local cross-section area in the diffuser, A^* = the throat area of the nozzle.

As local P is measured and the remaining parameters are known the mean Mach No. (the Fanno Mach No.) M can be computed at each point of the diffuser. For this Mach No. the isentropic ratio P/P_0 is found and for a given P the mean value of P_0 can be obtained indirectly.

In Fig. 9 one observes the distribution of the static pressured measured inside the diffuser, normalized by the reservoir pressure P_0 one observes the strongest rise in the static pressures close to the diffuser exit (at $X = 3.38''$), presumably downstream of a weak shock wave located below the second throat

embedded in a thick boundary layer. The position of the second throat and the distribution of the cross-section areas for this gap are also shown in Fig. 10.

The distribution of the mean Mach No. (Fanno Mach No) inside the diffuser is shown on Fig. 11. The greatest drop in the Mach No. seems to occur upstream of the conical spike i.e. before the flow meets the conical wave system. May be

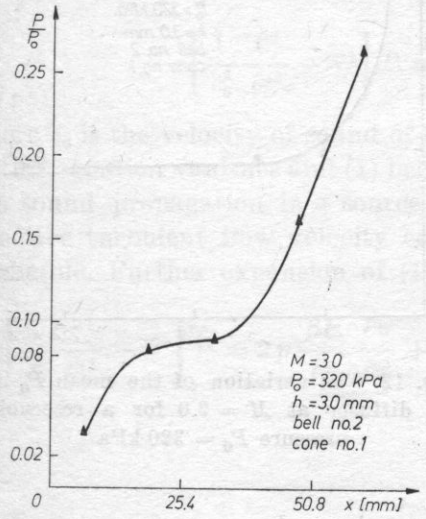

Fig. 9. Static pressure distribution in the diffuser at $M = 3.0$

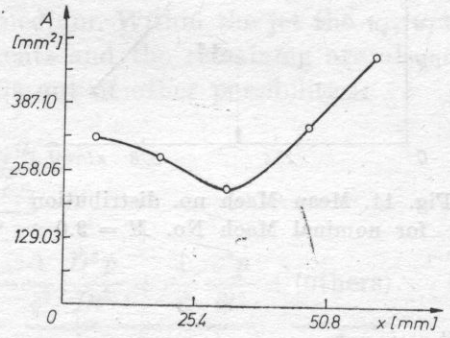

Fig. 10. Area distribution and position of the second throat for $h = 3$ mm Bell. No. 2, Cone no. 1

this is due to the slight roughness at the joint of the plates regulating the distance between the exit of the nozzle and the noise of the spike. Thus the conical waves occur at a comparatively small Mach No. Such a wave system is very weak and the eddies leaving the nozzle crossing them would generate a weak noise source. One notes that the Mach No, crosses $M = 1.0$ downstream of the second throat. Its location is shown in Fig. 10.

In Fig. 12 is shown the variation of the mean P_0 inside the diffuser. The monotonic drop in P_0 is expeded in an adiabatic system as a consequence of the II Law of Thermodynamics. Here again the greatest drop associated with the largest entropy increase is observed at the early stages of the flow that confirms that the shock wave system generated by the conical spike is weak.

Fig. 13 shows the relative position of the conical spike [for the gap $h = 0.12$ inch (3.0 mm)].

A coarse turbulence is associated with low frequency aerodymical noise. In this design of the diffuser the distance between the conical spike and the wall of the diffuser bell is steadily reduced up to the point when the gap h becomes constant. This is shown in Fig. 14 for $h = 0.12$ inch. Thus the transversal size of the eddies moving in the diffuser is in this case reduced 4-folds (assuming

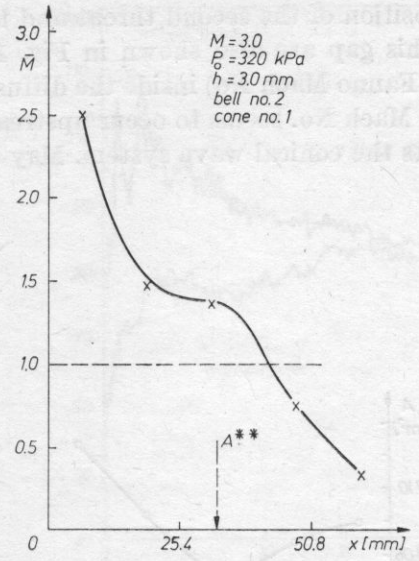

Fig. 11. Mean Mach no. distribution for nominal Mach No. $M = 3.0$

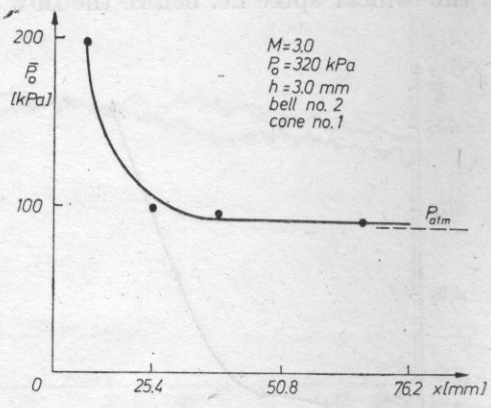

Fig. 12. The variation of the mean P_0 in the diffuser at $M = 3.0$ for a reservoir pressure $P_0 = 320$ kPa

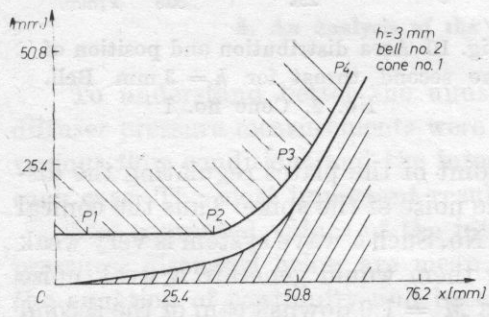

Fig. 13. The position of the conical spike No. 1 relative to the nozzle exit plane at $X = 0.0$ and of the pressure taps

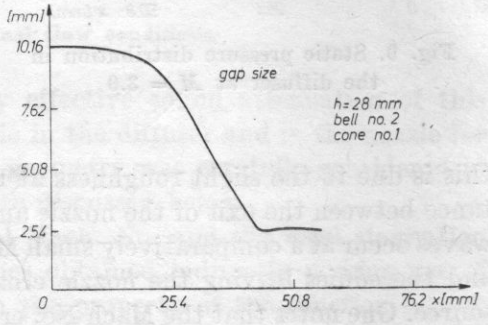

Fig. 14. The gap size inside the diffuser assumed initially as radius of the nozzle for $h = 2.8$ mm (0.11 inch)

that the initial width is equal to the nozzle radius). This also helps to understand the reduction in the low frequency noise levels as indicated by the acoustic measurements.

4. Theoretical aspects of sound generated aerodynamically

4.1 A review of the fundamental features of the current theories

It appears that one of the inherent weaknesses of all the aerodynamical sound theories is the essential ambiguity in identifying the physical causes and

sources of the observed noise field. The confidence in any conjectures in this regard can only be established by examining the details of sound production in very simple flows that are reasonably well known. Unfortunately only few compressible flow fields belong to this category. Progress in aerodynamic noise theory has been achieved by a formal but rather arbitrary source identification. LIGHTHILL'S [1] full equation restated in pressure terms is

$$\left[\frac{1}{c_0^2}\frac{\partial^2}{\partial t^2} - \nabla^2\right] P = \frac{\partial^2 p\, u_i u_j}{\partial x_i \partial x_j} - \frac{\partial^2}{\partial t^2}\left[p - \frac{P}{c_0^2}\right], \tag{1}$$

where c_0 is the velocity of sound of the ambient air. Outside the jet the R.H.S. of this equation vanishes and (1) becomes a homogenous wave equation describing sound propagation in a source free medium. Within the jet the u_i, u_j are effective turbulent flow velocity components and the remaining are also not negligible. Further expansion of (1) yields out of other possibilities:

$$\left[\frac{1}{c_0^2}\frac{\partial^2}{\partial t^2} - \nabla^2\right] P = 2p \underbrace{\frac{\partial U}{\partial y}\frac{\partial v}{\partial x}}_{a} + p \underbrace{\frac{\partial^2 u_i u_j}{\partial x_i \partial x_j}}_{b} - \underbrace{\frac{1}{c^2}\frac{D^2 p}{Dt^2} + \frac{1}{c_0^2}\frac{\partial^2 p}{\partial t^2}}_{c} + \underbrace{(\text{others})}_{d}. \tag{2}$$

The transversely sheared flow $U(y)$ or $U(x_2)$ has a superimposed turbulent component $u_i (i = 1, 2, 3)$ and $x_1, x_2 = x, y$, $v = u_2$ and c is the velocity of sound within the jet field.

The term (a) is a source responsible for noise due to shear

The term (b) is the "self noise" source due to turbulence

The term (c) is due to the convection of the sound waves but is not a source as can be seen by transferring the term (c) to the L.H.S.

The term (d) is due to other sources not classified above real or equivalent in the mathematical sense. The solution of LIGHTHILL'S equation gives the famous eighth power law of noise intensity $I \sim U^8$ (true for subsonic flows).

RIBNER [16] has shown that the above presentation of LIGHTHILL'S equation leads directly to a from very similar to the often quoted LILLEY'S wave equation

$$\frac{1}{c^2}\frac{D^2 p}{Dt^2} - \nabla^2 p - 2p\frac{\partial U}{\partial y}\frac{\partial v}{\partial x} = p\frac{\partial^2 u_i u_j}{\partial x_i \partial x_j} + (\text{others}) \tag{3}$$

which is identical with Eq. (2) after rearranging the terms. One observes above that the wave convection term (c) and the mean flow shear term appear on the L.H.S. LILLEY'S equation has been used widely to describe the jet noise with the argument that it represents more correctly the physics of noise generation because the R.H.S., the "self noise" term is considered as "real" noise source and note merely mathematically "equivalent".

This short discussion emphasizes the previous observations that the same results can be obtained without identifying exactly the sources of noise. Is has been also observed by RIBNER [16] that the sources of noise in Eq. (2) are not unique and many more source term expansion have been published. The acceptable variety of sources as well as "equivalent sources" in the mathematical sense have contributed to a great confusion for many years.

4.2 Some guidelines from the theory

The experimental scientist who looks for guidance on noise abatement from these general equations like (2) and (3) can expect much less in this area his fluid mechanics counterpart who uses Navier Stokes equation for boundary layer problems. It appears that there is a general consensus that the "self noise" term (*b*) in Eq. (2) is an unmistakable real source of aerodynamic noise generation. Thus any device which would reduce the turbulence level or the size of the eddies would be beneficial. Fig. 15 gives a schematic view of a high speed jet without wave patterns, in which two regions are distinguished. Region *A*,

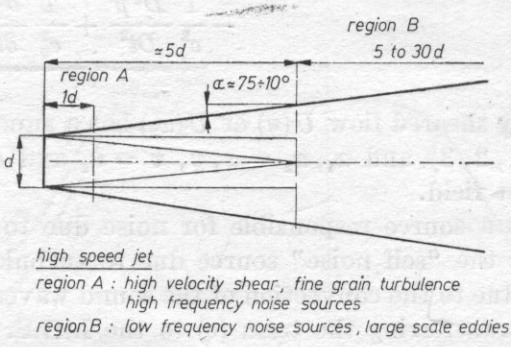

Fig. 15. Diagram of a subsonic jet with regions *A* and *B* related to high frequency and low frequency noise sources corresponding to fine grain and coarse scale turbulence respectively

very close to the exit of the jet, is characterized by nigh frequency noise sources, fine grain turbulence and high velocity shear. In region *B*, at about $5d$ distance from the jet exit, low frequency noise sources prevail as well as large scale eddies. In this context the aerodynamical noise theory indicates that very compact noise sources are inefective [17] the measure of smallness is the acoustic wave length λ. One may assume for the sake of the argument that sources smaller than $(1/4)\lambda$ are not very effective. On the other hand those larger than $(1/4)\lambda$ are more powerful sound generators. This is illustrated in Fig. 16 for a velocity of sound of 340 m/s. A reduction in the size of the eddies due to a narrowing gap inside the diffuser should contribute to the compactness of the noise sources a situation very different to that of a free jet.

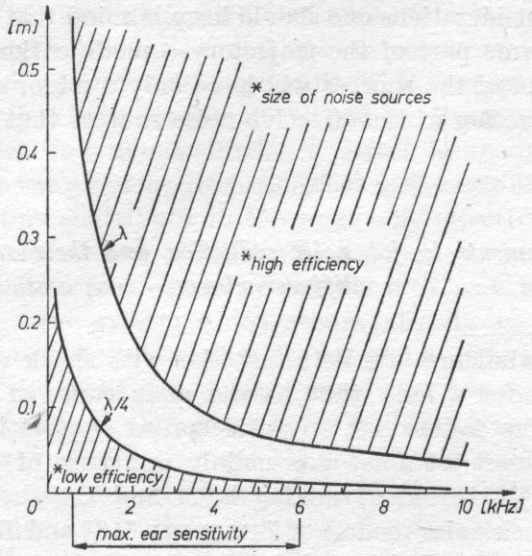

Fig. 16. The acoustic wave length as a function of the frequency compared to the size of efficient noise sources assumed larger than λ and to the inefficient ones assumed smaller than $(1/4)\lambda$

If one believes in the shear term of Eq. (2) as a real noise source a reduction in the transversal component v along the trajectory and of the sheared gradient dU/dy could contribute to the noise abatement. These two factors occur inside the diffuser because of the narrowing gap and the continuous reduction in the mean flow velocity U. The "self noise" term (b) in Eq. (2) can be explained in physical terms as an instantaneous pressure rise due to a collision between two adjacent eddies. In a three dimensional flow if the streamlines are strongly diverging transversally to the mean flow direction such collisions between two adjacent eddies should be less frequent thus reducing the "self noise" source intensity. A situation occurring within the diverging part of the radial diffuser.

With reference to the "other sources" (d) in the bracket of Eq. (2) and (3) a most powerful contribution to noise generation are vortices crossing a fixed shock wave pattern. Advantage is sough in this diffuser by decreasing the shock wave strength through a system of conical waves instead of plane waves.

Any boundary layer separation causes turbulence and vorticity which is the main noise source particularly if combined with shock waves. It boundary layer separation could be avoided by making the streamlines diverge between themselves due to three-dimensional effect without diverging from the wall as is the case in two-dimensional configurations this could also contribute to a reduction in the generation of noise.

LIGHTHILL'S equations (2) and (3) do not explicitly contain effects of viscosity. Its role is still debated it appears that moderate friction combined with small size eddies could be beneficial to reduce the noise level.

In all these considerations one should keep in mind that if real noise sources are active along some part of the trajectory a modification of that trajectory further downstream of the sources will have only a minor effect. It is only by suppression or reduction of the effective noise sources that positive gains may be achieved.

4.3 Recent developments in jet noise reduction and their relation to the radial diffuser-silencer

The role of turbulence and its interaction with shock waves has been recognized in theory for a long time as the main cause of aerodynamic noise supersonic jets. The failure for any widespread application of the existing theories to the aircraft jet noise was mainly due lack of detailed knowledge of the supersonic jet turbulent mixing layer and the shock structure itself. The theoretical shock noise models of LIGHTHILL [18] and RIBNER [19] employ integrals requiring a detailed knowledge of the shock strength, their position and of the turbulent components of the flow related to the stress tensor upstream of each shock cell. It is worth mentioning that according to these theories the "self-noise" source is associated with high pitch while the shear flow is responsible of low pitch noise sources.

On the experimental side interesting new development are to be noted. One of them is the use of a porous centerbody inserted in the jet exit. It has been first suggested Maestrello [20], [21] and afterwards further developed by BAUER [22], KIBENS and WLEZIEN [24]. Although the noise reduction by the porous centerbody in subsonic flow is disputed, a considerable in the noise level has been confirmed in supersonic condition when shock waves in the flow field. The centerbody the shock waves strength and their structure and also does not allow the jet to coalesce and produce focussing of the compression waves. Friction on the centerbody and mixing reduce gradually the energy of the jet without high noise penalty. Also SEINER and NORUM [25] have shown that the jet noise intensity in axi-symmetric flow increases in streamwise direction and reaches a maximum between the third and the sixth shock cell. Similarly TANNA et al. [26] have shown that a major reduction in noise is associated with the elimination of a highly organized shock structure.

It appears that the geometry of the centerbody also modifies the characteristics of the shear layer in such a way as to reduce the noise.

Similarly noise reduction by using a multi-jet suppressor nozzle or corrugated nozzles developed by the Boeing Co. [14] is most likely due to a change in the mixing pattern of the flow and a reduction in the scale of turbulence when the flow crosses a honeycomb-like multitube structure.

It may be also noted that most of the acoustic theories have not taken viscosity into account and its role remains up till now obscure. CANTRELL et al.

[27] and MORFEY [28] have suggested that acoustic energy is not always conserved and that sound sources and sound sinks can occur in regions of flow which is not potential and where viscosity prevails. This concept of acoustic sink in flow with viscosity has been further developed by BECHERT [29] who applied it successfully to jet flow demonstrating a defect in acoustic energy.

It appears from the previous discussion that in the case of the radial diffuser-silencer several factors contribute to the unusually effective noise attenuation and these may be enumerated as follows not in order of importance: i) Initial friction losses dissipate a part of energy directly into heat. ii) The conical spike produces a conical wave system which occurs already at a lower Mach No. than the nozzle. This system is weaker than a plane wave system and because of the closeness of the walls and quickly narrowing gap few shock wave cells can develop. iii) Streamlines diverge while the walls converge beyond the second throat. The waves are embedded in a quickly growing boundary layer. Such a wave system is not prone to be a strong noise source when crossed by the eddies. iv) A monotonic reduction in the gap size in the direction of motion together with flow deceleration reduces the size of the eddies and the turbulence scale as well as the shear stresses. These two factors affect the self noise source as well as the shear noise source and this reduces effectively the low pitch part of the spectrum. v) The mixing pattern is completely altered as compared to the free jet. The presence of the walls tends to dissipate the energy through viscosity into thermal motion. The concept acoustic sink may be important in this context. vi) A great part of the kinetic energy is conserved due to recompression and therefore less is available for acoustic dissipation also low speed flow emerges from the exit.

5. Concluding remarks

It should be mentioned that this type of diffuser-silencer conserves energy by recompression and works on a different principle than muffler type nozzles [30]. It is not clear however what role in noise attenuation is played by successful recompression as is the case in this diffuser. Low speed flow at the exit of this silencer makes it not applicable to aircraft to aircraft in flying conditions or to suppress the noise of industrial jets. A design is already in progress to maintain the same internal features only with a higher velocity at the exit. Preliminary tests of this diffuser-silencer on a four stroke engine indicated sound reduction comparable to a standard muffler with the difference however that for higher exit flow velocities the efficiency of the engine increased because of its discharge to a partial vacuum, while with a muffler the efficiency decreases.

More systematic research is required for this promising sound attenuator, and the role of the size of the jet must be assesed.

Acknowledgement

The authors would like to acknowledge the assistance of the Natural Sciences and Engineering Research Council of Canada for sponsoring this research and to Dr. A. DOIGE for the help in the acoustic measurements.

References

[1] M. J. LIGHTHILL, *On Sound Generated Aerodynamically. I. General Theory*, Proceedings of the Royal Society, Ser. A, **211**, 564–587 (1952).

[2] M. J. LIGHTHILL, *On Sound Generated Aerodynamically. II. Turbulence as a Source of Sound*, Proceedings of the Royal Society, Ser. A, **222**, 1–32 (1954).

[3] G. M. LILLEY, *The Generation and Radiation of Supersonic Jet Noise. IV. Theory of Turbulence Generated Jet Noise, Noise Radiation from Upstream Sources and Combustion Noise*, United States Air Force Aero Propulsion Laboratory, TR-72-53, July 1972.

[4] A. POWELL, *Theory of Vortex Sound*, Journal of the Acoustical Society of America, **36**, 1, 177–195 (1964).

[5] H. S. RIBNER, *New Theory of Jet-Noise Generation, Directionality and Spectra*, Journal of the Acoustical Society of America, **31**, 245–246 (1959).

[6] H. S. RIBNER, *Aerodynamic Sound from Fluid Dilatations: A Theory of Sound from Jets and Other Flows*, Univ. of Toronto, Institute for Aerospace Studies, Rept. 86, AFORS TN 3430, July 1962.

[7] E. MOLLO-CHRISTENSEN, M. A. KOLPIN and J. R. MARTUCELLI, *Experiments on Jet Flows and Set Noise Far-Field Spectra and Directivity Patterns*, Journal of Fluid Mechanics, **18**, 285–301 (1964).

[8] A. MICHALKE, *New Aspects of Sound Generation by Circular Jets*, Fluid Dynamic Transactions, **6**, 439–448 (1971).

[9] A. MICHALKE, *An Expansion Scheme for the Noise from Circular Jets*, Zeitschrift für Flugwissenschaft, **20**, 229–237 (1972).

[10] I. S. F. JONES, *Jet Noise Suppression by an Impedance Shroud*, Boeing Scientific Research Lab., Doc. DI-82-0984 (1970).

[11] H. S. RIBNER, *Shock-Turbulence Interaction and the Generation of Noise*, NACA TN 3255, July 1954 and NACA Rept. 1233, 1955.

[12] J. E. FLOWCS WILLIAMS, *The Noise from Turbulence Convected at High Speed*, Philosophical Transactions of the Royal Society of London, Ser. A, **255**, 469–503 (1963).

[13] M. A. HOLLINGSWORTH, E. J. RICHARDS, *A Schlieren Study of the Interaction Between a Vortex and a Shock Wave in a Shock Tube*, Aeronautical Research Council Britain, **17**, 985, 2323 (1955).

[14] J. B. LARGE, J. F. WILBY, E. GRANDE, A. O. ANDERSSON, *The Development of Engineering Practices in Jet*, Compressor, and Boundary Layer Noise, Aerodynamic Noise, Proceedings of AFOSR-UTIAS Symposium held at Toronto, 20–21 May, 1968.

[15] J. de KRASINSKI, W. WAWSZCZAK, *Aerodynamic Aspects of a Radial Diffuser in High Subsonic and Supersonic Flows*, Department of Mechanical Engineering, June 1985 (in press).

[16] H. S. RIBNER, *Perspectives on Jet Noise*, Acoustic, AIAA Journal, **19**, 12 (1981).

[17] J. E. FFOWCS WILLIAMS, *Sound Sources in Aerodynamics — Fact and Fiction*, Acoustics, AIAA Journal, **20**, 3 (1982).

[18] M. J. LIGHTHILL, *On the Energy Scattered from the Interaction of Turbulence with Sound of Shock Waves*, Proceedings of the Cambridge Philosophical Society, **49**, 531–551 (1953).

[19] H. S. RIBNER, *Acoustic Energy Flux from Shock-Turbulence Interaction*, Journal of Fluid Mechanics, **35**, 2, 299–310 (1969).

[20] L. MAESTRELLO, *Initial Results of a Porous Plug Nozzle for Supersonic Jet Noise Suppression*, NASA TM-78802, 1978.

[21] L. MAESTRELLO, *An Experimental Study on Porous Plug Jet Noise Suppressors*, AIAA Paper 79–0673, 1979.

[22] A. B. BAUER, *Jet Noise Suppression by Porous Plug Nozzles*, AIAA Paper 81–1993, 1981.

[23] A. B. BAUER, V. KIBENS, R. W. WLEZIEN, *Jet Noise Suppression by Porous Plug Nozzles*, NASA CR-3613, 1982.

[24] V. KIBENS, R. W. WLEZIEN, *Porous-Plug Flowfield Mechanisms for Reducing Supersonic Jet Noise*, AIAA Paper 83–0774, 1983.

[25] J. M. SEINER, T. D. NORUM, *Aerodynamic Aspects of Shock Containing Jet Plumes*, AIAA Paper 80–0965 (1980).

[26] H. K. TANNA, C. K. W. TAM, W. H. BROWN, *Shock Associated Noise Reduction from Inverted-Velocity-Profile Coannular Jet*, NASA CR-3454, 1981.

[27] R. H. CANTRELL, R. W. HART, *Interaction Between Sound and Flow in Acoustic Cavities: Mass, Momentum and Energy Considerations*, J.A.S.A. **36**, 697–706 (1984).

[28] C. L. MORFEY, *Acoustic Energy in Non-Uniform Flows*, J. Sound and Vib. **14**, 159–170 (1971).

[29] D. BECHERT, *Sound Sinks in Flows, a Real Possibility?*, Mechanics of Sound Generation in Flows, Joint Symposium Göttingen/Germany, August 28–31, Max Planck Institut für Stromungsforschung 1979.

[30] L. PEIZI, N. A. HALLIWELL, *Noise Control of Industrial Jets: An Investigation of Nozzle Performance*, Inter-Noise 83, Institute of Sound and Vibration Research, University of Southampton, Southampton, SO9 5NH.

Paper prepared for the XVII Fluid Mechanics Symposium, Polish Academy of Sciences, Warsaw, September 1985

ARCHIVES OF ACOUSTICS
11, 2, 137-150 (1986)

EXHAUST SILENCERS WITH MINIMUM POWER LOSS

F. B. SHENODA

Acoustic Laboratory, National Institute for Standards (Dokki, Cairo, Egypt)

Based on the principle of reflection free duct termination, silencers were designed. These silencers were applied to reduce the exhaust noise of internal combustion engines.

Acoustical and mechanical measurements have been taken as a function of engine speed for both full and partial load. For comparison, the same measurements have also been carried out on a conventional dissipative silencer of equal length, and also, for purposes of reference, on the exhaust pipe without a silencer.

A high level of acoustic absorption could be realized over a wide frequency range, without changing both the electric power and the fuel consumption of the applied engine, with respect to those for an untreated pipe.

Introduction

It is well known that internal combustion engines have uncomfortable noise. With increasing stringent noise legislation, manufacturs of internal combustion engines are faced with considerable difficulties in meeting these enacted requirements. Extensive investigations [1]–[3] have shown, that exhaust noise is one of the predominant noise sources of internal combustion engines.

In reducting exhaust noise, it seems, that the design of a suitable silencer is prefered to an attempt of lowering the noise generated at the source. The insertion of a silencer in the exhaust duct can attenuate the pressure pulsation, before they reach the surrounding atmosphere.

According to the mechanism of attenuation, silencers are divided into reactive silencers, dissipative silencers and acoustic resonators. A reactive silencer [4] provides an impedance mismatch for the acoustic energy travelling along the exhaust duct. This silencer type causes high backpressure and high pressure loss for the gas flow, which passes through it. As a result, a reactive silencer has a negative effect on the mechanical performance of the engine, on which it is mounted. The acoustical performance of a dissipative silencer is determined mainly by the presence of a sound absorbing material, which does

an efficient job of filtering high frequencies. An acousting resonator is incorporated to provide a relatively narrow band of attenuation [5]. Usually a low frequency resonator has an irregular shape and large volume, which is not always available.

Different types of silencers mentioned above may produce good noise results for a given system or application and produce poor results for another. Although many investigations [6]–[8] of exhaust silencing have been made, little was done to account for the behaviour of exhaust silencing with minimum power losses.

Exhaust silencers presented in this paper have been designed to be applied on internal combustion engines. The basic concept of these silencers is based on an earlier design made by the author [9]. This design is a reflection free duct termination, which gives a good matching impedance for an acoustic wave travelling along a pipe without change in its cross-section.

The designed silencers were mounted on a turbo — charged diesel engine. Acoustical and mechanical measurements have been assumed as a function of engine speed for both full and partial load. For comparison, the same measurements have been carried out on a conventional dissipative silencer of equal length, and also; for purposes of reference, on the exhaust pipe without a silencer.

Description of silencers

The basic concept of the construction uses a reflection free duct termination [10]–[13] by means of a gradually changing flow resistance along the walls of the exhaust pipe. This is realized by a suitable perforation of the pipe walls in combination with a sound absorbing material. The treatment covers 2 meters of pipe length.

Fig. 1 shows the construction principle of silencers designed in the present work, which are briefly described as follows:

Silencer S1

It consits of a straight pipe with a length ($l = 2$ m) and diameter ($d = 7$ cm) equal to the diameter of the common exhaust pipe of the applied engine. This pipe has a single slit at the pipe walls showing an exponential change in width $b(x)$ according to the relation

$$b(x) = b_0 e^{\delta x} \quad [\text{mm}], \tag{1}$$

where $b_0 = 1$ mm is the slit width at $x = 0$ and δ was chosen to be equal $= 0.00207$ to give a suitable width $b(x) = 63$ mm at the end of the treated pipe ($x = l = 2000$ mm). From the acoustics point of view, this variable slit can be replaced practically by a variable perforated area (more than 35% of the

slit area is perforated), which follows the above relation (1). An absorptive material is packed (in a half cylinder – shaped closed chamber of a 15 cm radius) with a constant density, so that it gives a flow resistance of about ϱc (the air characteristic impendance).

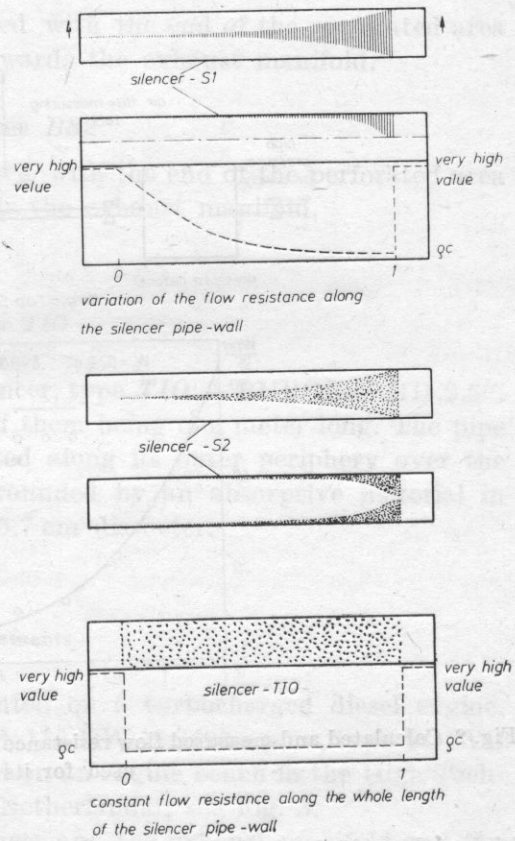

Fig. 1. Principal of construction of the measured silencers

Using this method (i.e.; constant flow resistance + variable perforated area), a gradually changing flow resistance according to the variation in width of the perforated area (relation (1)), can be obtained. To realize experimentally such a gradually changing flow resistance, a 2 m long plate of the same thickness as that of the pipe wall is variably perforated according to relation (1) and divided into ten equal parts (each 20 cm long) with the holes lying in the middle of an area equal to the cross section of a suitable holder (20×23.5 cm^2), made for a flow resistance measuring apparatus. Each perforated part acts as a face to the absorptive material which is packed at a depth of 15 cm, equal to that of the closed chamber of the silencer. The density of the absorptive material is chosen, so that it gives approximately the mean value of the flow resistance, which lies at the same length of a calculated curved. These measurements showed

that the densities of the absorptive material used with the different perforated parts are slightly different from each other. Consequently, a mean density was chosen to be used in the designed silencers. Fig. 2 shows the x-dependance of the calculated and measured flow resistance. The flow resistance has a very

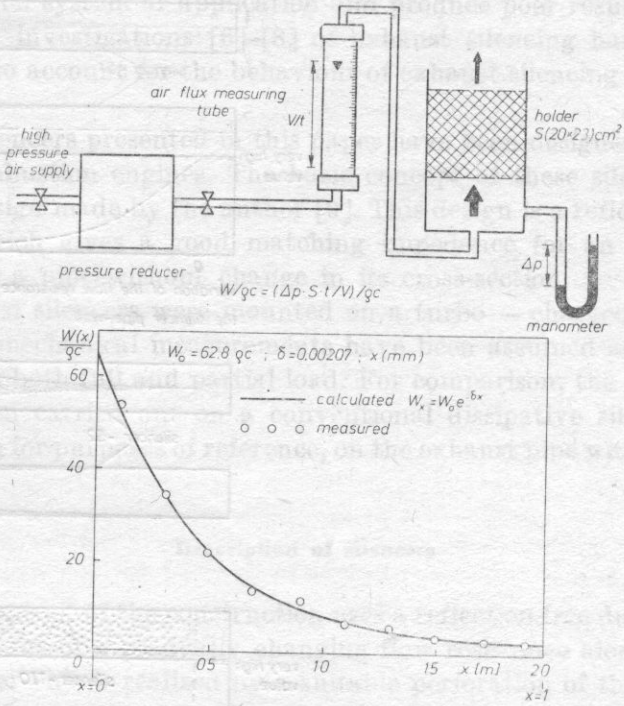

Fig. 2. Calculated and measured flow resistance along the silencer pipe-wall and the apparatus used for its measuring

high value (62.8 ϱc) at the side of the exhaust manifold and decreases exponentially to a definite value of about ϱc at the end of the treated pipe towards the tail-pipe.

Several kinds of absorptive materials have been used such as glass wool, mineral wool and steel wool in order to choose a suitable one with optimal effectiveness.

Silencer S2

It consists of two equally variable perforated areas at two opposite sides of the pipe walls (each perforated area is typical to hat of the silencer — *S1*). Each is covered with an absorbtive material packed in a half cylinder shaped

closed chamber (of 15 cm radius) with a constant density, so that it gives the same variation of the flow resistance along the pipe wall as that of *S1*.

The silencer *S2* is applied in two forms, namely:

1 Silencer *FS2*

In this case, the silencer *S2* was used with the end of the perforated area being smaller in width ($b_0 = 1$ mm) towards the exhaust manifold.

2 Silencer *BS2*

In this case, the silencer *S2* was used with the end of the perforated area being greater in width (63 mm) towards the exhaust manifold.

Silencer TIO

It is a conventional dissipative silencer, type *TIO* – BURGESS-HD 2.5″. It consists of two treated pipes, each of them being one meter long. The pipe is uniformly and continuously perforated along its outer periphery over the whole length. The treated pipe is surrounded by an absorptive material in a cylinder-shaped closed chamber of 15.7 cm diameter.

Measurements

The described silencers were mounted on a turbocharged diesel engine, 6 cylinder in line, cubic capacity 6.7 dm^3, 130 KW at 2400 r.p.m., type VOLVO TD70-B. The measurements were carried on an engine bench in the High Technical School Autotechnik in Apeldora (Netherlands); see Fig. 3.

The exhaust pipe between the silencer and the exhaust monifold and the tail-pipe is long enough, so that the measurements are made sufficiently far away from the engine and outside the engine room, in order to isolate the structural noise from the exhaust noise. The lengths of the exhaust and tail-pipes were kept constant in all measurements.

A BRUEL and KJAER (B & K) 1/2″-microphone covered with a wind shield, was located 40 cm from the exhaust exit, making an angle of 45° with the axis the tail-pipe, and about 3 m above the ground for normal incidence. Before each series of measurements, the sound level amplification was checked and adjusted using a standard noise source to ensure accurate measurements. The complete acoustic system was calibrated by using a piston-phone. The calibration signal was recorded on magnetic tape at the beginning and end of each series to provide a reference for the analysing system and in order to check the system stability.

The ambient temperature was controlled to keep it nearly the same in all measurements. In the present case, the microphone is very near the exit of the tail-pipe and accordingly the ambient temperature does not affect the recorded sound level. To avoid the effect of wind, the measurements were carried out

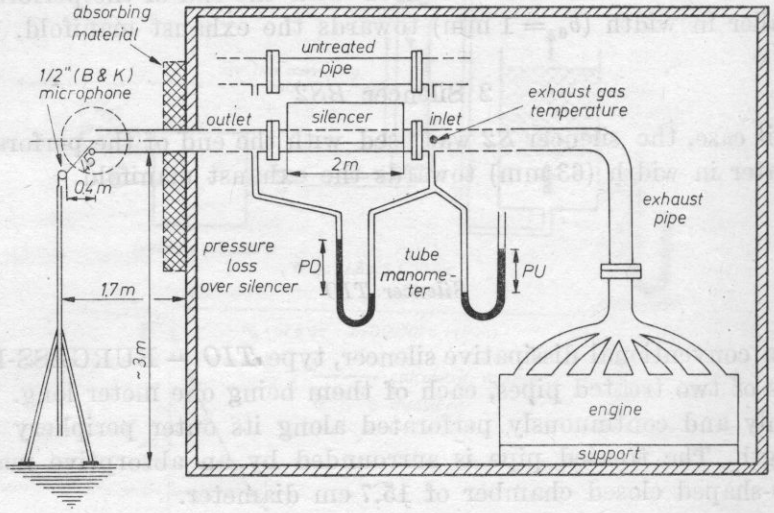

Fig. 3. The measuring arrangement and block diagram of an engine bench at the H.T.S. Autotechnik in Apeldoorn, Netherlands

when the wind speed was below 12 miles/hour. Humidity conditions and barometric pressure were also controlled during measurements. The sound absorption by the surface of the ground and the effect reflections from any surrounding objects were very small and could be neglected.

Prior to every test, the engine was warmed to an operating temperature. The engine speed n varied from 1400 to 2400 r.p.m. and was kept at ± 5 r.p.m. at each test. Measurements were carried out for partial load and full load of the engine every 200 r.p.m. increments. The exhaust gas temperature T °C at the front of the silencers under was measured by means of Cr—Ni thermocouple and thermoelectric-Digitime unit.

Acoustic measurement were carried out to determine the A-weighted sound pressure level L_A [dB (A)] at the microphone position and the insertion loss I_A, defined by the difference in sound level between the measurements with the untreated pipe and the pipe with silencer.

To study the influence of silencers on engine performance, several engine parameters have been measured as a function of engine speed and engine load. For purpose of reference, the same measurement have also been carried out on an untreated pipe with equivalent length (Fig. 3) to silencers.

The exhaust gas volume flow V [m³/s] in the silencer has been computed from the temperature T [K] and the pressure ($PU+1$ atm) values at the front of the silencer. The velocity of the exhaust gas G_v is determined from

$$G_v[\mathrm{m/s}] = \frac{4\dot{V}}{\pi d^2}, \tag{2}$$

where d is the diameter of the exhaust pipe.

The exhaust gas pressure difference PD over the silencer was also measured. The difference ΔPD with respect to the untreated pipe is the back pressure due to the silencer. The dissipated power W_d has been calculated from the relation:

$$W_d = \dot{V}PD \tag{3}$$

and accordingly the power loss due to the silencer ΔW_d can be determined from

$$\Delta W_d = W_d(\text{over silencer}) - W_d(\text{over untreated pipe}).$$

The effective electric power EP of the test engine was also measured

$$EP = \frac{F_m n \cdot 0.736}{1000} \quad [\mathrm{kW}], \tag{4}$$

where F_m is the mechanical power in Newtons and n is the rotational engine speed. Accordingly, EP with respect to the untreated pipe is computed:

$$EP = EP \text{ with silencer} - EP \text{ with untreated pipe.}$$

The fuel consumption F_c was determined from the relation:

$$F_c = \frac{V_f \varrho}{t} \quad [\mathrm{g/s}], \tag{5}$$

where t is time in seconds, in which a volume V_f of the fuel is consumed and ϱ is the density of the level (for gasolin $\varrho = 0.84\ \mathrm{kg/m^3}$). The change in fuel consumption $\Delta F_c(\%)$ due to the silencer with respect to that for the untreated pipe also determined,

$$\Delta F_c(\%) = 100 \frac{F_c \text{ with silencer} - F_c \text{ with untreated pipe}}{F_c \text{ with untreated pipe}}.$$

Results and discussion

Analysis of the exhaust noise of the applied engine was made at different engine speeds and for both partial load and full load, in order to show the characteristic frequency patterns of the unsilenced noise level. For example, Fig. 4 shows the unsilenced and silenced A-weighted third octave noise level at 2000 r. p.m. for partial load. At low frequency below 315 Hz the exhaust noise level

is a complex blend of its fundamental firing frequency and its higher harmonics as well as the resonance of all components of the exhaust system. From 315 Hz to about 630 Hz, the unsilected noise level increases slowly and afterwards a steady noise level can be stated till 5 kHz. In general, it was found, that the unsilected noise level depends on engine speed. At low engine speed, it depends strongly on engine load. The silenced noise levels obtained with both *FS2* and *BS2* silencers are similar and equal over most of the frequency range. From 250 Hz to 1000 Hz,

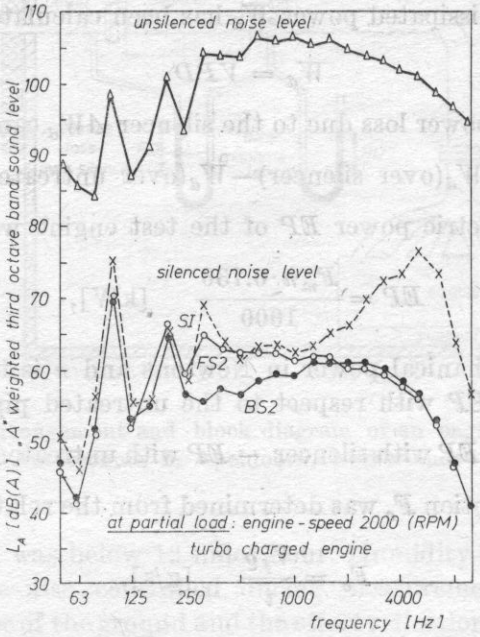

Fig. 4. *A*-weighted third octave band noise level

the silenced noise level obtained with the *BS2* silencer is 5 dB (*A*) in the mean lower than that obtained with the *FS2* silencer. The silenced noise level obtained with the *S1* silencer is slightly higher than those for *FS2* and *BS2* till 2000 Hz. Afterwards, the silenced noise level (for *S1*) becomes higher and this is due to the radiation effect, when the sound wave passes through the silencer unaffected by the absorbing material.

The effect of absorbing materials on the insertion loss I_A has been measured. For this purpose, absorptive materials such as glass wool, mineral wool and steel wool were used. Using these materials, the insertion loss I_A of the silencers *S1*, *FS2* and *BS2* were measured as a function of engine speed for both partial load and full load and compared with I_A measured with the conventional silencer *TIO* in the same conditions. Obtained results are represented in Fig. 5

from which the following results have been achieved:

1. In general, I_A depends on both engine speed and engine load and this may be due to different velocities of the exhaust gas at different operating conditions.

2. Glass wool, which is used only in silencer *S1*, is more effective than both

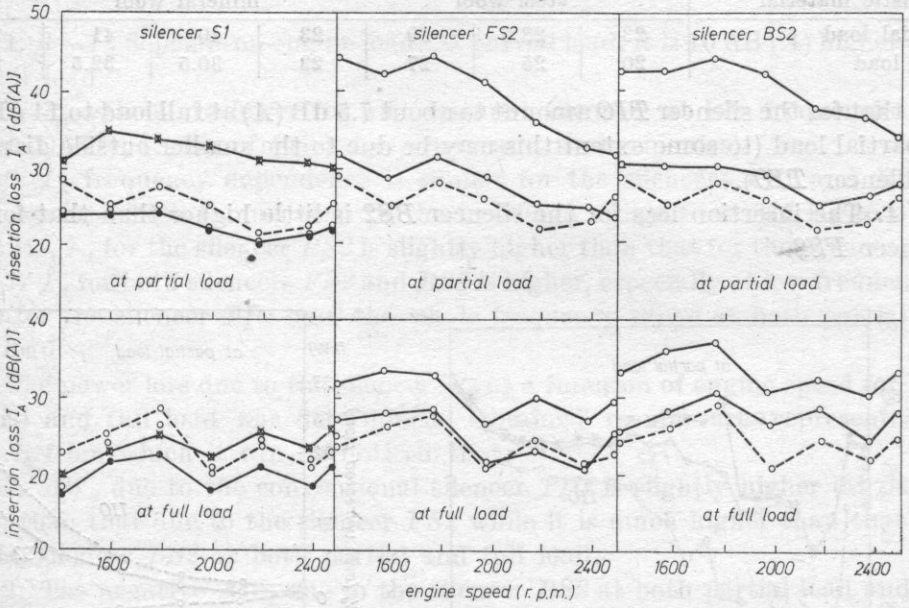

Fig. 5. *A*-weighted insertion loss I_A dB (*A*) against engine speed n (r.p.m.). x ——— x (glass wool), o ——— o (mineral wool), • ——— • (steel wool), o------o Silencer *TIO* (conventional silencer)

mineral wool and steel wool at partial load. At full load, I_A obtained with glass wool becomes lower and this is due to the strong variation of its acoustic performance as a function of gas temperature and local velocity effects. The little difference in I_A — values obtained with glass wool and mineral wool at full load seems to confirm this. For this reason glass wool is not preferable to be used in exhaust silencers.

3. The figure clearly shows, that mineral wool is more effective then steel wool.

To compare the effectiveness of these materials, the I_A — mean values (at different engine speeds) are determined and represented in Table 1.

From Table 1, it can be seen that:

1. The difference in insertion loss I_A between the single slit silencer *S1* and the double slit silencer *FS2* or (*BS2*) is very clear.

2. Mineral wool as absorptive material has a 10 dB (*A*) at partial load and a 5 dB (*A*) at full load higher insertion loss compared with that for steel wool.

3. If mineral wool is preferred as absorptive material for both silencers *FS2* and *BS2*, the difference in I_A — mean values for silencers *FS2* and *BS2*

Table 1

	I_A – mean value dB (*A*)						
Silencer	*S1*	*FS2*	*BS2*	*S1*	*FS2*	*BS2*	*TIO*
Acoustic material	steel wool			mineral wool			
Partial load	23	28.5	29	23	40	41	26
Full load	20	25	27	23	30.5	32.5	24

and that for the silencer *TIO* amount to about 7.5 dB (*A*) at full load to 14 dB (*A*) at partial load (to some extent this may be due to the smaller outside diameter of silencer *TIO*).

4. The insertion loss for the silencer *BS2* is little higher than that for the silencer *FS2*.

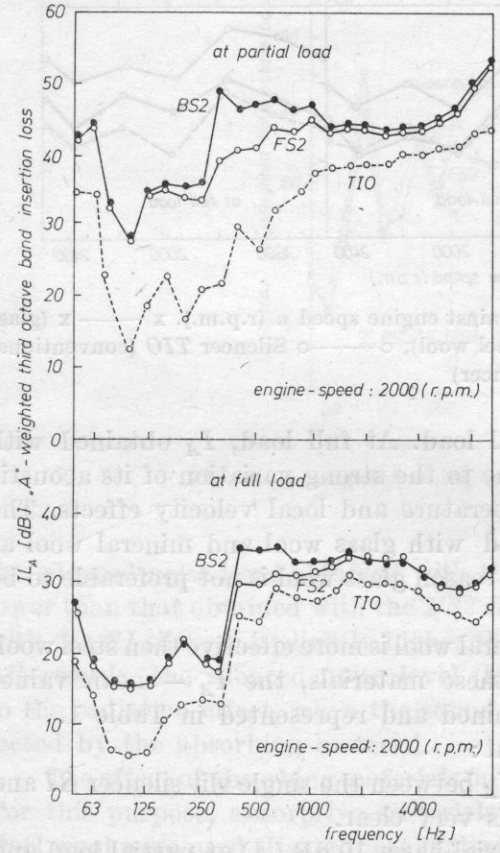

Fig. 6. *A*-weighted insertion loss I_A dB (*A*) against frequency *f* [Hz] mineral wool used as absorptive material

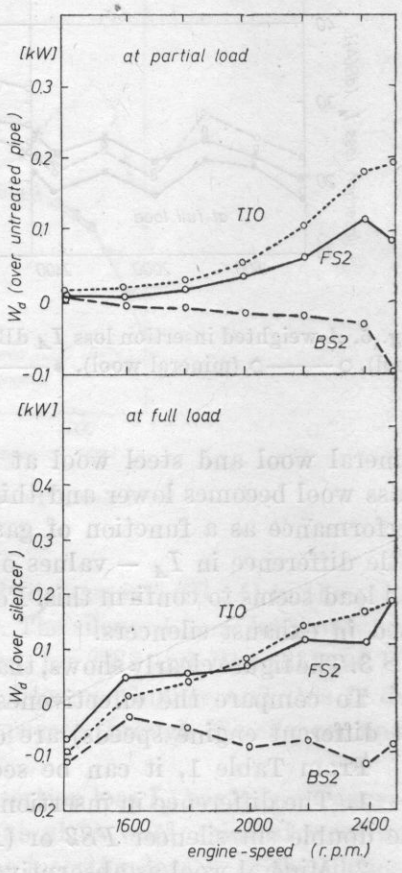

Fig. 7. Dissipative power loss ΔW_d [kW] against engine speed *n* (r.p.m.)

The frequency dependence of the *A*-weighted third octave band insertion loss I_A was measured for the silencers *FS2*, *BS2* (mineral wool as absorptive material) and silencer *TIO* at different engine speeds for both partial and full load. For example results obtained at engine speed 2000 r.p.m. for both partial load and full load are represented in Fig. 6. From the figure, it can be noticed, that:

1. $I - I_A$ depends on engine load. At partial load, it is 10 dB (*A*) higher than at full load.

2. I_A values are lower for all measured silencers at low frequencies (till about 315 Hz, region of firing frequency and its harmonics).

3. I_A frequency dependence is similar for the silencers *FS2* and *BS2* at both low and high frequencies. In the frequency range from 315 Hz to about 1000 Hz, I_A for the silencer *BS2* is slightly higher than that for the silencer *FS2*.

4. I_A for both silencers *FS2* and *BS2* is higher, especially at low frequencies, than for the silencer *TIO* over the whole frequency range at both partial and full load.

The power loss due to the silencer W_d as a function of engine speed for both partial and full load was determined. Obtained results are represented in Fig. 7, from which it can be noticed that:

1. ΔW_d due to the conventional silencer *TIO* is slightly higher (at partial load) than that due to the silencer *FS2* while it is much higher than that due to the silencer *BS2* at both partial and full load.

2. The negative ΔW_d due to the silencer *BS2* at both partial load and full load means that the power loss due to the silencer *BS2* is smaller than that due to the untreated pipe.

The measured and computed mechanical parameters obtained for the untreated pipe (2 m length and 7 cm diameter) as a reference are represented in Table 2 for both partial and full load. Table 3 gives the differences between these parameters for each silencer and for the untreated pipe, at different engine speeds for both partial and full load.

Table 2

	n (r.p.m.)	*PD* (cm H_2O)	*PU* (cm H_2O)	*Gv* [m/s]	*EP* [kW]
At partial load	1600	3.72	8.61	36.78	31.9
	1800	5.18	10.4	44.64	40.4
	2000	7.82	14.9	55.76	55.0
	2200	10.1	20.3	72.32	73.0
	2400	12.9	27.0	91.08	93.9
At full load	1600	7.82	15.8	66.08	98.3
	1800	11.2	21.9	77.75	109.1
	2000	14.7	25.4	89.89	119.7
	2200	16.9	30.5	99.83	125.6
	2400	20.2	39.9	110.3	129.6

In Table 3: Δ = measured parameter with silencer − measured parameter with untreated pipe.

Data represented in Table 3 leads to the following results:

1. The back pressure due to the *PD* silencers depends on both engine speed and engine load. At partial load, it increases for both silencers *FS2* and *TIO*, at increasing engine speed. At full load, it is slightly lower than at partial load at the same engine speed. The back pressure due to the silencer *BS2* is approximately independent from engine speed at partial load, while it decreases with

Table 3

	n (r.p.m)	ΔPD [cm H_2O]			ΔPU [cm H_2O]			ΔGv [m/s]			ΔEP [kW]			$\Delta\bar{\varepsilon}$ [%]		
		FS2	BS2	TIO	FS2	BS2	TIO	FS2	BS2	TIO	FS2	BS2	TIO	FS2	BS2	TIO
at partial load	1600	0.9	-0.1	1.2	-0.2	-1.4	0.2	-1.8	-1.3	-1.9	-0.2	-0.1	-0.1	-0.3	0.0	0.1
	1800	1.4	-0.2	1.6	1.3	-0.6	0.0	1.6	-0.8	-1.9	-0.1	-0.1	00.1	0.7	0.1	-0.2
	2000	1.8	-0.8	2.8	0.9	-1.6	2.1	-0.4	-0.3	-1.0	00.0	00.0	00.2	0.2	0.8	1.8
	2200	2.4	-0.5	4.2	0.2	-1.3	2.4	-1.5	-1.8	-2.5	00.2	00.0	00.2	0.5	-1.3	1.3
	2400	3.6	-0.5	6.0	0.2	-3.5	3.1	-1.1	-1.3	-4.5	-2.3	-2.3	-1.9	-0.8	0.2	0.4
	mean	1.7	-0.4	3.2	0.5	-1.7	1.6	-0.6	-1.1	-2.4	-0.5	-0.5	-0.3	0.06	0.04	0.7
at full load	1600	2.0	-0.9	1.0	0.2	-1.1	-0.3	0.9	-0.3	-2.0	-0.8	-2.4	-1.7	0.9	-1.0	0.6
	1800	1.5	-1.5	1.7	-0.4	-2.7	-0.4	2.5	2.3	-0.7	-0.2	-0.6	-0.6	-0.2	0.0	0.2
	2000	1.2	-2.7	2.2	1.6	-1.5	2.0	3.4	1.7	-1.5	-1.1	-2.1	-2.3	0.9	0.7	0.7
	2200	2.4	-2.4	3.9	1.4	-1.6	2.8	3.7	4.0	-1.2	-0.8	-1.4	-1.7	-0.4	1.4	0.9
	2400	1.5	-3.5	4.2	-3.7	-7.4	-0.4	5.3	4.4	-1.2	-1.4	-2.3	-2.7	1.4	1.1	1.2
	mean	1.7	-2.2	2.6	-0.2	-2.9	0.7	3.2	2.4	-1.3	-0.9	-1.8	-1.8	0.5	0.4	0.7

engine speed at full load. The negative ΔPD due for the silencer *BS2* means that the pressure difference over the silencer *BS2* is lower than over an untreated pipe with equivalent length; what is at this moment unexplained. The back pressure ΔPD due to the conventional silencer *TIO* is clearly higher than that due to both silencers *FS2* and *BS2* at all engine speeds, and for both partial and full load.

2. The pressure of the exhaust gas at the front of the silencers (PU + 1 atm) with respect to that for the untreated pipe ΔPU behaves differently at different engine speeds and different loads. The negative sign means that the pressure of the exhaust gas at the front of the silencer is lower than that at the front of the untreated pipe.

3. At partial load, the velocity of the exhaust gas *GV* is lower for all silencers than for the untreated pipe. The lowest *GV* values noticed are those for the silencer *TIO*. At full load, it is lower than for the untreated pipe in case of the silencer *TIO*, but the difference is somewhat smaller than at partial load. In case of the silencers *FS2* and *BS2*, it is higher than for the untreated pipe. It increases with increasing engine speed.

4. The electric power *EP* [kW] of the engine is slightly lower with the silencers than for the untreated pipe. It is lower than for an untreated pipe by about 0.7% in the mean at partial load and about 1.5% for the *TIO* and *BS2* silencers while it is only 0.77% lower for the *FS2* silencer in the mean.

5. The fuel consumption F_c is only silightly different from that of the untreated pipe.

Conclusions

Measurements and results lead to the following conclusions:

1. At a constant flow resistance, mineral wool as absorptive material is more effective than steel wool.

2. The insertion loss of a dissipative silencer becomes lower at both high engine speed and full load. This may be due to higher velocity at these two conditions.

3. A high level of acoustic absorption could be realized over a wide frequency range without

a) changing the electric power of the applied engine

b) changing the fuel consumption

with respect to an untreated pipe.

4. The measured low back-pressure due to the designed silencers *FS2* and *BS2* compared to those measured for the conventional *TIO* and the untreated pipe, leads to a minimum power loss of the exhaust gas. In case of silencer *BS2*, a power gain noticed over the whole range of engine speed and for both partial and full load. As a result, the characteristic of the engine, on which those silencers are mounted does not alter and the combustion process can show improvement.

Acknowledgements

The silencers described here are designed and tested by the author in Cairo at the National Institute for Standards, by means of a study financed by the Dutch Ministry of Public Health and Environment. Measurements were taken for this silencer after mounting it on the exhaust system of an engine bench in the High Technical School (H.T.S.) Autotechnik in Apeldoorn (Netherlands). The author wishes to thank Dr Ing. MEYER and Dipl. Ing. WAL at M + P Akoestische Adviseurs Amstelveen, Netherlands for their help and valuable discussions.

References

[1] T. PRIEDE, *Some studies into origins of automobile diesel engine*, 11th Int. Automobile Technischen Kongress, Juni 1966, Munich, F.I.S.T.A., Paper C 12.

[2] T. PRIEDE, *Relation between form of cylinder pressure diagram and noise in diesel engines*, Proc. Inst. Mech. Engrs. (A. D.) 1, 63–77 (1961).

[3] E. UNGAR, D. ROSS, *Vibration and noise due to piston slap in reciprocating machinery*, J. Sound Vib., **2**, 2, 132–146 (1955).
[4] L. L. BERANEK, *Noise and Vibration Control*, McGraw-Hill Book Company, New York 1960, Chapter 12.
[5] J. W. SULLIVAN, M. J. CROCKER, J. Acoust. Soc. Am., **68**, 1, 207 (1978).
[6] C. D. HAYNES, E. L. KELL, *Engine exhaust silencing, first report*, M.I.R.A. Report No. 1964/3, Nuneaton 1964.
[7] C. D. HAYNES, *Second Report*, Report No 1965/2 Nuneaton 1965.
[8] C. D. HAYNES, *Third Report*, No. 1965/12, Nuneaton 1965.
[9] F. B. SHENODA, *Reflexionsarme Abschlüsse für durchströmte Kanäle*, VDI-Akustik und Schwingungstechnik, Stuttgart, DAGA 269 (1972).
[10] F. B. SHENODA, *Reflexionsarme Abschlüsse für durchströmte Kanäle*, Dissertation T. U. Berlin (West) 1973.
[11] F. B. SHENODA, H. ISING, *Schalldompfer für Rennsportwagen mit leistungsteigernder Wirkung Kampf*, dem Lärm 25, 123 (1978).
[12] F. B. SHENODA, H. H. Von der WAL, A. Von MEIER, *Dissipative silencers with minimized back-pressure*, Inter. Noise, Amsterdam 1981.
[13] F. B. SHENODA, *A new silencer with good matching performance for air ducts and exhaust systems*, Acoustica, **50**, 338–341 (1982).

Received on September 19, 1985

ARCHIVES OF ACOUSTICS
11, 2, 151-162 (1986)

WAVE PROPAGATION ALONG AN EDGE OF A SOLID

WINCENTY PAJEWSKI, MAREK SZALEWSKI, PAWEŁ KIEŁCZYŃSKI

Institute of Fundamental Technological Research, Polish Academy of Sciences
(00-049 Warsaw, ul. Świętokrzyska 21)

Investigation results of waves propagating along edges of isotropic and anisotropic bodies are presented in this paper. Also methods of producing wave-guides, generation methods of line waves, the influence of anisotropy on distribution of vibrations and applications of these waves in the acoustic convolution process are discussed.

1. Introduction

Beside volume and surface waves also waves propagating along the intersection edges of planes occur in limited solid bodies. These waves are called edge or line waves. They have three components of particle motion and their amplitude decreases with the distance from the edge of both planes and inside the material. There are two fundamental line wave modes in an isotropic body, differing in the deformation manner. In an anisotropic body the deformation manner of an egde when the wave is propagating is more complex and pure modes do not occur.

Wave-guides of edge waves are characterized by high power density due to strong wave energy concentration. Acoustic power is concentrated near the edge in a range of a section of the order of λ^2.

Making a sharp edge is the main difficulty in producing such wave-guides. Difficulties in obtaining edges with an adequate quality limit the frequency range, in which line wave wave-guides can be applied. In the frequency range up to 200 MHz, adequatly sharp edges are obtained with the utilization of the phenomenon of cleavage. Edges used in the range up to 100 MHz are obtained with the application of a diamond saw with a high rotational speed (about 20 000 r.p.m.) [1].

2. Methods of generating line waves

There are several methods of generating line waves. One of them consists in the transformation of a RAYLEIGH surface wave into a line wave. The transformation occurs when the surface wave incides under an adequate angle onto the edge. It was experimentally proved that in case of glass, at the incidence angle of 75°, about 60% of the energy of the incident wave is converted into the energy of a line wave. Therefore, this is a quite efficient generation process.

Also plate piezoelectric transducers located next to the edge, directly on the wave-guide can be applied in line wave generation (Fig. 1). Transducers with adequate vibrations generate a line wave of a definite type, depending on the location of transducers in terms of the plane of symmetry of the dihedral angle.

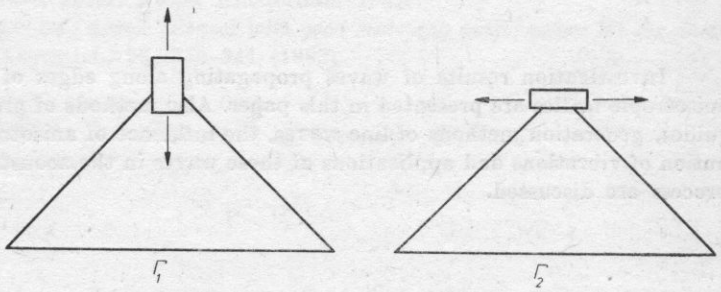

Fig. 1. Generation of line waves with plate transducers

Line waves can be also generated with the application of a interdigital, sawtooth or a single-phase electrode array transducer, located near the edge. In this case an adequate electromechanic coupling must occur in order to generate a wave. This generation method can be rationalised by applying a modified multistrip coupler (MSC), which matches the phase of the generated dy the transducer Rayleigh wave with the line wave [1].

3. Propagation of a line wave on an isotropic body

The symmetric mode Γ_1, and antisymmetric mode, Γ_2, are the basic modes of line waves on an isotropic body. In the Γ_1 mode deformations on the edge are located on the plane of symmetry of the dihedral angle and deformations on planes forming this angle are symmetric (Fig. 2a). In the Γ_2 mode, deformations on the edge are perpendicular to the plane of symmetry and deformations on planes forming the angle are antisymmertic in respect to the plane of symmetry of the dihedral angle (Fig. 2b). Theoretical analysis proves that the Γ_1 mode is a dispersive mode, while Γ_2 is a non-dispersive mode. Experiments confirm this conclusion.

The propagation of line waves along the edges of glass samples has been investigated experimentally. Fig. 3 and 4 present oscillograms of Γ_1 and Γ_2 wave pulses on glass; excitation with *PZT* plate transducers, frequency 4 MHz. Pressure exerted on the edge caused signal attenuation.

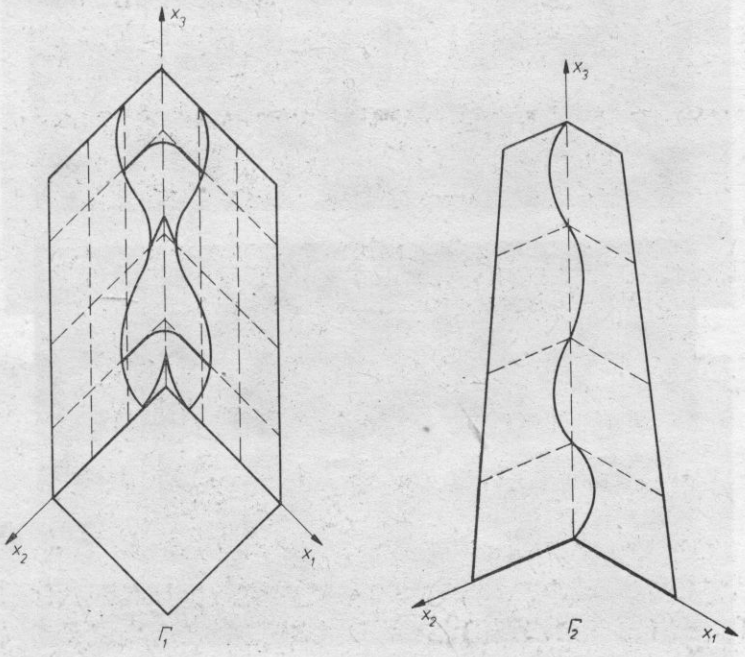

Fig. 2. Line waves on an isotropic body. a – symmetric mode Γ_1, b – antisymmetric mode Γ_2

Both modes can propagate along curved edges. Fig. 5 presents pulses of the Γ_2 wave, propagating along the edge of a glass half-disc with a 30 mm radius.

4. Propagation of a line wave on an anisotropic body

The deformation of the edge during wave propagation is more complicated in an anisotropic body. Due to the anisotropy, line waves are only more or less close to the Γ_1 or Γ_2 mode in dependence on the prevailing deformation – parallel or perpendicular to the plane of symmetry of the dihedral angle.

Investigations were carried out on quartz rods placed along the X axis with Y and Z planes and on rods placed along the Y axis with X and Z planes. Conducted calculations [2] have led to the determination of the particle vibration components in the Y and Z or X and Z planes, respectively. Fig. 6 presents relative amplitudes of vibrations for quartz rods X in terms of the distance from the edge for two directions. The calculated mode approximates the symmetric

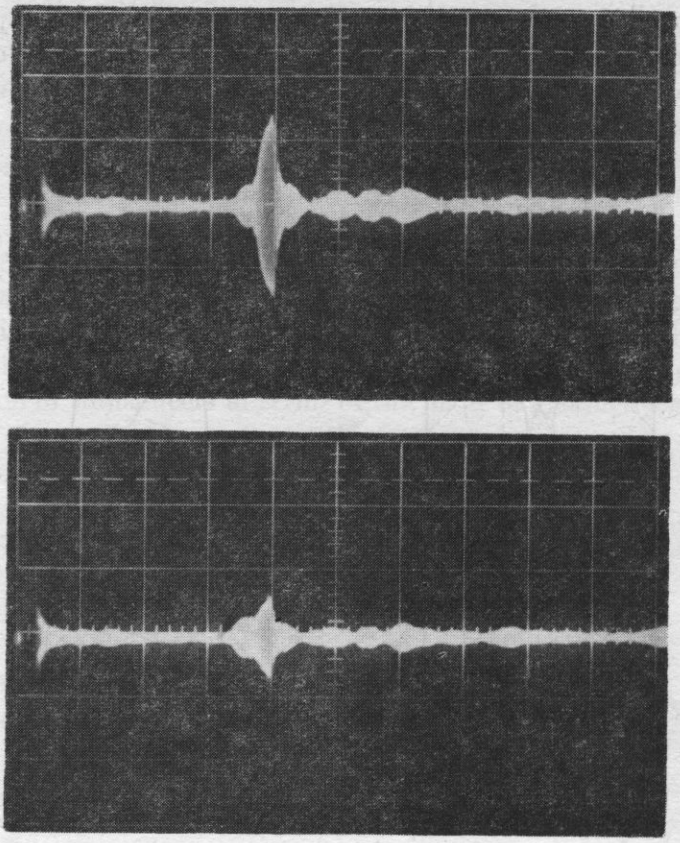

Fig. 3. Wave Γ_1 on glass. a – free surfaces, b – pressure on the edge

mode Γ_1, because the resultant vector of particle motion on the edge is inclined to the bisector of the dihedral angle at an angle of 18°. In this case also a mode approximating the Γ_2 mode is generated. The angle between the resultant vector of particle motion and the bisector of the dihedral angle is equal 66° for this mode. Relative amplitudes of the x, y, z components of a line wave in a quartz rod Y are shown in Fig. 7. The calculated angle between the bisector of the dihedral angle and the resultant vector of particle motion on the edge equals 63°; the measured angle is 69°. Therefore, in this case the wave approximates the Γ_2 mode. Similar calculations and measurements have been also conducted for ST quartz. Fig. 8 presents the calculated vibration distribution. Line waves in quartz samples have been generated by SiO_2 plate transducers (Y-cut) which work on the fundamental frequency and on harmonics [2].

Experiments were also conducted on lithium niobate wave-guides, where the edge of intersection of the cleavage plane and the turned Y plane, inclined to the cleavage plane at an angle of 84°54′, was utilized; direction of propagation X. The cleavage plane (012) is positioned along the X axis at an angle of

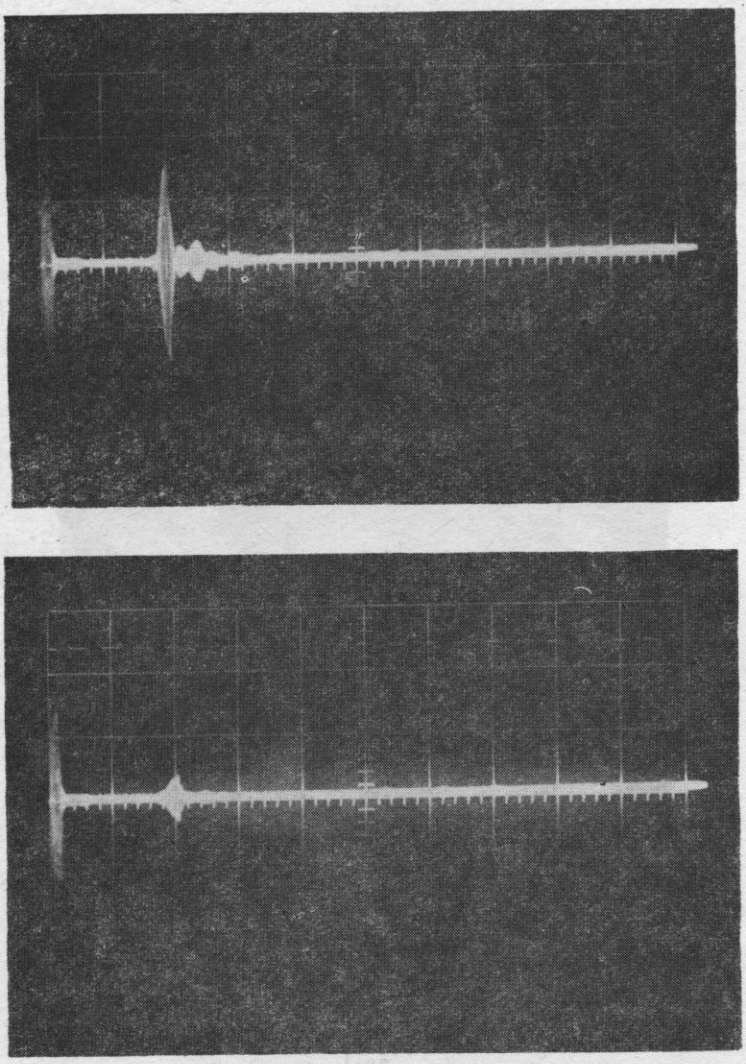

Fig. 4. Wave Γ_2 on glass. a – free surfaces, b – pressure on the edge

57°14′ to the Y axis [3]. Waves were excited by $LiNbO_3$ plate transducers (Y 163-cut); fundamental frequency 10 MHz. Fig. 9 presents oscillograms of signals for a wave approximating the Γ_2 mode. For this orientation of $LiNbO_3$ the resultant vector of particle motion on the edge is almost perpendicular to the bisector of the dihedral angle and the deviation equals 4°30′. Photographs show the volume wave pulse preceding the line wave pulse. This pulse comes from the transverse volume wave, which propagates in the direction X. These pulses can be separated by extending the sample, due to the velocity difference of the volume (about 4300 m/s) and line wave (about 3500 m/s). Lithium

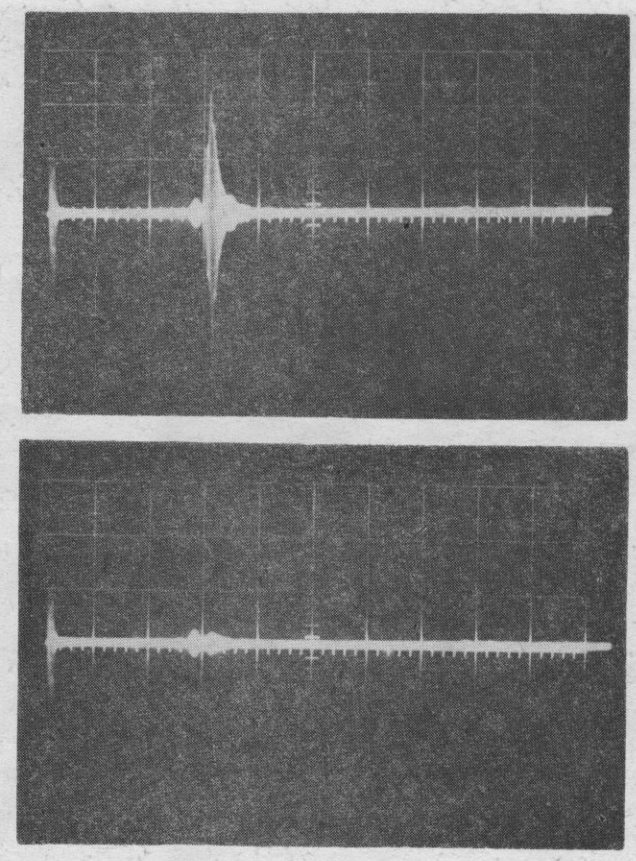

Fig. 5. Line wave on a glass semi-disc, 4 MHz. a — free surfaces, b — pressure on the edge

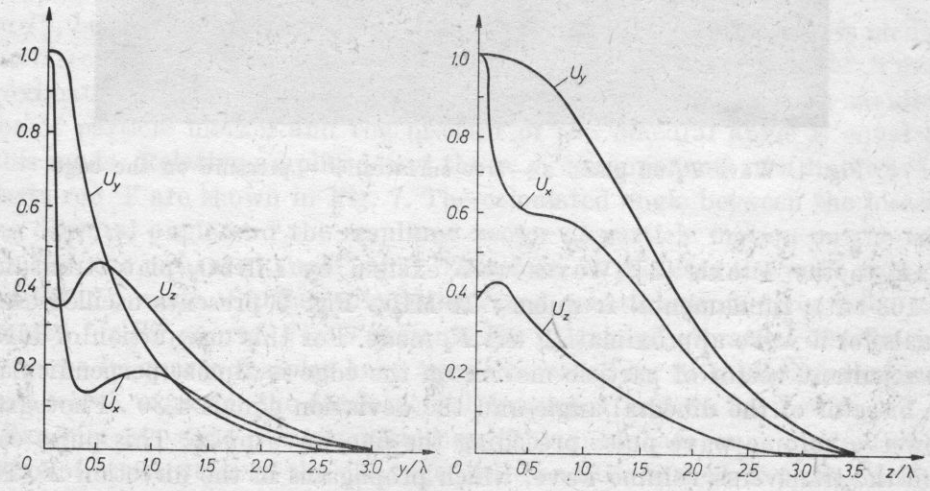

Fig. 6. Relative amplitudes of vibration components of a line wave in terms of distance l/λ from the edge, SiO_2, direction of propagation X

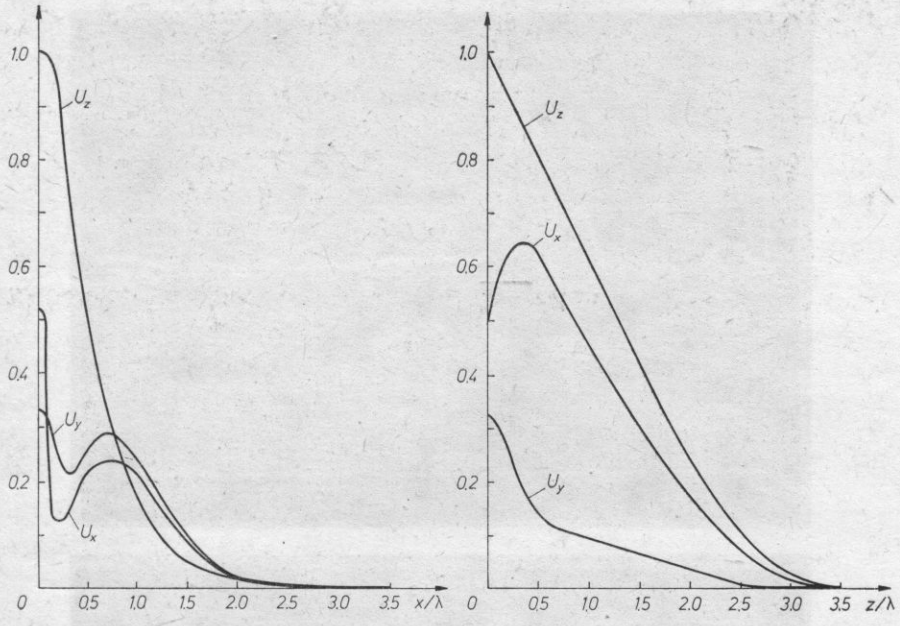

Fig. 7. Relative amplitudes of vibration components of a line wave in terms of distance l/λ from the edge, SiO_2, direction of propagation Y

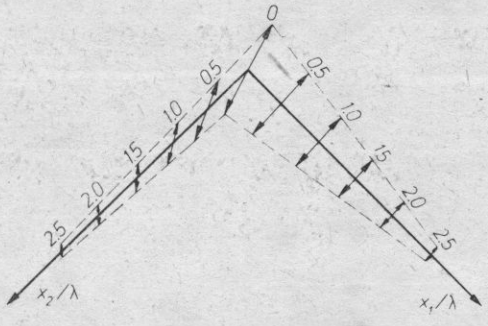

Fig. 8. Distribution of vibrations for a line wave on ST quartz sample, x_1 – distance from the edge on plane ST

niobate with edges on the intersection of the X and Y planes (direction of propagation Z), were also investigated. Fig. 10 presents oscillograph records for a wave approximating the Γ_2 mode; frequency 9.6 MHz.

5. Convolution with line waves

Convolution systems have found application in signal processing. They make it possible to obtain the convolution of two input signals. If two signals, $V_1(t)$ and $V_2(t)$, are supplied to the system, then on the output we receive

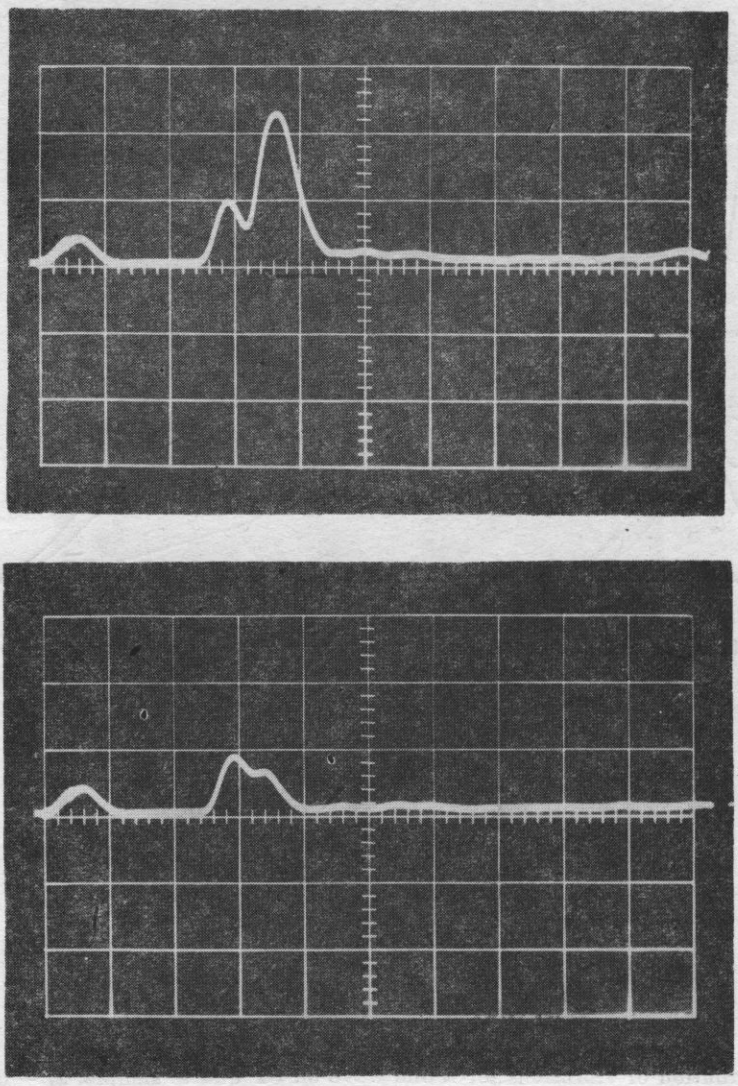

Fig. 9. Line wave on a $LiNbO_3$ sample with an edge formed by the intersection of the cleavage plane and turned plane Y. a – free surfaces, b – pressure on the edge

a signal

$$V_3(t) = A \int_{-\infty}^{+\infty} V_1(\tau)\, V_2(2t-\tau)\, d\tau. \quad . \tag{1}$$

When signals $V_1(t)$ and $V_2(t)$ are identical, rectangular pulses with a f_1 carrier frequency, then the pulse on the output has a triangular envelope and $2f_1$ carrier frequency. The output signal pedestal width and the width of input pulses are equal. A time scale change occurs due to the opposite propagation

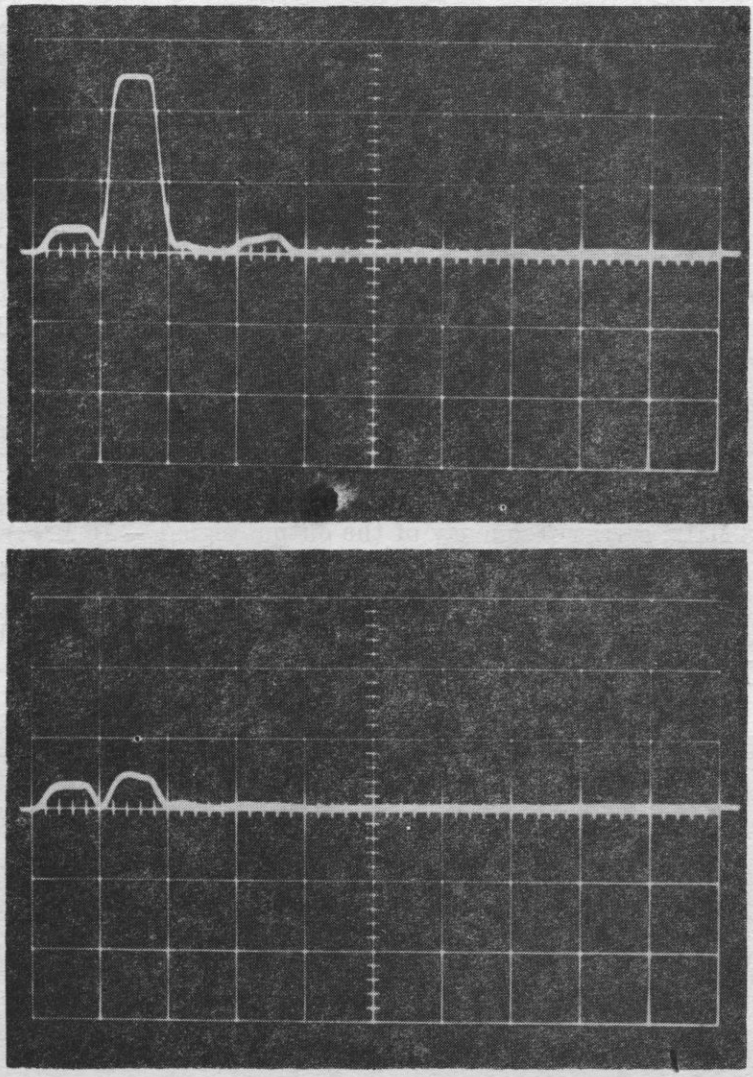

Fig. 10. Line wave on a $LiNbO_3$ sample with an edge formed by the intersection of planes X and Y. a – free surfaces, b – pressure on the edge

direction of waves. The output voltage is proportional to the input signal width and acoustic power per unit width of the wave beam.

Line waves are strongly confined near the edge. Nonlinear effects can be observed due to high power density. The power density of 600 W/mm² can be obtained for $LiNbO_3$ at a frequency of approximately 200 MHz. In similar conditions, the power density of about 20 W/mm² is obtained in $LiNbO_3$ for a Rayleigh wave. The lack of dispersion (mode Γ_2) and diffraction effect, which cause signal distorsion and efficiency decrease in convolution systems with Rayleigh waves, is an additional advantage of line waves [4]. Dispersion also

limits the possibility of applying thin-layer wave-guides, which focus the beam of surface waves, in convolution systems [5].

Non-linear interactions of two line waves of the Γ_2 mode, which propagate opposite each other, lead to the formation of a surface potential, symmetric in relation to the bisector of the dihedral angle [6]. In such a case symmetrically arranged in relation to the edge receiving electrodes can not be applied. The convolution electrode has to be situated at an approximately λ distance from the edge; the second surface in entirely metalized.

Convolution systems were observed in *PZT* ceramics and in lithium niobate. The lateral faces of the edge and the direction of the edge for $LiNbO_3$ were selected as follows: *Y*-128° and natural cleavage planes, direction of propagation *X*; *Y* and *X* planes, direction of propagation *Z*. Convolution electrodes were located on the *Y*-128° and *Y* plane, respectively. Fig. 11 presents oscillograms of signals of a Γ_2 type line wave on a *PZT* sample; frequency 8.75 MHz. Convolution signals for a line wave on *PZT* ceramics (carrier frequency of input signals — 8 MHz, carrier frequency of the output signal — 16 MHz) are shown in Fig. 12. Fig. 13 presents a signal obtained from the convolution of two double signals — top oscillogram, bottom oscillogram — the shape of the input signal. A signal convolution was obtained also for line wave on $LiNbO_3$ for both orientations [7].

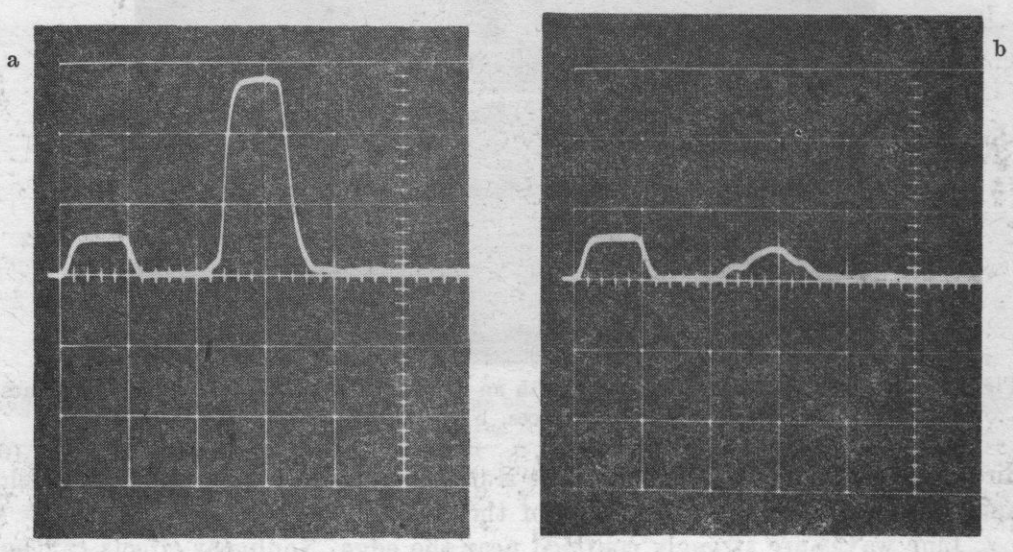

Fig. 11. Line wave on *PZT* ceramics. a — free surfaces, b — pressure on the edge

Investigations have been performed in a carrier frequency range of input signals from 8 to 12 MHz.

An increase of frequency would lead to a stronger wave concentration and an increase of the output signal at the same level of input power. The bilinear

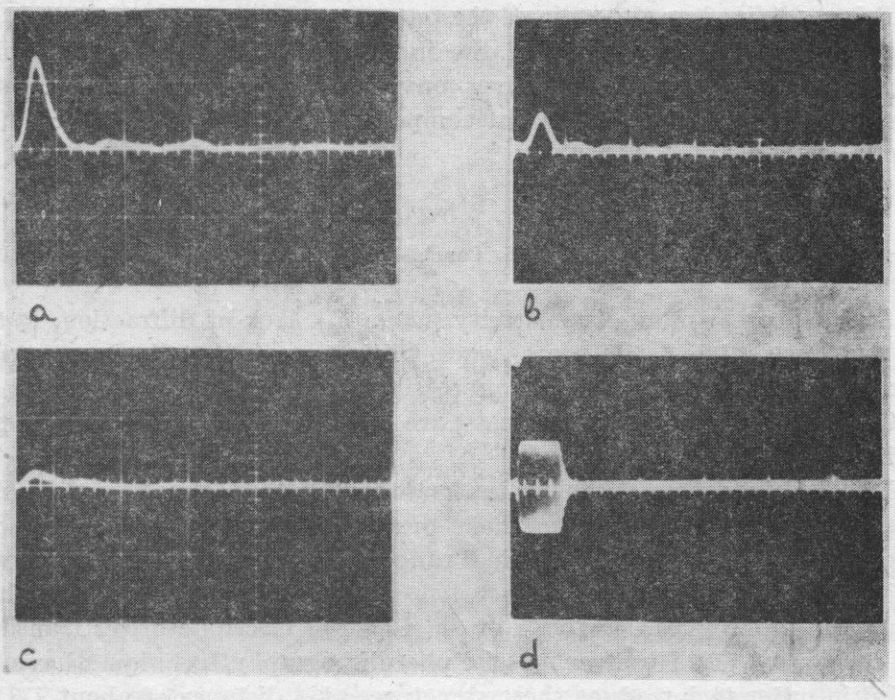

Fig. 12. Signals in the acoustic convolution, line waves on *PZT* ceramics. a — width of input pulse, 4 μs, b — width of input pulse, 3 μs, c — pressure on the edge, d — shape of input signal

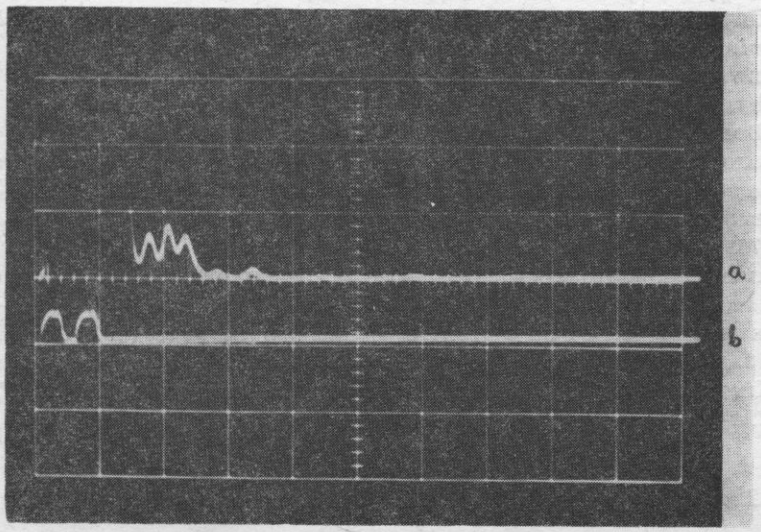

Fig. 13. Convolution of two double pulses, line waves on *PZT* ceramics. a — output signal, 16 MHz, b — input signal, 8 MHz

coefficient, defined as the ratio of the output power and the product of input acoustic powers, is a measure of the interaction efficiency in a convolution system. The application of line waves convolution systems subjected to optimization can give a bilinear coefficient comparable to the coefficient obtained in a diode system [8].

6. Conclusions

Such features as non-dispersitivity (mode Γ_2), lack of diffraction, low propagation losses and strong beam concentration prove that line waves can be utilized in delay lines and signal processing systems. Non-linear effects (convolution of signals, parametric effects) are easily obtainable due to high power density [6].

It is decisive for practical application to master the technology of producing sufficiently sharp edges and methods of effective generation of line waves. Our experiments have shown that in a range up to several tens MHz line waves can be easily and effectively generated with plate transducers. For higher frequencies interdigital, sawtooth or single-phase electrode array transducers have to be used [1]. However, special photolithography techniques have to be applied in order to introduce these structures at a distance of about $\lambda/3$ from the edge.

References

[1] R. L. Miller, K. J. Anderson, E. G. Bogus, J. Bodett, *Recent progress in line acoustic wave devices*, 1982 IEEE Ultrasonics Symp. Proc., pp. 385–388.

[2] W. Pajewski, M. Szalewski, P. Kiełczyński, *Ondes acoustiques sur l'arête d'un solide*, Rev. Phys. Appl., to be published.

[3] W. L. Bond, *Crystal Technology*, Wiley, New York 1976.

[4] O. P. Baiocchi, I. M. Mason, *The influence of diffraction and dispersion on the fidelity of degenerate convolution*, IEEE Trans. Sonics and Ultrason., SU-**22**, 5, 347–354 (1975).

[5] P. Defranould, C. Maerfeld, *A SAW planar piezoelectric convolver*, Proc. IEEE, **64**, 5, 748–753 (1976).

[6] R. L. Adler, M. J. Hoskins, S. Datta, B. J. Hunsinger, Unusual parametric effects on line acoustic waves, IEEE Trans. Sonics and Ultrason., SU-**26**, 5, 345–347 (1979).

[7] W. Pajewski, M. Szalewski, *Acoustic convolution on edge waves* (in Polish), Elektronika, no 11–12, 9–11 (1985).

[8] G. S. Kino, Acoustoelectric interaction in acoustic-surface-wave devices, Proc. IEEE, **64**, 5, 724–748 (1976).

Received on November 30, 1984; revised version on April 21, 1986

ARCHIVES OF ACOUSTICS
11, 2, 163-170 (1986)

ACOUSTIC PROPERTIES OF TWO PARALLEL ELASTIC PLATES

ZBIGNIEW WESOŁOWSKI

Institute of Fundamental Technological Research Polish Academy of Sciences
(00-049 Warsaw, ul. Świętokrzyska 21)

Two parallel elastic plates are submerget in gas. A plane sinusoidal wave propagates perpendicularily to the plates. Such a system models a paned window. In order to present the physical phenomenon without excessively developing the mathematical description, the plates are modelled by rigid plane screens suspended elastically. The displacement of the screen is proportional to the force, and the suspension rigidity is proportional to the third power of the screen thickness (as in a bended plate).

On the basis of motion equations and continuity equations, the displacement behind both plates is determined. The attenuation coefficient depends on the frequency, plate thickness and their spacing. Plates with different thicknesses give a better characteristic than those with identical thicknesses. The attenuation coefficient does not depend on the sequence of plates and it has two maximum in the acoustical range. Frequencies corresponding to them differ from the frequencies of free vibrations of the plates and the cavity.

1. Model

We are analysing two simple-supported elastic plates submerged in gas (Fig. 1). These plates have equal moduli of elasticity but different thicknesses. A plane sinusoidal wave incides perpendicularily onto the plates and passes through them undergoing attenuation. The described system is a model of a window closed by two panels. This paper is aimed at the determination of the resulting displacement field with special pressure put to the analysis of the influence of plate thickness, their distance and sequence on this field.

Let us begin with the analysis of a single circular plate. Displacement, w (in the direction of the x-axis, Fig. 1) satisfies equation [1]

$$\frac{\partial^4 w}{\partial r^4} + C_1 \frac{\partial^2 w}{\partial r^2} + q = C_2 \frac{\partial^2 w}{\partial t^2}, \tag{1}$$

where q is the external load and r is the distance from the centre.

Constant coefficients of the equation were denoted by C_1, C_2. The load q is induced by a known incident wave and by the reflected and refracted waves of unknown intensities dependent (on plane $x = 0$) only on r, $A_r(r)$, $A_t(r)$. Due to motion, every plate surface element is a source of a spherical wave which loads all plate surface elements. Therefore, the load q in point r can be expressed as integrals, over the whole plate, of the function $(A_r(r) - A_t(r))$. Substituting them in equation (1) we obtain an integral-differential equation for quantities: $w(r, t)$, $A_r(r)$, $A_t(r)$. Other, unmentioned here, equations are displacement and velocity continuity equations. Such a system of equations can not be solved analytically. Obviously, the situation for a rectangular plate or a system of plates is even more complex. For this reason we are limiting our investigations to an analysis of a simplified model presented in Fig. 2.

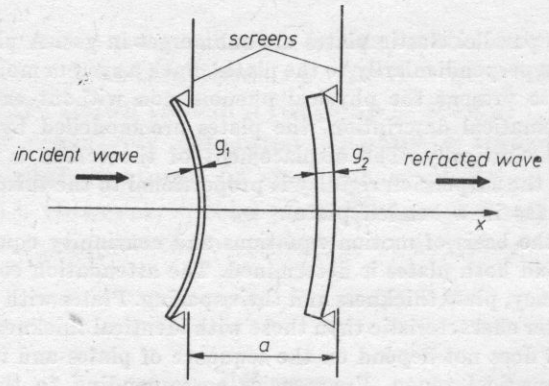

Fig. 1. Analyzed system

Two ridig diaphragms of g_1 and g_2 thicknesses are suspended elastically at a distance, a, and can move in the direction of the x-axis. In order to model a system of plates in the best possible way we assume that suspension rigidities, Q_1 and Q_2, are proportional to the third power of the diaphragm thickness, $Q_1 \approx g_1^3$, $Q_2 \approx g_1^3$ (because the rigidity of a bended plate is proportional to the third power of its thickness). Masses of a unit diaphragm surface, m_1 and m_2, are proportional to their thicknesses: $m_1 \approx g_1$, $m_2 \approx g_2$. It can be expected that the attenuation properties of the system presented in Fig. 2 have a characteristic approximating the characteristic of attenuation properties of the system presented in Fig. 1.

2. Acoustical properties of a single diaphragm

We are analysis a diaphragm of a g-thickness placed at $x = \bar{x}$. A plane sinusoidal wave, moving to the right, incides onto the diaphragm (Fig. 3):

$$A_i e^{i\omega(t-x/c)}$$

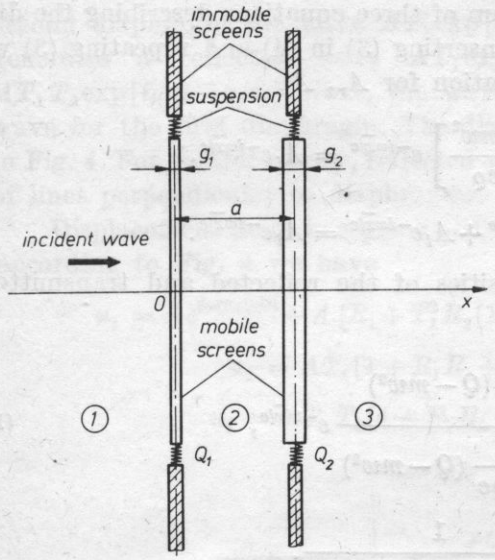

Fig. 2. Substitute model

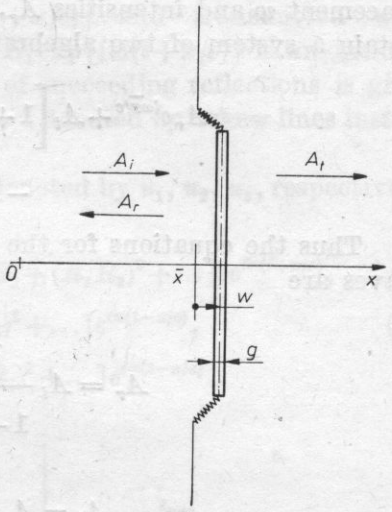

Fig. 3. System with a single diaphragm

and generates a reflected wave (moving to the left)

$$A_r e^{i\omega(t+x/c)},$$

and a transmitted wave (moving to the right) $A_t e^{i\omega(t-x/c)}$ A_i and ω are assumed known. Intensities A_r, A_t should be determined from the motion equations and continuity equations. The calculation methodology is discussed in papers [2] and [3]. Denoting the displacement on the left side of the diaphragm by u, and the right side by v, we obtain

$$u = A_i e^{i\omega(t-x/c)} + A_r e^{i\omega(t+x/c)}, \qquad v = A_t e^{i\omega(t-x/c)}. \tag{2}$$

The displacement of the diaphragm is denoted by $w = w(t)$. At $x = \bar{x}$ the displacements u and v, are identical and equal w. Thus we have

$$(A_i e^{-i\omega\bar{x}/c} + A_r e^{i\omega\bar{x}/c}) e^{i\omega t} = A_t e^{-i\omega\bar{x}/c} e^{i\omega t} = w. \tag{3}$$

As the air elasticity modulus is $E = \varrho c^2$, then waves (2) interact with the mobile diaphragm with a force (acting in the direction $+x$).

$$i\omega\varrho c[(A_i - A_t)e^{-i\omega\bar{x}/c} - A_r e^{i\omega\bar{x}/c}]e^{i\omega t}.$$

Also the force $-Qw$ acts on a unit surface and it is the reaction of the elastic suspension. Including finally the force of inertia $m\ddot{w}$ we achieve the motion equation diaphragm for the

$$i\omega\varrho c[(A_i - A_t)e^{-i\omega\bar{x}/c} - A_r e^{i\omega\bar{x}/c}]e^{i\omega t} = m\ddot{w} + Qw. \tag{4}$$

Equations (3) and (4) give a system of three equations describing the displacement w and intensities A_r, A_t. Inserting (3) in (4) and repeating (3) we obtain a system of two algebraic equation for A_r, A_t

$$A_r e^{i\omega\bar{x}/c} + A_t\left[1 + \frac{Q - mw^2}{i\omega c\varrho}\right] e^{-i\omega\bar{x}/c} = A_i e^{-i\omega\bar{x}/c},$$

$$-A_r e^{i\omega\bar{x}/c} + A_t e^{-i\omega\bar{x}/c} = A_i e^{-i\omega\bar{x}/c}.$$

Thus the equations for the intensities of the reflected and transmitted waves are

$$A_r = A_i \frac{\dfrac{i}{2\omega\varrho c}(Q - mw^2)}{1 - \dfrac{i}{2\omega\varrho c}(Q - mw^2)} e^{-2i\bar{x}/c}, \tag{5}$$

$$A_t = A_i \frac{1}{1 - \dfrac{i}{2\omega\varrho c}(Q - mw^2)}.$$

Further analysis does not require the formula for w, therefore we are not giving it here. Let's notice that for a resonance frequency $\omega^2 = Q/m$ we have.

$$A_r = 0, \quad A_t = A_i.$$

According to (5) for waves sent at $\bar{x} = 0$ (see Fig. 2) we obtain

$$A_r = R_1 A_i, \quad A_t = T_1 A_i, \tag{6}$$

where

$$R_1 = \frac{-M_1^2 + iM_1}{1 + M_1^2}, \quad T = \frac{1 + iM_1}{1 + M_1^2}, \quad M_1 = \frac{Q_1 - m_1 w^2}{2\omega\varrho c}. \tag{7}$$

These formulas are also true for waves propagating in the direction $-x$. For a second diaphragm situated at $x = a$ we have

$$A_r = R_2 A_1, \quad A_t = T_2 A_i, \tag{8}$$

where

$$R_2 = \frac{M_2^2 + iM_2}{1 + M_2} e^{-2i\omega a/c}, \quad T_2 = \frac{1 + iM_2}{1 + M_2^2}, \quad M_2 = \frac{Q_2 - m_2 w^2}{2\omega\varrho c}. \tag{9}$$

3. Two diaphragms

We will utilize previous results in this paragraph. The wave $A\exp[i\omega(t - x/c)]$ inciding onto the first diaphragm produces a reflected wave $AR_1\exp[i\omega(t + x/c)]$ and a transmitted wave $AT_1\exp[i\omega(t - x/c)]$. In regard to the

second diaphragm the wave $AT_1\exp[i\omega(t-x/c)]$ is an incident wave, which generates a reflected wave $AT_1\exp[i\omega(t+x/c)]$ and transmitted wave $AT_1T_2\exp[i\omega(t-x/c)]$. Next, the wave $AT_1R_1\exp[i\omega(t+x/c)]$ is an incident wave for the first diaphragm. The diagram of succeeding reflections is given in Fig. 4. For greater clarity, reflected waves are denoted by askew lines instead of lines perpendicular to diaphragms.

Displacement fields in regions 1, 2, 3 are denoted by u_1, u_2, u_3, respectively. According to Fig. 4 we have

$$\begin{aligned} u_1 &= Ae^{i\omega(t+x/c)}+A\{R_1+T_1^2R_2[1+R_1R_2+(R_1R_2)^2+\ldots]\}e^{i\omega(t+x/c)},\\ u_2 &= AT_1[1+R_1R_2+(R_1R_2)^2+\ldots]e^{i\omega(t-x/c)},\\ u_3 &= AT_1T_2[1+R_1R_2+(R_1R_2)^2+\ldots]e^{i\omega(t-x/c)}. \end{aligned} \tag{10}$$

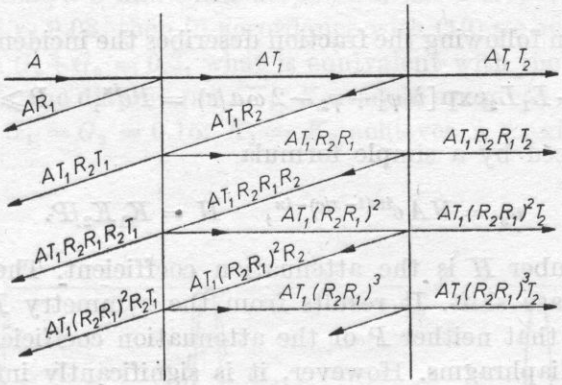

Fig. 4. Diagram of succeeding reflections from two diaphragms

Terms in square brackets are the sums of infinite geometrical progressions. On the basis of formulas for the sums of such progressions we achieve

$$\begin{aligned} u_1 &= Ae^{i\omega(t-x/c)}+A\left(R_1+\frac{T_1^2R_2}{1-R_1R_2}\right)e^{i\omega(t+x/c)},\\ u_2 &= A\frac{T_1}{1-R_1R_2}e^{i\omega(t-x/c)}+A\frac{T_1R_2}{1-R_1R_2}e^{i\omega(t+x/c)},\\ u_3 &= A\frac{T_1T_2}{1-R_1R_2}e^{i\omega(t-x/c)}. \end{aligned} \tag{11}$$

From the point of view of noise control the formula for u_3 is the most important. Having numeric calculations in mind we will express the coefficients T_1, T_2, R_1, R_2 in the exponential form

$$T_1=K_1e^{i\varphi_1},\quad T_2=K_2e^{i\varphi_2},\quad R_1=L_1e^{i\psi_1},\quad R_2=L_2e^{i\psi_2'}, \tag{12}$$

where K_1, K_2, L_1, L_2 are non-negative constants. In complience with formulas (7) and (9) we have

$$K_1 = \frac{1}{\sqrt{1+M_1^2}}, \quad K_2 = \frac{1}{\sqrt{1+M_2^2}}, \quad L_1 = K_1|M_1|, \quad L_2 = K_2|M_2|, \tag{13}$$

$$\varphi_1 = \operatorname{arctg} M_1, \quad \varphi_2 = \operatorname{arctg} M_2, \quad \psi_1 = \operatorname{arctg}(1/M_1)+\pi,$$

$$\psi_2 = \operatorname{arctg}(1/M_2)+\pi,$$

where M_1, M_2 are described by fromulas (7) and (9).

Applying (12), (13) we obtain from formula (11)

$$u_3 = \frac{K_1 K_2}{1-L_1 L_2 \exp[i(\psi_1+\psi_2-2\omega a/c)]} A e^{i\omega(t-x/c)}. \tag{14}$$

The expression following the fraction describes the incident wave. Denoting

$$1-L_1 L_2 \exp[i(\psi_1+\psi_2-2\omega a/c) = Pe^{i\varkappa}, \quad P \geqslant 0 \tag{15}$$

(14) can be replaced by a simple formula

$$u_3 = HA e^{i\omega(t-x/c)-i\varkappa}, \quad H = K_1 K_2/P. \tag{16}$$

The real number H is the attenuation coefficient. The term $\exp(-i\varkappa)$ represents the phase shift. It results from the symmetry $L_1 L_2 = L_2 L_1$ and $\varphi_1+\varphi_2 = \psi_2+\psi_1$, that neither P or the attenuation coefficient H depends on the sequence of diaphragms. However, it is significantly influenced by their thickness.

4. Attenuation

Diagrams of the functions K_1, K_2 and H in terms of frequence ω, will be given here. We will introduce dimensionless thicknesses

$$G_1 = g_1/a, \quad G_2 = g_2/a \tag{17}$$

and the following frequencies

$$\omega_0 = \frac{\varrho c}{\varrho_s a}, \quad \omega_1 = \sqrt{\frac{Q_1}{m_1}}, \quad \omega_2 = \sqrt{\frac{Q_2}{m_2}}, \quad \omega_a = \pi\frac{c}{a}. \tag{18}$$

Frequencies, ω_1 and ω_2, are the frequencies of free vibrations of diaphragms 1 and 2. The frequency ω_a is the free frequency of the space between the diaphragms. It is proportional to the number of distances, a, which the wave travels during a unit of time.

In accordance with the assumption that $Q_1 \approx g_1^3 m_1 \approx g_1$ and in accordance with (18) we have

$$\omega_1 = CG_1, \qquad \omega_2 = CG_2, \tag{19}$$

where C is a certain factor of proportionality.

Further calculations are conducted for typical values equivalent for a window in a building, namely:

diaphragm spacing	$a = 0.1$ m
wave velocity in air	$c = 330$ m/s
vave velocity in glass	$c_1 = c_2 = 4000$ m/s
air density	$\varrho = 1$ kg/m^3
glass density	$\varrho_s = 3300$ kg/m^3

We assume that a 3-mm-thick diaphragm has a free vibration frequency of 30 s^{-1}. Since $G = 0.03$, then in accordance with (19) we accept $C = 1000$ s^{-1}.

We establish $G_1 + G_2 = 0.3$, what is equivalent with the assumption about a constant mass of the diaphragms. K_1, K_2 and H are given as frequency functions. In Fig. 5, $G_1 = G_2 = 0.15$. $K_1 = K_2$ achieves a maximum of 1 for the

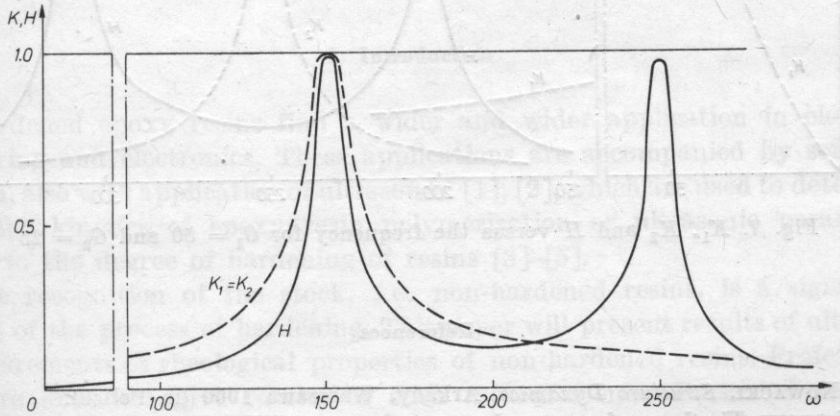

Fig. 5. $K_1 = K_2$ and H versus the frequency for $G_1 = 0.15$

frequency $\omega = 150$ s^{-1}. Also H achieves a maximum equal to 1 for this frequency. For $\omega = 250$ s^{-1} function H achieves next maximum, lower than 1. In Fig. 6, $G_1 = 0.1$, $G_2 = 0.2$. The maximal values of the attenuation coefficient are lower than 1. Maxima are shifted in regards to the maxima of coefficients K_1, K_2. Fig. 7 presents K_1, K_2 and H for $G_1 = 0.5$, $G_2 = 25$. Also in this case H is everywhere lower than 1.

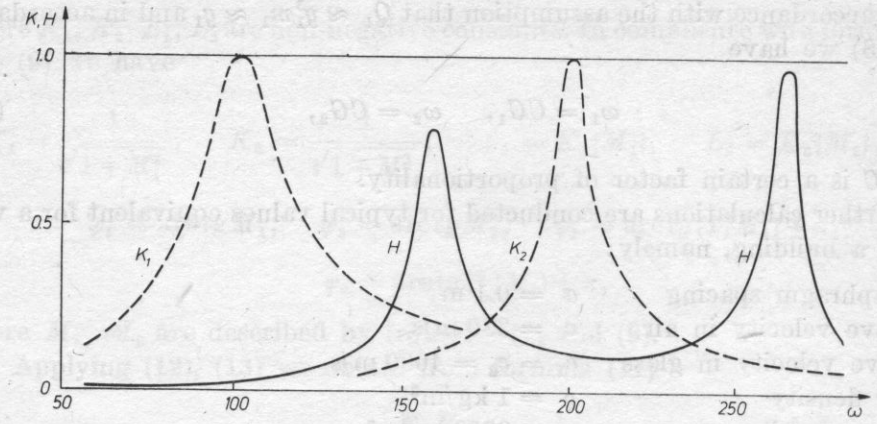

Fig. 6. K_1, K_2 and H versus the frequency for $G_1 = 0.1$ and $G_2 = 0.2$

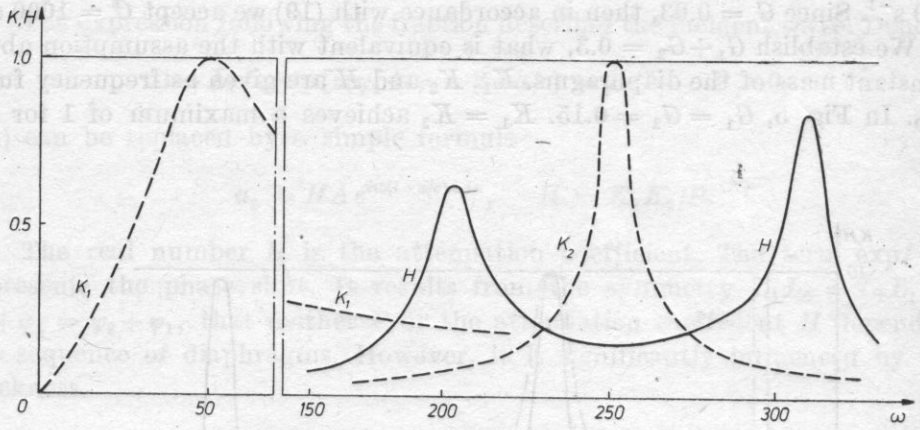

Fig. 7. K_1, K_2 and H versus the frequency for $G_1 = 50$ and $G_2 = 25$

References

[1] W. NOWACKI, *Structure Dynamics*, Arkady, Warszawa 1960 (in Polish).
[2] I. MALECKI, *The theory of waves and acoustical systems*, PWN, Warszawa 1964 (in Polish).
[3] Z. WESOŁOWSKI, *Acoustics of an elastic body*, PWN (in print) (in Polish).

Received on July 30, 1985; revised version on March 26, 1986

ARCHIVES OF ACOUSTICS
11, 2, 171-182 (1986)

RHEOLOGICAL PROPERTIES OF EPOXY RESINS IN AN SHEAR ULTRASONIC FIELD

RYSZARD PŁOWIEC

Institute of Fundamental Technical Research, Polish Academy of Sciences
(00-049 Warsaw, ul. Świętokrzyska 21)

Ultrasonic shear measurements were perfomed on epoxy resins: araldit *F* and epidian 5 in a temperature range from -30 to 80°C and a frequency range from 10 to 800 MHz. Using reduced variables a "master curve", following the *BEL* model, was determined for $K = 1.8$ and 1.6, and $\beta = 0.47$ and 0.44, respectively. Both elasticity moduli and dynamic viscosity are given as frequency functions. It was found that rheological properties of both resins are close each other in an ultrasonic shear field.

1. Introduction

Hardened epoxy resins find a wider and wider application in electrical engineering and electronics. These applications are accompanied by scientific research, also with application of ultrasound [1], [2], which are used to determine either the kinetics of epoxy resin polymerization or ultrasonic parameters related to the degree of hardening of resins [3]–[5].

The recognition of the stock, i.e. non-hardened resins, is a significant element of the process of hardening. This paper will present results of ultrasonic measurements of rheological properties of non-hardened resins. Professional literature does not give results of such measurements. Presented research will lead to the determination of the reaction of the resin to shear strain in a wide ultrasonic frequency range through the measurement of acoustical impedance to shear. This parameter allows us to calculate the changes of the shear modulus, the loss modulus and dynamic viscosity, as well as the viscoelastic relaxation range.

In ultrasonic measurements conducted with a transverse wave, the epoxy resin is used as a coupling layer, because here oil can not be applied although it finds wide application in investigations conducted with a longitudinal wave. This property of the resin can be explained through the determination of the moduli of elasticity in terms of frequency.

In order to establish the ultrasonic difference, two types of epoxy resins were chosen: epidian 5 from the Sarzyna works (Poland) and araldit *F* produced by Ciba-Geigy (Switzerland).

2. Measuring method

The mechanical shear impedance of the resin was determined with the application of transverse vibrations with a ω frequency. The relation between the impedance $Z^*_{j\omega}$ and the complex modulus of elasticity of a liquid $G_{j\omega}$ for this frequency, ω, is expressed by

$$(Z^*_{j\omega})^2 = \varrho G^*_{j\omega}, \tag{1}$$

where ϱ is the liquid density

$$Z^*_{j\omega} = R + jX, \quad G^*_{j\omega} = G' + jG''.$$

The mechanical shear impedance is most oftenly determined from the measurement of the amplitude reflection coefficient, k, and phase, θ, of the ultrasonic wave on the boundary of two media, i.e., solid body and liquid. The mechanical shear impendance of a liquid in the case of a plane wave inciding perpendicularily to the boundary surface, is:

$$Z^*_{j\omega} = Z_Q \frac{1 - k^2 + j2k\sin\theta}{1 + k^2 + 2k\sin\theta}, \tag{2}$$

where Z_Q is the impedance of the solid body.

For most liquids the wave phase shift related to the reflection is small, as the impedance of a liquid $|Z| < 0.1 < |Z_Q|$; therefore, it can be accepted that $\cos\theta = 1$. Then equation (2) has a form as follows:

$$Z^*_{j\omega} \cong Z_Q \left(\frac{1 - k^2}{(1+k)^2} + j \frac{2k\sin\theta}{(1+k)^2} \right) = R + jX. \tag{3}$$

The error due to the assumption that $\cos\theta = 1$ does not exceed $1^0/_0$. Using equation (3) the real part of the impedance can be calculated with the knowledge of the amplitude reflection coefficient, solely:

$$R = Z_Q \left(\frac{1-k}{1+k} \right). \tag{4}$$

Having R and X the components of the shear modulus of a liquid, $G^*_{j\omega}$, are

$$G'_\omega = \frac{R^2 - X^2}{\varrho}, \quad G''_\omega = \frac{2RX}{\varrho} \tag{5}$$

while the dynamic viscosity is expressed by equation

$$\eta'_\omega = \frac{2RX}{\omega\varrho}.$$

Investigations were performed on measuring set-ups built at the Department of Physical Acoustics of the IFTR for frequencies: 10 and 30 MHz [6], 400 and 800 MHz [7]. An apparatus produced by "MATEC" was used for control measurements performed at a frequency of 50 MHz.

The echo method was applied in measurements of the pulse reflection coefficient. A delay line made from fused quartz was used for frequencies of 10, 30 and 50 MHz. Measurements for frequencies of 400 and 800 MHz were done with the use of a tuned resonant cavity with a crystal of lithium niobate as the delay line.

For every individual temperature the reflection coefficient, k, was measured twice; first measurement for an unloaded delay line, second — for a delay line loaded with measured medium. The attenuation difference of first ten reflections of the line was determined through the comparison with a standard pulse with a controlled amplitude. Then the value of resistance was calculated from equation (4).

Considering the tendency of epoxy resins to form conglomerates and resulting layer heterogeneities, the investigated samples, before every series of measurements, were heated to the temperature of 95°C and then measurements were done on samples cooled to an adequate temperature. This procedure gave a satisfactory measurement accouracy. If the scatter of results was too great, measurements for that temperature were repeated several times and the average value was calculated.

Generally it can be stated that the epidian 5 epoxy resin gave a greater scatter of results than the araldit F resin.

3. Characteristic of investigated samples

An epoxy resin is a linear polymer with the average specific gravity, M_n, in the range 340–382 [8]. The epoxy group is the characteristic element of the resin structure. It is a there-part oxycyclopoprane ring consisting of two carbon atoms and one oxygen atom

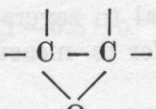

The general formula of a resin with characteristic epoxy groups at the ends is presented in Fig. 1.

Investigations of non-hardened epoxy resins include structure identification with chemical and spectral methods, quantitative analysis of typical functional groups: epoxy and hydroxyl, and estimation of organically bound chlorine, α-glycol groups and ionic chlorine, which occur due to the imperfection of the synthesis process.

Physical properties, such as: molecular weight, viscosity, density, have been also determined. The two last properties are of special interest in the course of ultrasonic investigations with shear waves. Because the density and stationary viscosity, and their changes with regard to temperature, have to be known in order to determine the rheologic properties of the resin and to state

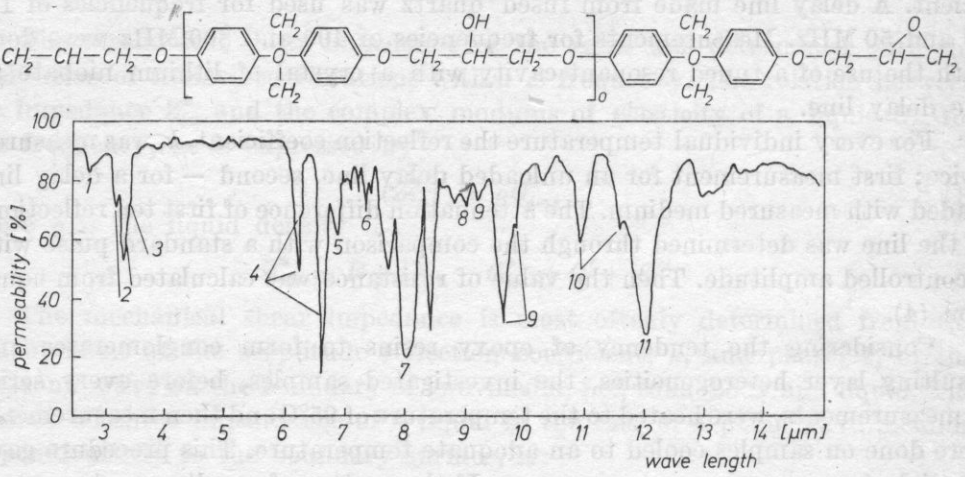

Fig. 1. The epoxyresion formula and its infrared spectrum. The numbers mark groups: *1* — hydroxyl, *2* — methyl, *3, 5* — methylene, *4, 9, 11* — substitution in the aromatic ring, *7* — etheral, *8* — diphenyl ethers, *10* — epoxy

changes of dynamic viscosity and moduli of elasticity in terms of the strain frequency, described by equations (5) and (6). These quantities (especially viscosity) differ for various resin in dependence on the producer and on the imperfection of the synthesis process.

Viscosity

Standard viscometers, such as the Engler, Ford or Hoepler viscometers, can be used in viscosity measurements. However, the Brookfield rotary viscometer is used particularily frequently in control measurements, for its measurement simplicity in a range from several to several milion mPa·s. Therefore, resin viscosity data on the package refer to measurements conducted with the described viscometer.

A Ferranti-Shirley type cone-plate viscometer or a Weissenberg rheoviscometer are used in laboratory measurements. A liquid sample in these viscometers (approx. 0.5 cm^3) is subjected to shearing between a fixed flat plate and a cone rotor. The viscous resistance of the liquid, which acts on the rotating cone is the source of the momentum transmitted to a precise mechanic-electric dynamometer with an indicator calibrated in viscosity units. The Weissenberg viscometer beside the tangent component of stress, allows also the measurement of the normal component, which characterizes viscoelastic liquids.

Fig. 2 presents the epidian 5 viscosity in terms of temperature [9], measured with the rotary viscometer. Viscosities given by Ciba-Geigy [10] and measured with a Ferranti-Shirley viscometer at the Materials Quality Assaurance Directorate (England) have been also denoted in the diagram.

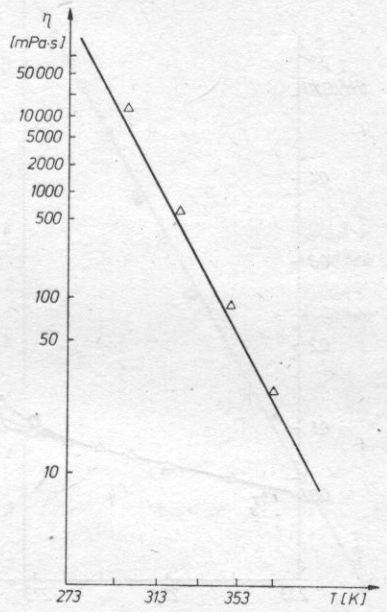

Fig. 2. Changers of the epidian 5 epoxy resin viscosity in terms of temperature [9]. The points mark the viscosity of araldit *F*, given by the producer [10]

Density

Considering the small density influence on the calculation results of the moduli of elasticity and the relaxation spectrum, it has been assumed that the density of both resins changes with temperature in the same manner and accordingly to data reported in literature [11]

$$\varrho = 1.229(1 - 6.8 \cdot 10^{-4})t - 20°\mathrm{C}.$$

4. Measurement results

Measurement of the high frequency limiting shear compliance, J_∞

The measurement of the shear compliance, J_∞, was done for araldit *F* at frequencies: 30 and 800 MHz, and for epidian 5 for frequencies 30 and 400 MHz.

Measurement results are given in Fig. 3 in the forms of a quotient $\varrho/R^2 = J_\infty$.

The transtion from the viscoelastic behaviour of the resin to the elastic behaviour, where the compliance changes linearly with temperature, can be clearly seen. The arrow marks the temperature of glass transition T_g.

Within the limit of error it can be accepting that compliance changes of both resins, in terms of temperature, are alike.

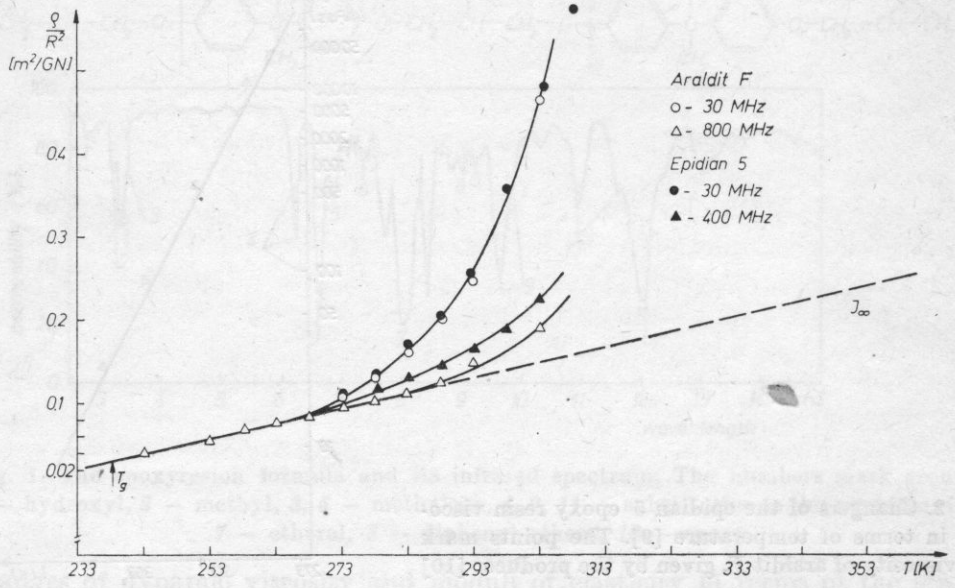

Fig. 3. Changes of the shear compliance, J_∞, in terms of temperature. Araldit F: ○ – 30 MHz, △ – 800 MHz, Epidian 5: ● – 30 MHz, ▲ – 400 MHz

Measurement of the real component of the acoustical impedance of resins

Fig. 4 presents measurement results of the real component of the acoustical shear impedance of the resin, done at a frequency of 10 MHz, while Fig. 5 presents those done at the frequency of 30 MHz.

For comparative purposes, measurements of the araldit F resin at the frequency of 50 MHz have been additionally performed with the application of the American "Matec" apparatus.

5. Discussion

Presentation of measurement results

Applying the principle reduce variable [12], the results of described above impedance measurements performed for various frequencies and at various temperatures have made up one "master curve" which marks impedance changes

of both resin samples as a function of frequency ω. This frequency has been related to the relaxation frequency $\omega_m = 1/\tau_M$ of a simple Maxwell model. These curves are presented in Fig. 6.

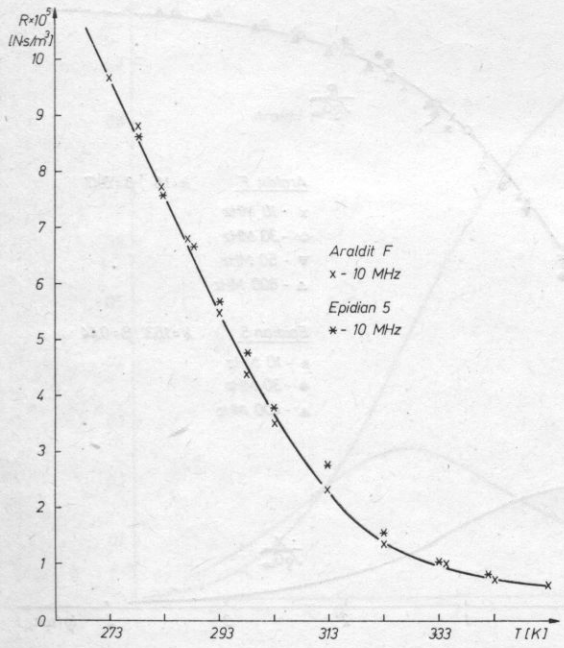

Fig. 4. Measurement results of the real component of impedance in terms of temperature for araldit (X) and epidian (*) for the frequency of 10 MHz

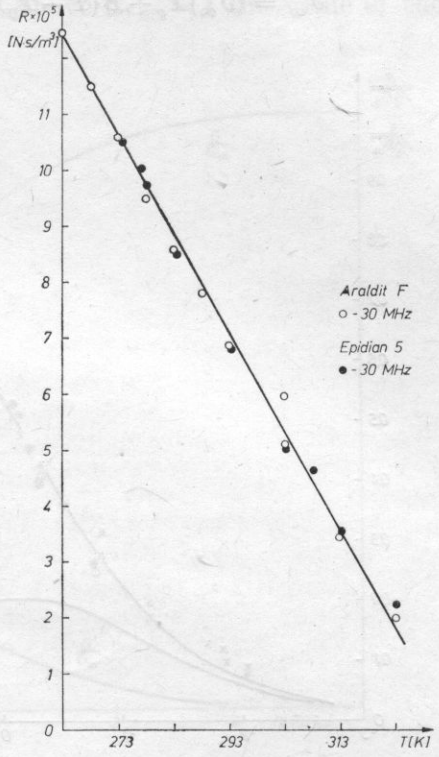

Fig. 5. Measurement results of the real component of impedance in terms of temperature for araldit (○) and epidian (●) for the frequency of 30 MHz

Such a presentation of the results is generally accepted in literature, for it allows the presentation of impedance changes in a vide range of frequencies and an easy comparison of results obtained for various liquids. The reduction of the results on the vertical axis is done through relating the measured impedance for a given value ω to the boundary impedance (equal to $\sqrt{\varrho G_\infty}$, i.e. the impedance for an infinitely great frequency).

Discussion

Presented in Fig. 3 measurements of the boundary shear compliance (J_∞) did not vary significantly for both resins. In both cases the glass transition temperature of the resins was estimated at $T_g = -35°C$, with an error of $\pm 5°C$,

resulting from the difficulties of viscosity measurements in the range of negative temperatures. It can be proved that the changes of the boundary shear compliance, J_∞, with temperature can be expressed by the equation:

$$J_\infty = (J_\infty)T_g + B(T - T_g) = 3.4 \cdot 10^{-11} + 1.89 \cdot 10^{-12}(T - 238.1).$$

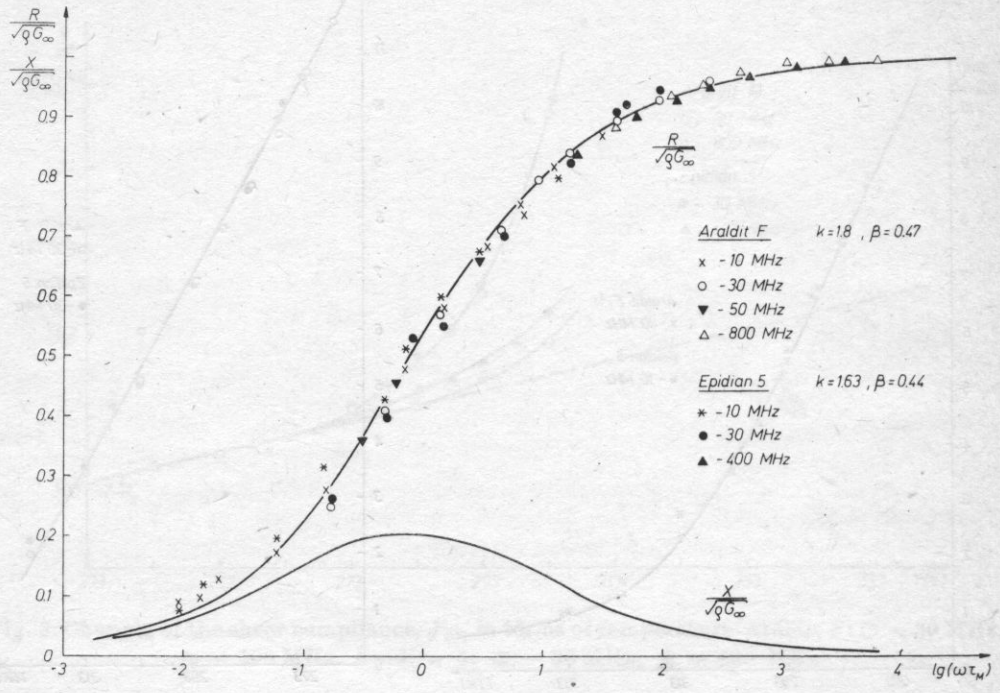

Fig. 6. Measurement results of the real component of impendance in the reduced system for araldit and epidian for different frequencies. Solid line was calculated from eq. (7)

Impedance values used for the determination of the temperature relationship of J_∞, determine the upper part of the relaxation curve presented in Fig. 6. Impedance values measured at 30 MHz determine the middle part of this curve, while those measured at 10 MHz — the lower part. The results fit each other confirming the use of reduce variable. The relaxation curves for both resins include four frequency decades. The full line marks the theoretical curve which has been calculated for a generalized BEL liquid model. This model expressed by the equation:

$$\frac{1}{G^*} = \frac{1}{G_\infty} + \frac{1}{j\omega\tau} + \frac{2K}{G_\infty (j\omega\tau)\beta}. \tag{7}$$

Parameters, K and β, which approximate the theoretical curve to the measurement results in araldit, equal $K = 1.8, \beta = 0.47$. While these parameters for epidian 5 equal $K = 1.6$, $\beta = 0.44$.

Fig. 7 presents curves of the reduced modulus of elasticity, G'/G, and the loss modulus, G''/G_∞, in the relaxation range in terms of the reduced frequency, for araldit F. The loss modulus has its maximum at $\omega\tau = 3$–5. Below $\omega\tau = 1$ the value of the loss modulus is higher than the value of the modulus of elasticity, what proves viscous character of the resin. Above $\omega\tau_M = 1$ the value of the

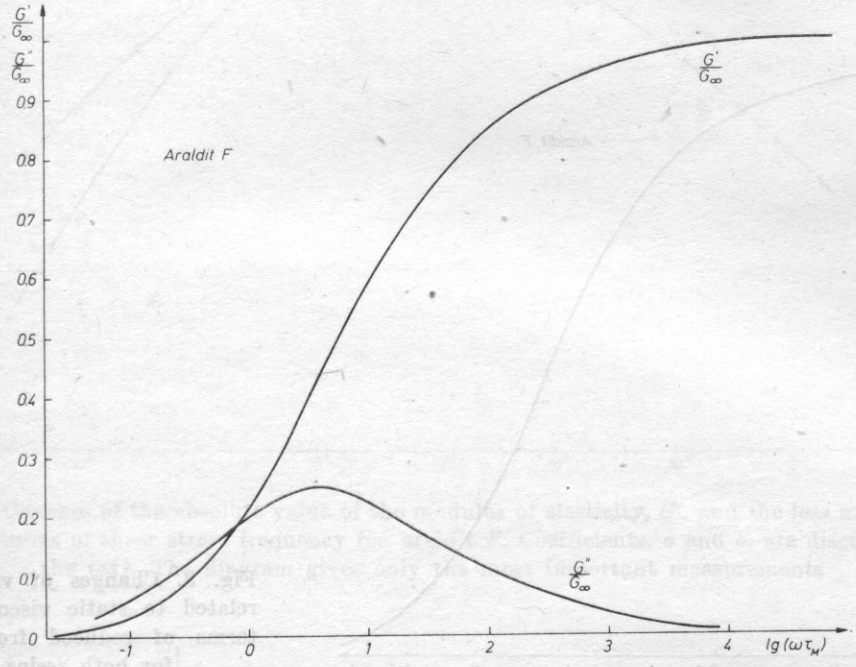

Fig. 7. The reduced modulus of elasticity, G'/G, and the loss modulus, G''/G, in terms of reduced frequency, for both resins

modulus of elasticity exceeds the value of the loss modulus, determining the elastic character of the resin. The value of the modulus of elasticity increases quickly to the maximum value in this range and achives this value within the range of four frequency decades.

The viscous character of the resin and the rate of decrease of viscosity in terms of frequency can be clearly seen in Fig. 8. At $\omega\tau = 2.5$ the resin viscosity constitutes hardly one tenth of its maximal value.

Functions presented in Fig. 7 and Fig. 8 characterizing resins in terms of the reduced frequency, can be related directly to the measured frequency. This can be done considering resin viscosity and density changes as functions of temperature in the form of the following coefficients:

$$ab = \frac{\eta}{\eta^*}, \qquad b = \frac{\varrho T}{\varrho^* T^*},$$

where the values of these coefficients for the reference temperature (accepted at 293.1) are equal to 1. The moduli changes in terms of frequency are presented in Fig. 9 for both resins.

The value of the modulus of elasticity, G', for the frequency of 10^5 Hz equals 10^6 Pa and increases with the rise of frequency achieving a maximal value of $1.25 \cdot 10^9$ Pa for the frequency of 10^{11} Hz. The loss modulus value,

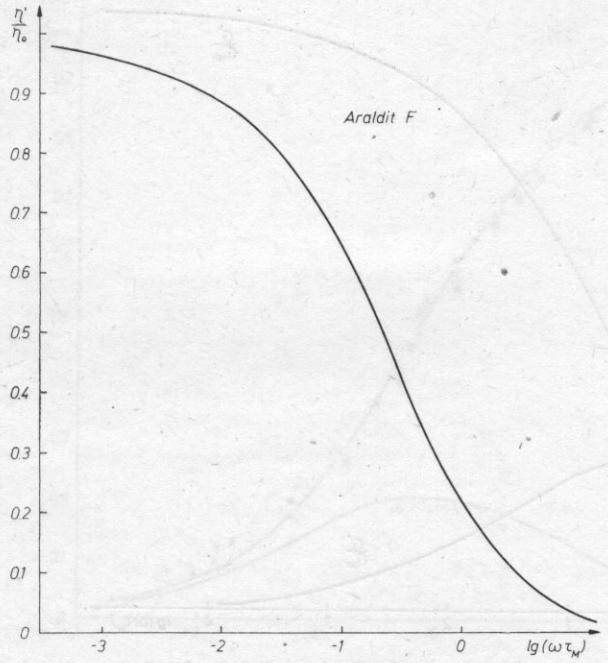

Fig. 8. Changes of viscosity related to static viscosity in terms of reduced frequency for both resins

G'', for the frequency of 10^5 Hz is by an order of magnitude higher than the value of the modulus of elasticity for this frequency. It achieves a flat maximum of $2 \cdot 10^8$ Pa in the frequency range 10^7–10^8 Hz and then decreases slowly. The moduli are equal at the frequency of $5.5 \cdot 10^6$ Hz, for the elasticity value of $1.5 \cdot 10^8$ Pa. For this characteristic frequency the value of $\operatorname{tg}\delta (= G'/G'')$ equals 1. For higher frequencies the resin reacts elastically to shear. From this it follows that the epoxy resin used as a coupling layer, can perform its function for frequencies exceeding the value of 5.5 MHz. The value of this frequency is by an order of magnitude lower in comparison with mineral oils [15] and synthetic oils [16].

Fig. 10 presents the changes of the absolute value of the dynamic viscosity for araldit *F* in terms of a quantity proportional to frequency (*af*). The static viscosity in the temperature of 20°C equals 180 mPa·s. For the shear frequency of 10^5 Hz the dynamic viscosity amounts to 144 mPa·s and quickly decreases with the rise of the shear frequency, because for the frequency of 10^8 Hz it equals only 3 mPa·s. The run of the curve for epidian 5 is very close to araldit *F*.

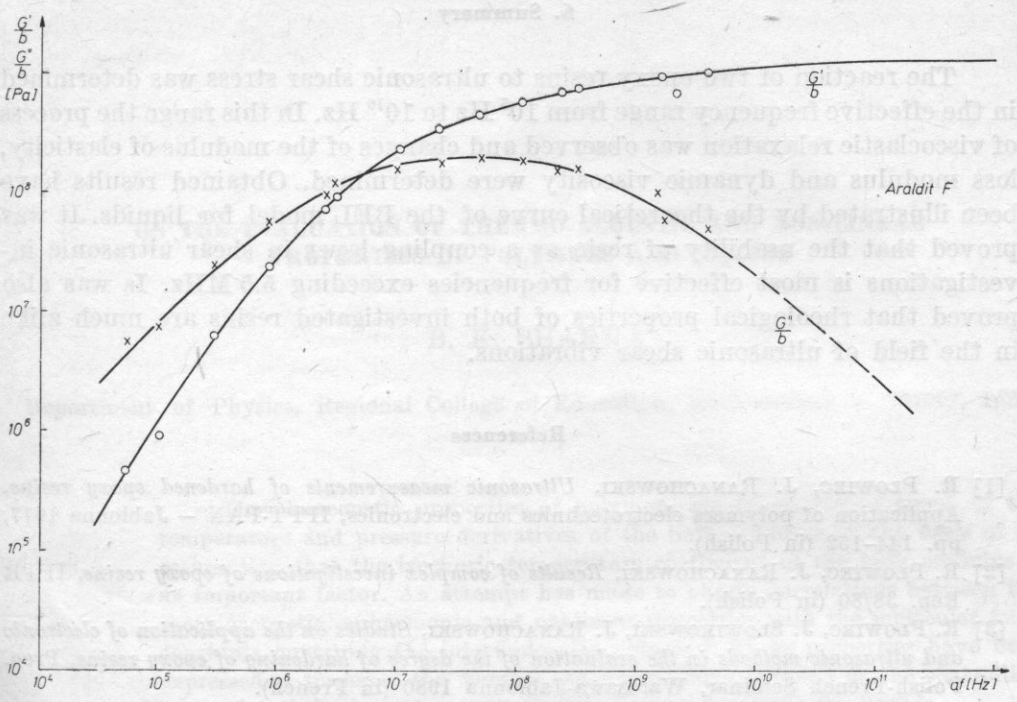

Fig. 9. Changes of the absolute value of the modulus of elasticity, G', and the loss modulus, G'', in terms of shear strain frequency for araldit F. Coefficients, a and b, are discussed in the text. The diagram gives only the most important measurements

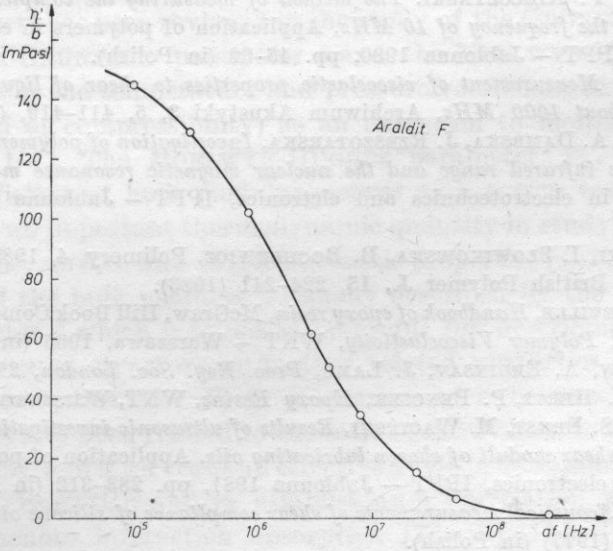

Fig. 10. Changes of the absolute value of the dynamic viscosity in terms of frequency, for araldit F. The diagram gives only the most important measurements

6. Summary

The reaction of two epoxy resins to ultrasonic shear stress was determined in the effective frequency range from 10^5 Hz to 10^{10} Hz. In this range the process of viscoelastic relaxation was observed and changes of the modulus of elasticity, loss modulus and dynamic viscosity were determined. Obtained results have been illustrated by the theoretical curve of the BEL model for liquids. It was proved that the usability of resin as a coupling layer in shear ultrasonic investigations is most effective for frequencies exceeding 5.5 MHz. Is was also proved that rheological properties of both investigated resins are much alike in the field of ultrasonic shear vibrations.

References

[1] R. PŁOWIEC, J. RANACHOWSKI, *Ultrasonic measurements of hardened epoxy resins*, Application of polymers electrotechnics and electronics, IPPT-PAN – Jabłonna 1977, pp. 144–152 (in Polish).

[2] R. PŁOWIEC, J. RANACHOWSKI, *Results of complex investigations of epoxy resins*, IFTR Rep. 38/80 (in Polish).

[3] R. PŁOWIEC, J. SŁOWIKOWSKI, J. RANACHOWSKI, *Studies on the application of electronic and ultrasonic methods in the evaluation of the degree of hardening of epoxy resins*, Proc. Polish-French Seminar, Warszawa-Jabłonna 1980 (in French).

[4] R. PŁOWIEC, *Ultrasonic measurements of the kinetics of the process of hardening of an epoxy resin*, Polimery **12**, 620–623 (1973) (in Polish).

[5] R. PŁOWIEC, *Ultrasonic measurements of the kinetic of polimerization processes in epoxy resins*, Proc. 3rd Conf. on Ultrasonic Investigation Methods of Condensed Matter, Żilina, 1972.

[6] R. PŁOWIEC, P. KIEŁCZYŃSKI, *The method of measuring the complex shear impedance of liquids for the frequency of 10 MHz*, Application of polymers in electrotechnics and electronics, IPPT – Jabłonna 1980, pp. 45–60 (in Polish).

[7] R. PŁOWIEC, *Measurement of viscoelastic properties to shear of liquids at deformation frequencies about 1000 MHz*, Archiwum Akustyki **3**, 5, 411–419, (1970) (in Polish).

[8] A. JANOWSKI, A. DĄMBSKA, J. RZESZOTARSKA, *Investigation of polymers with the spectrum method in the infrared range and the nuclear magnetic resonanse method*, Application of polymers in electrotechnics and eletronics, IPPT – Jabłonna 1977, pp. 96–120 (in Polish).

[9] A. KOZŁOWSKI, I. SŁOWIKOWSKA, B. BOCHLEWICZ, Polimery **4**, 1980, 139 (in Polish).

[10] W. WRIGHT, British Polymer J., **15**, 224–241 (1983).

[11] H. LEE, K. NEVILLE, *Handbook of epoxy resin*, McGraw, Hill Book Comp. 1976, pp. 17–21.

[12] I. D. FERRY, *Polymer Viscoelasticity*, WNT – Warszawa, 1965 (in Polish).

[13] A. J. BARLOW, A. ERGINSAV, J. LAMB, *Proc. Roy. Soc. London*, **298**, A. 481 (1967).

[14] Z. BROJER, Z. HERTZ, P. PENCZEK, *Epoxy Resins*, WNT, Warszawa 1972 (in Polish).

[15] R. PŁOWIEC, S. ERNST, M. WACIŃSKI, *Results of ultrasonic investigations of the dynamic viscosity and shear moduli of chosen lubricating oils*, Application of polymers in electrotechnics and electronics, IPPT – Jabłonna 1981, pp. 283–312 (in Polish).

[16] R. PŁOWIEC, *Acoustical measurements of shear compliance of silicone oil*, Arch. Akustyki, **12**, 1, 35–45 (1977) (in Polish).

Received on January 14, 1986; revised version on March 10, 1986

ARCHIVES OF ACOUSTICS
11, 2, 183-190 (1986)

ON THE EVALUATION OF THERMO-ACOUSTIC AND NON-LINEAR PROPERTIES OF POLYMERS AND LIQUIDS

B. K. SHARMA

Department of Physics, Regional College of Education, Bhubaneswar – 751007, India

Thermo-acoustic properties of polymers are calculated in terms of the temperature and pressure derivatives of the bulk modulus on the basis of an assumption that the isochoric temperature coefficient of the bulk modulus is an important factor. An attempt has made to obtain correlations between the thermoacoustic, anharmonic and nonlinear properties with the molecular force constants governing the intermolecular potential. These properties have been expressed in terms of the volume expansion which is found as the controlling factor for their dependence on temperature and volume for liquids.

1. Introduction

New interest has been revieved in the study of the GRÜNEISEN parameter Γ, the ANDERSON-GRÜNEISEN parameter δ and the MOELWYN-HUGHES parameter C_1 in the view of the temperature and pressure coefficient of the bulk modulus (the reciprocal of compressibility) as an extension to molten state, polymers and liquids [1–7]. The MOELWYN-HUGHES parameter C_1, expressed as the pressure coefficient of bulk modulus, serves as a severe test of the equation of state and is an important thermodynamic quantity in studying the molecular-thermodynamic, surface and thermo-acoustic properties [4–7]. The temperature dependence of the bulk modulus is usually described by the ANDERSON-GRÜNEISEN parameter δ which is found to be useful for describing the microscopic behaviour, internal structure and other related properties [2], [3], [6], [8]. The GRÜNEISEN parameter Γ, as a measure of anharmonicity of molecular vibrations, has also been related to the ratio of inter-chain to intra-chain normal mode vibrations, and it serves as an effective guide in determining the mechanism of ultrasonic absorption and in establishing a correlation with the results of phonom – phonom interaction absorption [7], [9]–[11]. The present paper deals with the correlations between these parameters with the molecular force constants governing the intermolecular potential, through the isobaric, iso-

thermal and isochronic acoustical parameters by RAO [12], CARNEVALE and LITOVITZ [13] and SHARMA [14]. The properties of interest are the bulk modulus, volume expansion and the sound speed, whose temperature and pressure dependence may be conveniently utilized to obtain such relationships.

2. Relationship between the thermo-acoustical parameters and intermolecular potential functions

Assuming the sound speed as a function of both volume and temperature, the isobaric, isothermal and isochronic acoustical parameters are related as [11], [14]

$$K' = K + K'' \tag{1}$$

in which

$$K'' = (K' - K) = \left(\frac{1}{\alpha}\right)\left(\frac{d\ln C}{dT}\right)_V, \tag{2}$$

$$K = -\left(\frac{1}{\alpha}\right)\left(\frac{d\ln C}{dT}\right)_P, \tag{3}$$

$$K' = B\left(\frac{d\ln C}{dP}\right)_T, \tag{4}$$

$$C^2 = BV, \tag{5}$$

where K and K' respectively represent the isobaric and isothermal acoustical parameters due to RAO [12], and that of CARNEVALE and LITOVITZ [13] and K'' is the isochoric acoustical parameter due to SHARMA [14]. C is the bulk sound speed, B is the bulk modulus, α is the volume expansion and V is the specific volume at pressure p and absolute temperature T.

Following SCHUYER [15], the RAO'S isobaric acoustical parameter may be expressed as

$$K = (m+n+1)/6, \tag{6}$$

where m and n are respectively the attractive and repulsive exponents of the intermolecular potential.

The expression for the ANDERSON-GRÜNEISEN parameter δ as obtained by BARKER [16] may be expressed in terms of m and n as

$$\delta = -\left(\frac{1}{\alpha}\right)\left(\frac{d\ln B}{dT}\right)_p = (m+n+4)/3. \tag{7}$$

From equations (6) and (7) it follows that [4]

$$\delta = 2K + 1 = 2\Gamma \tag{8}$$

in which the GRÜNEISEN parameter Γ is given by the temperature dependence of the bulk modulus as [4], [17],

$$\Gamma = -\left(\frac{1}{2\alpha}\right)\left(\frac{d\ln B}{dT}\right)_p. \tag{9}$$

Equation (8) resembles the relation obtained by warfield and HARTMANN [1] and SHARMA [4, 5].

The expressions for parameters K' and C_1 may be expressed as [4]

$$K' = (m+n+3)/6, \tag{10}$$

$$C_1 = \left(\frac{dB}{dp}\right)_T = 2K'+1 = \frac{m+n+6}{3} \tag{11}$$

BEYER'S parameter of nonlinearity (B/A) which is a particular combination of the temperature and pressure derivatives of the sound speed has been shown by SHARMA [4] to be related to K' at $V = Vo$ by the relation

$$(B/A)_0 = (C_1-1) = (m+n+3)/3 = 2K', \tag{12}$$

where $(B/A)_0$ is the value of (B/A) corresponding to the specific volume Vo which represents the value of V at zero temperature and pressure.

Usually the exponent m has the value of 6 and $n > m$ for substances [6], [19]. The value of n varies from about 13 to 19 for quasispherical, unassociated molecular liquids [6], [19].

For $m = 6$, equations (7) and (8) give

$$n = 3(\delta-4)+2 = 6K-7 = 6\Gamma-10. \tag{13}$$

Equations (7) and (12) lead to the relation between δ and $(B/A)_0$ as

$$\delta = \left(\frac{B}{A}\right)_0 + \frac{1}{3}. \tag{14}$$

Equations (13) and (14) establish the direct and close relationship between Γ, $(B/A)_0$ and n which can be expressed in terms of δ for a polymer. This suggests that the GRÜNEISEN parameter Γ as a measure of anharmonicity of molecular vibrations is related to the parameter $(B/A)_0$ describing the non-linearity effects in polymers. Thus intermolecular forces through the repulsive exponent n seem to play a vital role in establishing a close correlation between the anharmonic and nonlinear properties of the polymer.

Assuming the bulk modulus as a function of both volume and temperature, it can be shown from the thermodynamic considerations [11] that

$$\alpha B\left(\frac{d\ln B}{dp}\right)_T = \left[\left(\frac{d\ln B}{dT}\right)_v - \left(\frac{d\ln B}{dT}\right)_p\right]. \tag{15}$$

From equations (2), (5), (7) (11) and (15) it follows that

$$\left(\frac{d\ln B}{d\ln T}\right)_v = (C_1 - \delta)\alpha T = 2K''\alpha T. \tag{16}$$

Since the values of δ are greater than C_1, hence the isochronic acoustical parameter K'' is a negative quantity for polymers [11], while it is a positive quantity for liquids [14]. It implies that the bulk modulus should decrease with the rise of temperature at a constant volume in a polymer.

This implies that volume changes caused by temperature have a greater effect on bulk modulus or sound speed than volume changes caused by pressure in the polymer.

The relation between the isothermal acoustical parameter K' and free volume [20] may be expressed in terms of n, using equations (10) and (11), as

$$Va/V = (K'+1)^{-1} = \frac{2}{(C_1+1)} = 6/(n+15), \tag{17}$$

where $Va = (V - Vo)$ is the free volume, V is the volume at absolute temperature T and V_0 is the volume of the polymer at 0 K.

Equations (7)–(9), (11), (13), (14), (16) and (17) allow direct evaluation of the parameters δ, C_1, Γ, K, K', K'', n, $(B/A)_0$, $(d\ln B/d\ln T)_v$ and Va/V from the available data for the thermo-acoustic parameters involved. Such calculations for eight polymers are presented in Table 1 using the calculated values

Table 1. Calculated values of thermo-acoustic parameters of polymers

Polymer	T [K]	Γ	δ	C_1	$\left(\frac{B}{A}\right)_0$	$\left(\frac{d\ln B}{d\ln T}\right)_v$	n	Va/V
Phenolic polymer	303	7.6	15.2	12.6	14.9	−0.24	35.6	0.14
Polyphenyl quinoxaline	303	4.4	8.8	7.0	8.5	−0.14	16.4	0.25
Polymethyl methacrylate	298	4.8	9.8	8.0	9.3	−0.10	18.8	0.22
Polystyrene	298	4.4	8.8	8.8	8.5	−0.0	14.4	0.20
Polyethylene (high density)	298	5.1	10.2	8.2	9.9	−0.30	20.6	0.22
Polypropylene	298	11.0	22.0	18.0	21.7	−0.57	56.0	0.10
Polymethylene Oxide	298	6.3	12.6	11.2	12.3	−0.10	27.8	0.16
Poly(4-methyl pentene-1)	298	5.1	10.2	10.0	9.9	−0.02	20.6	0.18

of K, K' and K'' and the experimental data for volume expansion α from [11]. The calculated values of $(B/A)_0$ for most of the polymers are of the same order as those observed for fluorocarbon fluids [21]. However, the values of n vary from about 16 to 56 which is more than range of about 16 to 19 for quasi-spherical

molecular liquids [19]. Higher values of n for polymers as compared to liquids are expected since the polymers are strongly anisotropic and the anharmonicity is exhibited by interchain vibrations [9–11, 17]. The calculated values of (Va/V) for polymers under present investigation range from about 0.10 to 0.25 as compared to about 0.15 for fluorocarbon fluids [10] and 0.20 for saturated hydrocarbon fluids [19].

3. Computation of thermo-acoustical parameters of liquefied gases

Pastine [22] related the anharmonic parameter Γ in terms of the exponents m and n as

$$\Gamma = (m+n+3)/6. \tag{18}$$

Equation (18) for Γ resembles the equation (10) obtained for K' by Sharma [4].

Using equations (7), (8), (11), (14) and (18), the parameters $(B/A)_0$, K, δ and C_1 of a liquid may be expressed in terms of Γ as

$$\left(\frac{B}{A}\right)_0 = \delta - \left(\frac{1}{3}\right) = (C_1 - 1) = 2\Gamma = 2\left(K + \frac{1}{3}\right). \tag{19}$$

The parameter Γ can be estimated from the expression obtained for the Debye temperature for a liquid [23]. It has been shown [23] that the GRÜNEISEN parameter Γ can be expressed in terms of volume expansion of the liquid as

$$\Gamma = 1 + (2\alpha T)^{-1}. \tag{20}$$

Equations (19) and (20) lead to the expression for δ, K and $(B/A)_0$ in terms of α as

$$\delta = \frac{7}{3} + (\alpha T)^{-1}, \tag{21}$$

$$K = 2/3 + (2\alpha T)^{-1}, \tag{22}$$

$$\left(\frac{B}{A}\right)_0 = 2 + (\alpha T)^{-1}. \tag{23}$$

Equations (20)–(23) show that the volume expansion α is the controlling factor the dependence of the parameters Γ, δ and K of liquids on temperature and volume. For simple liquids these parameters are found to decrease with a rise in temperature [5], [24].

Equations (20) and (22) establish a direct relationship between Γ and K for liquids which can be expressed in terms of α only. This result agrees closely with the suggestion of HARTMANN [25] that the same anharmonicity of the intermolecular potential that gives rise to a volume or temperature dependence

of normal mode frequency also produces thermal expansion, so it is not surprising that Γ and α are related.

The temperature dependence of the parameter δ of a liquid can be treated qualitatively by considering equation (21) which yields the temperature derivatives of δ as

$$\left(\frac{\partial \delta}{\alpha T}\right)_p = -\left(\frac{\delta}{T}\right)\left[1+\frac{4/\delta}{3\delta-7}\right], \tag{24}$$

where the isobaric temperature derivative of α is given by [11], [14]

$$\left(\frac{d\ln \alpha}{dT}\right)_p = \frac{\alpha}{3}(7+4\alpha T).$$

Equation (24) correctly predicts a negative coefficient $(\partial\delta/\alpha T)_p$ showing a decrease in δ with a rise of temperature. This consequence is in qualitative accordance with the similar behaviour of K, Γ and C_1 observed for simple liquids [5], [9], [24].

The calculated values of Γ, δ, K and $(B/A)_0$ using equations (20)–(23) for several liquefied gases are presented in Table 2. Experimental data on α needed for the calculations were taken from literature [2–29]. The values of parameters δ

Table 2. Calculated values of the parameters K and (B/A) of liquefied gases

Liquefied gas	T [K]	$\alpha\cdot10^3$ [K^{-1}]	Γ	δ	K	$(B/A)_0$
Argon	84	4.37	2.36	5.05	2.03	4.72
Nitrogen	70	5.16	2.39	5.11	2.06	4.78
Oxygen	85	4.33	2.36	5.05	2.03	4.72
Neon	27	14.6	2.27	4.88	1.94	4.54
Krypton	120	3.20	2.30	4.94	1.97	4.60
Xenon	165	2.26	2.34	5.02	2.01	4.68
Methane	112	3.34	2.34	5.02	2.01	4.68
Hydrogen	20	15.68	2.59	5.52	2.26	5.18
Parahydrogen	20	15.87	2.57	5.48	2.24	5.14
Butane	273	2.13	1.86	4.06	1.53	3.72
Ethane	184.5	2.40	2.13	4.57	1.80	4.26
Carbon monoxide	81.6	5.27	2.16	4.66	1.83	4.32
Sulphur dioxide	263	1.70	2.12	4.58	1.79	4.24
Carbon dioxide	289	13.75	2.26	4.86	1.93	4.52
Hydrogen chloride	188	2.40	2.11	4.56	1.78	4.22
Hydrogen iodide	238	1.44	2.46	5.26	2.13	4.92

and $(B/A)_0$ vary from about 4 to 5.5 and those of K around 2 in the case of the liquefied gases under present investigation. A similar pattern has also been observed earlier for simple liquids [8], [23], [24].

4. Conclusions

From the considerations presented in this paper the following conclusions can be drawn:

1. The isobaric temperature and isothermal pressure derivatives of the bulk modulus or the sound speed are not independent but are related through their isochoric pressure or temperature derivatives.

2. The anharmonic and nonlinear properties of a polymer can be described in terms of temperature and pressure dependence of the bulk modulus.

3. The repulsive exponent of the intermolecular forces in a polymer seems to play a vital role in establishing a close correlation between the anharmonic and the nonlinear properties of the polymer.

4. Equation (17) makes possible the evaluation of (Va/V) of a polymer from the repulsive exponent calculated from the velocity and the pressure coefficient of the velocity of ultrasonic waves in the polymer.

5. Equations (20)–(23) make possible the evaluation of the anharmonic and the nonlinear properties of a liquid from the volume expansion alone showing a decrease with an increase in temperature.

6. The values of the parameters Γ and δ of a liquid are several times lower than that of a polymer, showing that polymers are strongly anisotropic and anharmonic as compared to liquids.

The author wishes to thank Dr. E. Soczkiewicz, Institute of Physics, Silesian Technical University, Gliwice, Poland for helpful correspondence.

References

[1] R. W. Warfield, B. Hartmann, J. Appl. Phys., **44**, 708 (1973).
[2] C. L. Gupta, M. N. Sharma, Phys. Stat. Solid (b), **101**, K47 (1980).
[3] Y. A. Chang, J. Phys. Chem. Solida, **28**, 697 (1967).
[4] B. K. Sharma, Polymer, **24**, 314 (1983).
[5] B. K. Sharma, Acustica, **43**, 221, 225 (1979); **45**, 65, (1980); **48**, 118, 121 (1981).
[6] B. K. Sharma, Acoust. Lett., **8**, **40**, 56 (1984).
[7] B. K. Sharma, Acoust. Lett., **5**, 95, 103 (1981); **6**, 25 (1982).
[8] B. K. Sharma, Acustica, **53**, 152 (1983).
[9] B. K. Sharma, Acoust. Lett., **8**, 11, 32 (1984).
[10] B. K. Sharma, Phys. Lett., A, **89**, 16 (1982); **95** (1983); **99**, 227 (1983).
[11] B. K. Sharma, J. Phys. D: Appl. Phys. **15**, 1273, 1735 (1982); **16**, 1959 (1983).
[12] M. R. Rao, J. Chem. Phys., **9**, 682 (1941).
[13] E. H. Carnevale, T. A. Litovitz, J. Acoust. Soc. Am. **27**, 547 (1955).
[14] B. K. Sharma, J. Acoust. Soc. AM., **73**, 106 (1983).
[15] J. Schuyer, J. Polym. Sci., **36**, 475 (1959).
[16] R. E. Barker, J. Appl. Phys., **38**, 4234 (1967).
[17] B. Hartmann, J. Appl. Polym. Sci., **19**, 3241 (1975).
[18] A. B. Coppens, R. T. Beyer, M. B. Seiden, J. Donohue, F. Guepin, R. H. Guepin, R. H. Hodson, C. Town Send, J. Acoust. Soc. Am., **38**, 797 (1965).
[19] E. Soczkiewicz, Archiv. Acoust., **2**, 325 (1977).

[20] B. K. Sharma, J. Polym. Mater., **1**, 193 (1984).
[21] W. M. Madigosky, I. Rosenbaum, R. Lucas, J. Acoust. Soc. Am., **69**, 1639 (1981).
[22] D. J. Pastine, Phys. Rev., **138**, 767 (1965).
[23] B. K. Sharma, Acoustica, **47**, 44 (1981).
[24] B. K. Sharma, Pramana, **14**, 477 (1980), **20**, 91 (1983).
[25] B. Hartmann, J. Acoust. Soc. Am., **65**, 1392 (1979).
[26] J. S. Rowlinson, Liquid and Liquid mixtures, Butterworth, London 1969.
[27] D. Nomoto, J. Phys. Soc. Japan, **18**, 1526 (1963).
[28] S. J. Yosim, J. Chem. Phys., **40**, 3069 (1964).
[29] A. Vanitterbeek, W. Van Dael, Physica, **27**, 1202 (1961).

Received on July 6, 1985

ARCHIVES OF ACOUSTICS
11, 2, 191-200 (1986)

ULTRASONIC BEHAVIOUR OF BINARY LIQUID MIXTURES CONTAINING *n*-OCTANOL AS A COMMON COMPONENT

K. GOPAL, B. RAJESWARA REDDY, N. PRABHAKARA RAO*

Department of Physics, College of Engineering, Sri Venkateswara University, (Tirupati – 517 502, India)

Ultrasonic wave propagation in binary liquid mixtures of benzene, tolune, *O*-xylene and ethyl-benzene in *n*-octanol was studied at 313.16 K. The compressibilities, available volumes, freelengths, relative associations, molar sound velocities and molar compressibilities were calculated from the density and velocity measurements. The systems studied show non-ideal behaviour and the deviations from linearity are explained on the basis of molecular dissociation of *n*-octanol in the solvents. The sound velocities in these systems have also been calculated theoretically, based on the Free Length Theory (FLT) due to Jacobson and Collision Factor Theory (CFT) due to Schaaffs.

Introduction

The non-linear variation of ultrasonic velocity and compressibility throws much light on the structural changes occurring in a liquid, as its concentration is varied in a mixture. This method has the ability of characterising the physico-chemical behaviour of liquid systems. Molecular association, dissociation in a liquid mixture as well as some important relations with the other parameters such as available volume, free lengths, relative associations, isothermal and adiabatic compressibilities etc, can be studied by ultrasonic measurements. The molar sound velocities (R) [1] and molar compressibilities (W) [2] gives information on the formation of a complex, molecular association and dissociation of the components. The sound velocities in binary mixtures can be calculated theoretically at different concentrations from the JACOBSON'S *Free Length Theory* (*FLT*) [3] and also from *Collision Factor Theory* (*CFT*) [4] due to SCHAAFF'S. Both the theories have been applied successfully by many workers [5–11].

A survey of the literature has shown that, more amount of work has been carried with lower aliphatic alcohols where as a little amount of work is attempt-

* Present address: Department of Physics, S.V.U. Post Graduate Centre, Kavali – 524 202, India.

ed with higher alcohols. Hence we report new experimental data for sound velocities and allied parameters of binary mixtures of *n*-octanol with benzene, tolune, *O*-xylene and ethylbenzene. The sound velocities were also calculated theoretically using *FLT* and *CFT* for these mixtures and the results were compared with the experimental data.

Theoretical

From the measured ultrasonic velocity (U) and density (ϱ) measurements, the adiabatic compressibilities can be calculated using the Laplace equation

$$\beta_{ad} = (U^2 \varrho)^{-1}. \tag{1}$$

The free lengths in the liquids can be calculated from the JACOBSON'S equation (2)

$$L_f' = \frac{K}{U \varrho^{1/2}} = K(\beta_{ad})^{1/2}, \tag{2}$$

where K is a temperature dependent constant ($K = 642$ at 313.16 K). In the case of mixtures free lengths can be calculated as

$$L_f^{M'} = \frac{K}{U_{\text{mix}} \varrho_{\text{mix}}^{1/2}}. \tag{3}$$

The free lengths in pure liquids or mixtures can also be calculated without involving velocity data using the relation

$$L_f = \frac{2V_a}{Y} = \frac{2(V_T - V_0)}{Y}, \tag{4}$$

where V_a is the available volume per mole V_T and V_0 are the molar volumes at the temperature T and absolute zero, respectively, Y is the surface area per mole of the liquid and is given by $Y = (36\pi N V_0^2)^{1/3}$, where N is Avogadro's number. From the knowledge of the pure liquids, the ideal free lengths $\supset L_f^M \supset$ in mixtures at different concentrations may be evaluated from the equation

$$L_f^M = \frac{2V_a^M}{X_A V_A + V_B Y_B}, \tag{5}$$

where X_A and X_B are mole fractions, Y_A and Y_B are surface areas per mole of the components A and B, respectively.

The relative association ($R.A.$) of the liquids or liquid mixtures [12] may be evaluted from the relation

$$R.A. = (L_f^{M'}/L_f^M)^3. \tag{6}$$

The molar sound velocities (R) and molar compressibilites (W) of the pure liquids as well as mixtures can be calculated by using the Eqs. (7) and (8) which are as follows:

$$R = (M/\varrho)\, V^{1/3}, \tag{7}$$

$$W = (M/\varrho)\beta_{ad}^{-1/3}, \tag{8}$$

where M is the molecular weight.

For the theoretical evaluation of velocities in pure liquids or binary mixtures, in addition to JACOBSON'S *Free Length Formula*, SCHAAFF'S *Collision Factory Theory* [4] may also be used. Schaaff presented the following formula for velocities in pure liquids

$$U = U_\infty s r_f = U_\infty S B/V, \tag{9}$$

where $U_\infty = 1600$ m/s, S is the collision factor and B is the actual volume of the mole given by

$$B = (4/3)\pi r^3 N. \tag{10}$$

The molecular radius r may be calculated from the formula due to SCHAAFF'S [4] and also GOPALA RAO and VENKATASESHAIAH [12] NUTACH-KUHNKIES [9] extended the theory to binary mixtures as

$$U_{\text{mix}} = U_\infty (X_A S_A + X_B S_B)\,(X_A B_A + X_B B_B)/V_{\text{mix}}, \tag{11}$$

where S_A and S_B are collision factors and B_A and B_B are the actual volumes of the pure components A and B respectively.

Experimental

Ultrasonic velocities were determined using a single crystal interferometer working at a fixed frequency of 2 MHz with an accuracy of 0.01%. Densities were measured using a double stem pyknowmeter having capillaries of narrow bore and the open ends which were fitted with "Teflon Caps" in order to prevent evaporation. The accuracy in density determination is 1 in 10^5 parts. All the measurements were made at a constant temperature 313.16 K, maintained to an accuracy of ± 0.01 K.

Results and Discussion

From the measured ultrasonic velocites and densities the available volumes, adiabatic compressibilities, free lengths relative associations, molar sound velocities and molar compressibilities were calculated for the binary mixtures of *n*-octanol with benzene, tolune *O*-xylene, and ethylbenzene and the results are given in Table 1. The ultrasonic velocities, free lengths and adiabatic compressibilities of the mixtures studied are polted against mole

fraction of the alcohol component $B(X_B)$ in Fig. 1. From the free lengths and surface areas of the pure components, the free lengths and sound velocities of mixtures were evaluated. From *CFT*, the collision factors for the pure liquids were calculated and are used in evaluating sound velocities in mixtures. Molecular radii were calculated from both the formulas due to SCHAAFF'S [4] and GOPALA RAO and VENKATASESHAIAH [12] and the mean is employed in the evalution of actual volume. The mean values of molecular radii and collision factors of; pure liquids are presented in Table 2. The sound velocities calculated theoretically are presented in Fig. 1 along with the experimental data.

The ultrasonic velocity, free length and compressibility curves of all the systems studied show a non-linear variation with mole fractions of *n*-octanol H_B. The curves have not exhibited any maximum in velocity or any dip in compressibility thereby indicating the absence of complex formation [13]–[15]. This will also be further evidenced by the following points of discussion.

The deviations from linearity in the binary mixtures are attributed mainly due to *a* the formation of complexes and *b* the molecular assotiation by weak bonds, if the deviations in free lengths are negative. If the deviations are negative in velocity curves and positive in free length curves, they are attributed to the molecular dissociation of an associated species caused by the addition of an inert solvent or an active solvent producing considerable, dissociation. In addition to these effects, non-lineartics can also be attributed to size difference of molecules and the difference of the boiling points of solute solvent. In the present systems absence of sudden variation in the curves of velocity and comperessibility indicates absence of complex formation.

The observed non-lineartics in velocity, free length and compressibility curves can be explained as follows. There is considerable evidence to show that

Table 1. Ultrasonic parameters in binary liquid mixtures at 313.16 K

Mole fraction X_B	Density ϱ [g/cm³]	Velocity U [m/s]	Compressibility $\beta \times 10^{11}$ [cm²/dyn]	Free length L_f^M [10^{-10}m]	Free length $L_f^{M'}$ [10^{-10}m]	Relative association $R.A.$	Molar sound velocity R	Molar compressibility W
1	2	3	4	5	6	7	8	9
benzene + *n*-octanol								
0.0000	0.85762	1232.25	7.684	0.5622	0.5627	1.002	977	2538
0.0532	0.85230	1222.25	7.854	0.5629	0.5689	1.032	1014	2635
0.1004	0.84831	1221.30	7.903	0.5638	0.5707	1.037	1050	2725
0.1501	0.84448	1220.44	7.950	0.5644	0.5724	1.043	1087	2820
0.2005	0.84098	1221.60	7.982	0.5646	0.5735	1.048	1125	2917
0.2991	0.83952	1227.58	7.904	0.5621	0.5707	1.147	1195	3096
0.4976	0.82992	1244.07	7.785	0.5463	0.5664	1.115	1348	3485
0.6935	0.82289	1266.11	7.581	0.5418	0.5589	1.098	1502	3875
0.8458	0.81906	1282.56	7.422	0.5359	0.5331	1.099	1620	4176
1.0000	0.81516	1299.03	7.269	0.5325	0.5473	1.085	1743	4486

Table 1 — cont.

Mole fraction X_B	Density ϱ [g/cm³]	Velocity U [m/s]	Compressibility $\beta \times 10^{11}$ [cm²/dyn]	Free length L_f^M [10^{-10}m]	Free length $L_f^{M'}$ [10^{-10}m]	Relative association $R.A.$	Molar sound velocity R	Molar compressibility W
1	2	3	4	5	6	7	8	9
tolune + *n*-octanol								
0.0000	0.84718	1240.84	7.660	0.5462	0.5619	1.106	1167	3028
0.0513	0.84474	1238.47	7.718	0.5474	0.5640	1.093	1196	3100
0.1017	0.84234	1236.42	7.765	0.5470	0.5657	1.105	1223	3170
0.2023	0.83725	1237.69	7.796	0.5484	0.5669	1.104	1280	3315
0.3613	0.83301	1244.33	7.753	0.5487	0.5653	1.093	1365	3537
0.4973	0.82571	1256.38	7.672	0.5481	0.5623	1.079	1451	3748
0.5985	0.82214	1264.27	7.609	0.5487	0.5600	1.063	1511	3899
0.6947	0.81955	1272.23	7.538	0.5472	0.5574	1.057	1568	4042
0.8960	0.81436	1289.52	7.384	0.5454	0.5517	1.034	1687	4344
1.0000	0.81516	1299.03	7.269	0.5325	0.5473	1.085	1743	4486
O-xylene + *n*-octanol								
0.0000	0.86279	1287.02	6.948	0.5179	0.5351	1.103	1339	3477
0.0506	0.85987	1285.14	7.022	0.5182	0.5380	1.118	1358	3524
0.1029	0.85672	1283.57	7.075	0.5193	0.5400	1.124	1378	3574
0.2016	0.84969	1280.63	7.176	0.5242	0.5438	1.106	1418	3675
0.3052	0.84433	1280.92	7.218	0.5269	0.5454	1.116	1460	3779
0.5014	0.83353	1283.52	7.282	0.5339	0.5478	1.080	1541	3982
0.6972	0.82459	1290.14	7.285	0.5376	0.5479	1.058	1623	4185
0.7952	0.82016	1292.67	7.296	0.5404	0.5484	1.044	1664	4287
0.8994	0.81660	1297.41	7.275	0.5399	0.5476	1.051	1705	4390
1.0000	0.81516	1299.03	7.269	0.5325	0.5473	1.085	1743	4486
ethylbenzene + *n*-octanol								
0.0000	0.84852	1256.20	7.468	0.5400	0.5548	1.084	1349	3499
0.0538	0.84675	1255.31	7.494	0.5378	0.5557	1.103	1368	3547
0.1046	0.84403	1252.95	7.547	0.5397	0.5577	1.103	1388	3595
0.2018	0.83923	1251.23	7.611	0.5455	0.5600	1.082	1417	3668
0.2640	0.83528	1253.97	7.613	0.5462	0.5601	1.216	1452	3757
0.5005	0.82732	1265.16	7.551	0.5503	0.5578	1.042	1545	3990
0.6968	0.81935	1275.64	7.500	0.5501	0.5559	1.032	1627	4193
0.7985	0.81741	1284.90	7.410	0.5457	0.5526	1.038	1667	4294
0.8906	0.81641	1290.36	7.356	0.5400	0.5506	1.059	1705	4390
1.0000	0.81516	1299.03	7.269	0.5325	0.5473	1.085	1743	4486

alcohols exist as closed ring structures as dimers and trimers [16]. It is important to notice eshaiah [12] and the mean is employed in the evaluation of actual volume. The mean values of molecular radii and collision factors of; pure liquids are presented in Table 2. The sound velocities calculated theoretically are presented in Fig. 1 along with the experimental data.

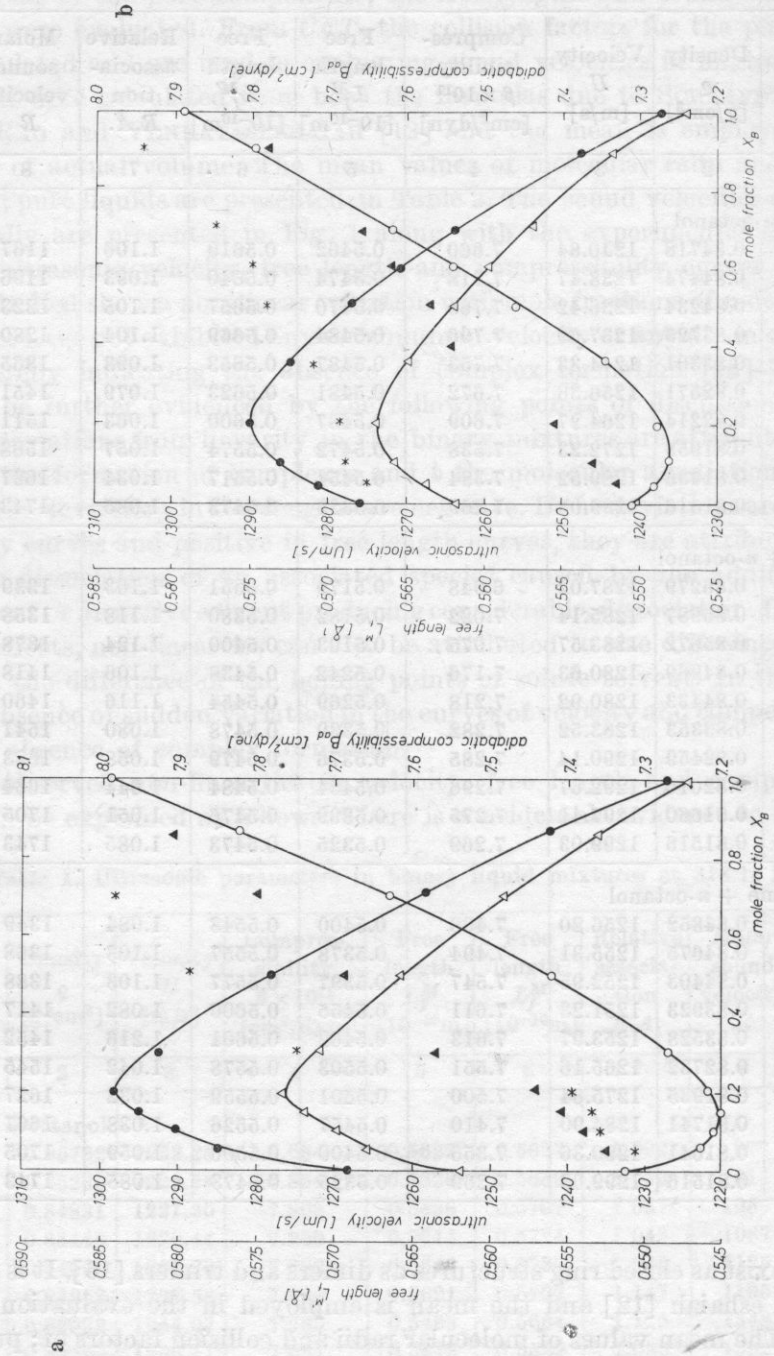
a
b
free length L_f^M [Å]
ultrasonic velocity [Um/s]
adiabatic compressibility β_{ad} [cm²/dyne]
mole fraction X_B

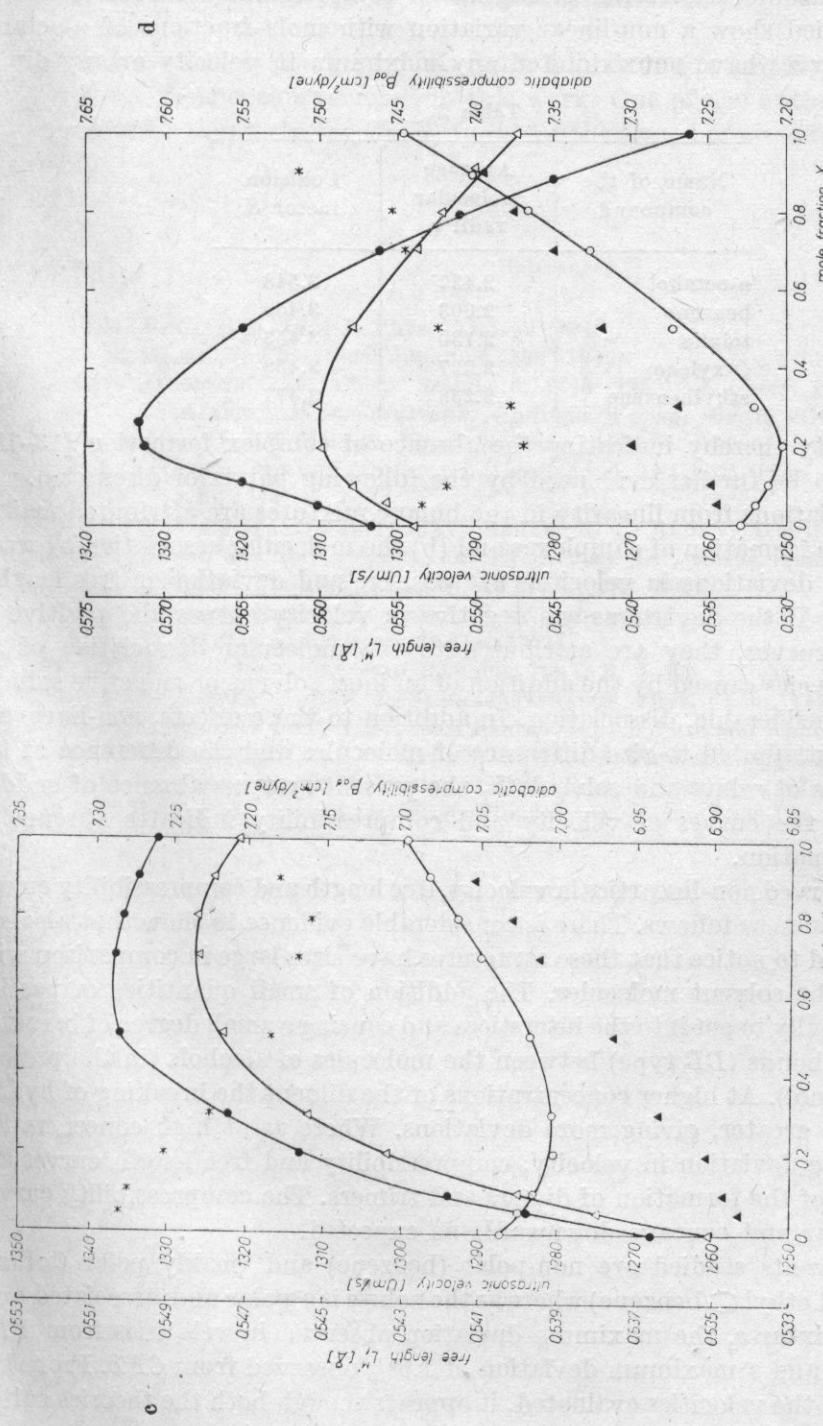

Fig. 1. Variation of ultrasonic velocity U (○○○), adiabatic compressibility (●●●), free-length L_f^M (▲▲▲), ultrasonic velocity calculated from CFT (△△△) and from FLT (***) as a function of mole fraction (X_B) of alcohol in the systems: (a) benzene + n-octanol, (b) tolune + n-octanol, (c) O-xylene + n-octanol, (d) ethylbenzene + n-octanol

The ultrasonic velocity, free length and compressibility curves of all the systems studied show a non-linear variation with mole fractions of *n*-octanol (X_B). The curves have not exhibited any maximum in velocity or any dip in

Table 2

Name of the compound	Average molecular radii *r*	Collision factor *S*
n-octanol	2.437	3.548
benzene	2.003	3.459
tolune	2.130	3.453
O-xylene	2.227	3.458
ethylbenzene	2.238	3.471

compressibility thereby indicating the absence of complex formation [13–15]. This will also be further evidenced by the following points of discussion.

The deviations from linearity in the binary mixtures are attributed mainly due to (a) the formation of complexes and (b) the molecular association by weak bonds, if the deviations in velocities are positive and deviation in free lenghts are negative. If the deviations are negative in velocity curves and positive in free length curves, they are attributed to the molecular dissociation of an associated species caused by the addition of an inert solvent or an active solvent producing considerable, dissociation. In addition to these effects, non-lineartics can also be attributed to size difference of molecules and the difference of the boiling points of solute and solvent. In the present systems absence of sudden variation in the curves of velocity and compressibility indicates absence of complex formation.

The observed non-lineartics in velocity, free length and compressibility curves can be explained as follows. There is considerable evidence to show that alcohols exist as closed to notice that these structures have sizes large in comparison with the size of the solvent molecules. The addition of small quantities of passive diluent is usually to get into the interstices and causing a small degree of breaking of hydrogen bonds (*BB* type) between the molecules of alcohols (in the present study *n*-octanol). At higher concentrations of the diluent the breaking of hydrogen bonds is greater, giving more deviations. Where as at high concentration of alcohol the deviation in velocity, compressibility and free length curves are less because of the formation of dimers and trimers. The compressibility curves are non-linear and concave downwards as expected.

The solvents studied are non-polar (benzene) and weakly polar (tolune, *O*-xylene and ethyl ⊃ benzene) where as the solute is a polar and associated one. In all the mixtures, the maximum deviation observed in velocities from *FLT* is about 3% and a maximum deviation of 1.9% observed from *CFT*. From the deviations of the velocities evaluated, it appears though both the theories suited well, however, *CFT*, has an edge over *FLT*.

Acknowledgements

The authors thank Prof. K. SREE RAMAMURTHY and Dr. R. GOPALAKRISHNAN for their encouragement in this work. One of the authors (K. GOPAL) expresses his thanks to the CSIR, India for the award of a senior Research Fellowship.

References

[1] M. RAMA RAO, Ind. J. Phys., **14**, 109 (1940).
[2] Y. WADA, J. Phys. Soc. Japan, **4**, 280 (1949).
[3] B. JACOBSON, Acta Chem. Scand., **6**, 1485 (1952); J. Chem. Phys. **20**, 927 (1952).
[4] W. SCHAAFFS, *Molekularakustik*, Springer Verlag, Berlin–Göttingen–Heidelberg, Chapts. XI and XII; Z. Phys. **115**, 69 (1940).
[5] PRASAD RAVINDRA, K. C. REDDY, Acustica, **39**, 39 (1977); Proc. Ind. Acad. Sci., B2A, 217 (1975).
[6] K. RAVINDRAPASAD, E. L. RAVI MEHAR, K. C. REDDY, Acoust. Let., **4**, 170 (1981).
[7] K. GOPAL and RAO PRABHAKARA, N. Acoust. Lst, **4**, 164 (1981).
[8] R. NUTSCH-KUHNKIES, Acustica, **15** Beih., 383 (1965).
[9] C. S. ADGAONKAR, S. N. JAJOO, V. S. DAOGAONKAR, Acoust. Lst, **2**, 34 (1978).
[10] M. V. KAULGUD, Acustica, **25**, 14 (1971).
[11] M. G. RAO SESHAGIRI, RAO RAMACHANDRA, B. J. Sci. Industr. Res., **218**, 331 (1962).
[12] R. V. GOPALA RAO, V. Z. VENKATASESHAIAH, Phys. Chem. **242**, 193 (1969).
[13] M. VENKATESWARLU, G. SIVARAM SASTRY, Ind. J. Pure and Appl. Phys., **6**, 393 (1968).
[14] K. RAMAMURTHY, P. S. VARADACHARI, Ind. J. Pure and Appl. Phys., **11**, 238 (1973).
[15] S. RAJAGOPALAN, G. S. VARMA, Nuova Cimento, **678**, 13 (1970).
[16] C. REID, T. M. CORNER, Hydrogen Bonding, Pergamon Press Ltd., London P.83 (1959).

Received on March 3, 1985